On Solving a Three Phase Flow Model with Capillary Forces

Cand. Scient. Thesis in Industrial and Applied Mathematics and Informatics; Applied Analysis

Hans Fredrik Nordhaug

Department of Mathematics

University of Bergen

10th July 1998

This version printed 18th September 2002.

Dedications

I would like to thank my supervisors, Professor Magne Espedal, Associative Professor Helge K. Dahle and Doctor Scient. Kenneth Hvistendahl Karlsen, for backing my up and keeping me going. They have all given me good advice and useful hints. Karlsen has been especially helpful with his insight in the jungle of conservation laws.

I would also like to thank all the students at the department. Our daily round of "Spar dame" has given me ups (and, unfortunately, downs) when I have been sick of my thesis. The weekly round in the Mathematical Hockey League has also given me something to look forward to. Hopefully I will be able to continue these activities for yet some years...

A special thank goes to my girlfriend Celia M. Berg for being a friend when I needed it, and not giving me up when I was at my most desperate - after a week in front of an electronic monster.

Hans Fredrik Nordhaug
Bergen, 10th July 1998

Figure 1: Dilbert is my friend.

Contents

Chapter 1

Introduction

Mathematical models that involve a combination of advection and diffusion processes are among the most widespread in all of science, engineering and other fields where mathematical modelling is important. Very often the models are advection dominated with sharp fronts building up. Because of these fronts difficulties will be experienced with standard numerical approximations. Thus many different methods have been proposed to overcome the difficulties, see [1]. Advection-diffusion equations occur for example in the study of three phase flow, atmospheric pollution and ground water transport.

In this thesis we will investigate the three phase flow model. The model describes the flow of oil, gas and water in a porous media. The solution of this 2×2 system of (coupled) equations are well understood for some cases, see for example [2, 3, 4]. However, we will assume that the flow of one of the phases is independent of the other leading to a system of equations where one equation is decoupled from the other, i.e., a *triangular* system. This assumption is not trivial, but it seems that at least for some systems it is a good approximation. We are going to solve the system with a corrected operator splitting method. In the first step we solve for the hyperbolic part of the problem, and in the second step for the diffusion part. In this process we make a splitting error. We therefore try to find a correction term that can reduce the splitting error. This leads to the *corrected operator splitting method* [5, 6]. The advection part will be solved by the means of *front tracking* [6, 7, 8], and the diffusive part will be solved by finite difference approximations. In this paper only one spatial dimension is considered. Generalisations to more space dimensions can be done using dimensional splitting, see [9, 10].

The main objectives of this thesis are to investigate the corrected operator splitting method and to compare the triangular model with the fully coupled model. The triangular model without diffusion is well understood, see [11, 12, 13]. We will build on this work when we introduce diffusion terms and the corrected operator splitting. We want to quantify when a fully coupled system can be approximated by a triangular system. Investigating this approximation is interesting since solving the triangular system is much faster than solving the fully coupled one.

In Chapter 2 a three phase flow model is briefly developed, and the assumptions used are stated. In Chapter 3 operator splitting will be presented. In Chapter 4 we define a

Riemann problem and construct a *Riemann solver*. The essential part of the construction of the construction of the Riemann solver is the H-sets, which are presented in this chapter. Front tracking and its implementation are given in Chapter 5. In Chapter 6 we solve the diffusion equation using explicit and implicit finite difference approximations. Numerical results are given in chapter 7. Finally, in Chapter 8, we present a summary and conclusions. Some further developments are suggested.

Chapter 2

The mathematical model

The equations for three phase flow are well known, and they can be found in numerous books in reservoir mechanics, e.g. [14]. We are going to do a short derivation of the equations describing the flow and point out the assumptions. The phases are :
Gas, oil and water (short: g, o and w).

The following terminology will be adopted in this thesis.

Symbol	Meaning $l = g, o, w$
V_b	bulk volume
V_p	volume of pores
V_l	volume of phase l
$\phi = V_p/V_b$	porosity
$S_l = V_l/V_p$	saturation of phase l
C_g^o	concentration of gas in oil
K	absolute permeability
k_{rl}	relative permeability of phase l
u_l	velocity of phase l
$u_t = u_g + u_o + u_w$	total velocity
μ_l	viscosity of phase l
$\lambda_l = k_{rl}/\mu_l$	mobility for phase l
$\lambda_t = \lambda_w + \lambda_g + \lambda_o$	total mobility
p_l	pressure of phase l
$P_{clk} = p_l - p_k$	capillary pressure
$\mathbb{R}_l$	density of component l
g	gravity constant
$\gamma_l = \mathbb{R}_l g$	specific gravity

2.1 Assumptions on the model

The following assumptions are commonly made in three phase flow models [14, 15]:

1. Incompressible flow $\Leftrightarrow \ \frac{d\mathbb{R}_l}{dp} = 0 \Leftrightarrow \mathbb{R}_l = \text{constant for } l = w, g, o$
2. Incompressible porosity $\Leftrightarrow \ \frac{\partial \phi}{\partial p} = 0 \Leftrightarrow \ \phi = \text{constant}$
3. The void space is completely saturated $\Leftrightarrow \ S_w + S_g + S_o = 1$
4. Constant viscosity for each phase $\Leftrightarrow \ \mu_l = \text{constant for } l = w, g, o$
5. "Black oil" - We look at oil as one component and disregard the the fact that oil typically contains several hundred components, i.e., we have three phases and three components. We allow only gas in the gas phase, only water in the water phase but both gas and oil in the oil phase.
6. The concentration of gas in oil phase is C_g^o, which we assume to be constant. Since there is no water in the oil phase (see 5. above), the concentration of oil in the oil phase is $1 - C_g^o$.
7. Isotropic and homogeneous reservoir $\Leftrightarrow \ K = \text{constant}$
8. No source and sink terms.

2.2 Derivation of governing equations

Darcy's law for a single fluid flowing in one dimension is

$$u = -\frac{K}{\mu}\left(\frac{\partial p}{\partial x} + \mathbb{R}\ g\cos\theta\right), \tag{2.1}$$

where u is the velocity, θ is the angle between the (positive) vertical and direction of flow, and K is permeability for the fluid. This equation is generalised to three phase flow by introducing mobilities and specific gravities:

$$u_l = -K\lambda_l\left(\frac{\partial p_l}{\partial x} + \gamma_l\cos\theta\right) \quad \text{for} \ \ l = w, g, \tag{2.2}$$

and in addition using the fact that there is gas desolved in the oil phase to get

$$u_o = -K\lambda_o\left(\frac{\partial p_o}{\partial x} + ((1 - C_g^o)\gamma_o + C_g^o\gamma_g)\cos\theta\right). \tag{2.3}$$

From assumption 3 we get $S_o = 1 - S_w - S_g$. It follows that we only have to solve for two phases, for instance water and gas.

If we use conservation of mass for each component and assumption 1, 2, 6 and 8, we get the following simple form of the conservation law for the phases after removing constants:

$$\phi\frac{\partial S_w}{\partial t} + \frac{\partial u_w}{\partial x} = 0, \tag{2.4}$$

$$\phi\frac{\partial S_g}{\partial t} + \frac{\partial u_g}{\partial x} = 0, \tag{2.5}$$

$$\phi\frac{\partial S_o}{\partial t} + \frac{\partial u_o}{\partial x} = 0. \tag{2.6}$$

By adding (2.4), (2.5) and (2.6) we get

$$\frac{\partial(u_g + u_o + u_w)}{\partial x} = \frac{\partial u_t}{\partial x} = 0 \Leftrightarrow \ u = \text{constant}. \tag{2.7}$$

Thus the total velocity is constant. This not true in higher dimensions.

2.3 Fractional flow formulas

By using the definition of the mobilities and capillary pressures together with Equations (2.2) and (2.3) we get, after some algebra [3], expressions for u_w/u_t and u_g/u_t as follows:

$$\frac{u_w}{u_t} = F_w + \frac{K}{u_t}\left(f_w(\lambda_o + \lambda_g)\frac{\partial P_{cow}}{\partial x} + f_w\lambda_g\frac{\partial P_{cgo}}{\partial x}\right), \tag{2.8}$$

$$\frac{u_g}{u_t} = F_g - \frac{K}{u_t}\left(f_g\lambda_w\frac{\partial P_{cow}}{\partial x} + f_g(\lambda_w + \lambda_o)\frac{\partial P_{cgo}}{\partial x}\right), \tag{2.9}$$

where F_w and F_g are the fractional flow function for the water and gas phase respectively:

$$F_w \stackrel{\text{def}}{=} f_w + f_{w_g} \tag{2.10}$$

$$\stackrel{\text{def}}{=} \frac{\lambda_w}{\lambda_t} + \frac{K}{u_t}\left(\frac{\lambda_g\lambda_w}{\lambda_t}(\gamma_g - \gamma_w) + \frac{\lambda_o\lambda_w}{\lambda_t}((1 - C_g^o)\gamma_o - \gamma_w + C_g^o\gamma_g)\right)\cos\theta,$$

$$F_g \stackrel{\text{def}}{=} f_g + f_{g_g} \tag{2.11}$$

$$\stackrel{\text{def}}{=} \frac{\lambda_g}{\lambda_t} + \frac{K}{u_t}\left(\frac{\lambda_g\lambda_w}{\lambda_t}(\gamma_w - \gamma_g) + \frac{\lambda_o\lambda_g}{\lambda_t}(\gamma_o - (1 - C_g^o)\gamma_g)\right)\cos\theta.$$

The first part (f_w and f_g) in Equations (2.10) and (2.11) measures the advection part of the flow and the last part (f_{w_g} and f_{g_g}) measures the gravity part of the flow.

The difference in phase pressures due to capillary forces leads to capillary dispersion or diffusion[1], i.e., advection-diffusion equations.

[1]Strictly speaking, capillary diffusion is incorrect terminology, although commonly used, since diffusion refers to mixing on the molecular level. The capillary forces lead to mixing on a pore-scale level, and the correct terminology is therefore a dispersion.

We substitute Equations (2.8) and (2.9) into Equations (2.4) and (2.5) to obtain advection-diffusion equations:

$$\frac{\partial S_w}{\partial t} + \frac{u_t}{\phi}\frac{\partial F_w}{\partial x} + \frac{K}{\phi}\left(f_w(\lambda_o + \lambda_g)\frac{\partial P_{cow}}{\partial x} + f_w\lambda_g\frac{\partial P_{cgo}}{\partial x}\right) = 0 \tag{2.12}$$

and

$$\frac{\partial S_g}{\partial t} + \frac{u_t}{\phi}\frac{\partial F_g}{\partial x} - \frac{K}{\phi}\left(f_g\lambda_w\frac{\partial P_{cow}}{\partial x} + f_g(\lambda_w + \lambda_o)\frac{\partial P_{cgo}}{\partial x}\right) = 0. \tag{2.13}$$

Since $P_{cow} = P_{cow}(S_w)$ and $P_{cgo} = P_{cgo}(S_g)$

$$\frac{\partial P_{cow}}{\partial x} = P'_{cow}\frac{\partial S_w}{\partial x} \quad \text{and} \quad \frac{\partial P_{cgo}}{\partial x} = P'_{cgo}\frac{\partial S_g}{\partial x}.$$

Using this Equations (2.12) and (2.13) can be written as

$$\frac{\partial S_w}{\partial t} + \frac{u_t}{\phi}\frac{\partial F_w}{\partial x} = -\frac{K}{\phi}\frac{\partial}{\partial x}\left(f_w(\lambda_o + \lambda_g)P'_{cow}\frac{\partial S_w}{\partial x} + f_w\lambda_g P'_{cgo}\frac{\partial S_g}{\partial x}\right) \tag{2.14}$$

and

$$\frac{\partial S_g}{\partial t} + \frac{u_t}{\phi}\frac{\partial F_g}{\partial x} = \frac{K}{\phi}\frac{\partial}{\partial x}\left(f_g\lambda_w P'_{cow}\frac{\partial S_w}{\partial x} + f_g(\lambda_w + \lambda_o)P'_{cgo}\frac{\partial S_g}{\partial x}\right). \tag{2.15}$$

Let

$$D(\mathbf{S}) = \begin{pmatrix} -f_w(\lambda_o + \lambda_g)P'_{cow} & -f_w\lambda_g P'_{cgo} \\ f_g\lambda_w P'_{cow} & f_g(\lambda_w + \lambda_o)P'_{cgo} \end{pmatrix}.$$

D is called the diffusion matrix. Typically, P_{cow} is a decreasing function of S_w and P_{cgo} an increasing function of S_g, see [16]. These properties of the capillary pressures guarantee that D is positive definite, i.e, it is symmetrisable and has positive real eigenvalues.

Let

$$\mathbf{S} = \begin{pmatrix} S_w \\ S_g \end{pmatrix} \quad \text{and} \quad A(\mathbf{S}) = \begin{pmatrix} \frac{\partial F_w}{\partial S_w} & \frac{\partial F_w}{\partial S_g} \\ \frac{\partial F_g}{\partial S_w} & \frac{\partial F_g}{\partial S_g} \end{pmatrix},$$

where $A(\mathbf{S})$ is the Jacobian matrix of $\mathbf{F} = \begin{pmatrix} F_w \\ F_g \end{pmatrix}$.

Equations (2.14) and (2.15) define a 2×2 system which now can be rewritten as

$$\mathbf{S}_t + \frac{u_t}{\phi} A(\mathbf{S})\mathbf{S}_x = \frac{K}{\phi} \left(D(\mathbf{S})\mathbf{S}_x\right)_x . \tag{2.16}$$

This system can easily be written in dimensionless form so that the saturations go from 0 to 1, see [2]. This introduces a parameter ϵ_l $(l = w, g)$ in front of the diffusion terms. Typically, this parameter is small for the problems considered here. For simplicity the dimensionless variables are not renamed and ϵ_w and ϵ_g are set equal to ϵ. The system can then be written as

$$\mathbf{S}_t + A(\mathbf{S})\mathbf{S}_x = \epsilon \ \left(D(\mathbf{S})\mathbf{S}_x\right)_x \quad \text{for} \ \ l = w, g. \tag{2.17}$$

The equations are coupled through the fractional flow functions and the diffusion matrix.

Fractional flow formulas without capillary forces

Neglecting the capillary forces is physically reasonable when u_t is large, i.e., the advection terms dominate the diffusion terms. This is also seen from Equation (2.17) when u_t goes to infinity.

$$\lim_{u_t \to \infty} \left[\mathbf{S}_t + A(\mathbf{S})\mathbf{S}_x\right] = \lim_{u_t \to \infty} \left[\epsilon \ \left(D(\mathbf{S})\mathbf{S}_x\right)_x\right] = 0$$

since $D(\mathbf{S})$ is finite and $\epsilon = O(1/u_t)$ when u_t goes to infinity. Thus Equation (2.17) reduces to

$$\mathbf{S}_t + A(\mathbf{S})\mathbf{S}_x = 0. \tag{2.18}$$

This is the same as we get if we neglect the capillary forces, i.e., set the phase pressures equal, $p_w = p_g = p_o = p$.

From Equation (2.8) and (2.9) we get that

$$\frac{u_l}{u_t} = F_l \ \ \text{for} \ \ l = w, g, \tag{2.19}$$

when u_t goes to infinity. Thus capillary pressure terms can be neglected.

No capillary forces give no diffusion terms in the conservation laws for the water and gas phase. The equations are coupled only in the fractional flow functions.

2.4 Triangular model

The advection-diffusion system (2.17) is coupled both in the fractional flow functions and via the diffusion matrix. To make the system easier to solve numerically we will make the following assumptions to reduce the difficulties:

1. The diffusion matrix is diagonal.
2. The diagonal elements are functions of one phase only, $D_{11} = D_w(S_w)$ and $D_{22} = D_g(S_g)$.
3. The fractional flow function for the gas phase is independent of the other phases.

As stated in Section 2.3, the diffusion matrix is diagonalisable since it is positive definite, see [16]. Thus, the matrix can be made diagonal by an appropriate transformation. The first assumption is therefore not essential. Normally the elements in the diffusion matrix are functions of both phases because of the phase mobilities. Assuming the diagonal (diffusion) elements to be functions of one phase only is done for convenience. The fact that gas mobility generally is larger than oil and water mobility motivates the assumption that gas flow is independent of the oil and the water phase.

From the statements above it follows that the equation for the gas phase is decoupled from the equation for the water phase. All functions in the gas equation are functions of the gas phase only. But still the water phase equation is coupled to the gas phase equation. Thus, the system is coupled through the fractional flow function for the water phase, F_w. The resulting system of equations is:

$$\frac{\partial S_w}{\partial t} + F_w(S_w, S_g)_x = \epsilon \frac{\partial}{\partial x}(D_w(S_w)\frac{\partial S_w}{\partial x}), \tag{2.20}$$

$$\frac{\partial S_g}{\partial t} + F_g(S_g)_x = \epsilon \frac{\partial}{\partial x}(D_g(S_g)\frac{\partial S_g}{\partial x}). \tag{2.21}$$

Since the Jacobian matrix for $[F_w, F_g]^T$ is (upper) triangular, this system will be denoted a *triangular* system[2]

The diffusion functions for the water and gas phase, D_w and D_g, respectively, are set equal to D_{eq}. In addition let $S_g = u$, $S_w = v$, $F_g = f$, $F_w = g$ and let d be the definite integral of the diffusion function D_{eq}, $d(\eta) = \int_0^\eta D_{eq}(\xi)\, d\xi$. It then follows that

$$[D_{eq}(\eta)\eta_x]_x = d(\eta)_{xx}.$$

The system of advection-diffusion equations we will investigate in the rest of this thesis thus becomes:

$$v_t + g(u, v)_x = \epsilon\, d(v)_{xx}, \tag{2.22}$$

$$u_t + f(u)_x = \epsilon\, d(u)_{xx}. \tag{2.23}$$

[2]Strictly speaking this terminology relates to the hyperbolic part of Equations (2.20-2.21).

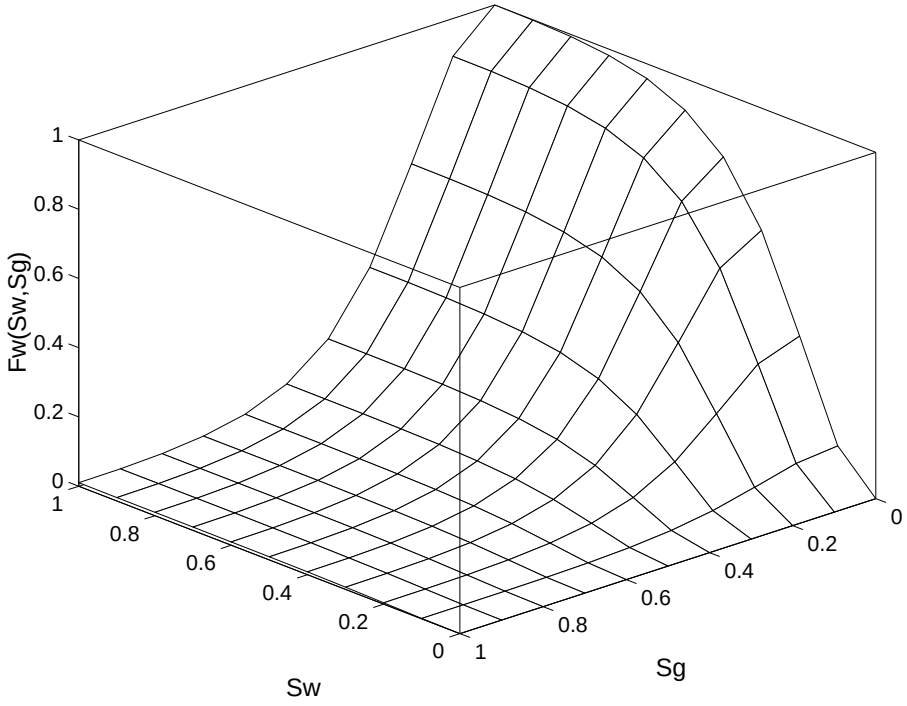

Figure 2.1: Fractional flow function for water

The essential assumption made above is that the fractional flow function for the gas phase is independent of the other phases since this makes the system triangular. This assumption was physically motivated by the fact that the gas mobility generally is larger than the oil and water mobility. In some models this is not the case, and we may not make the assumption. Looking at the fractional flow functions in the phase plane may also motivate the assumption that the gas flow is independent for some sets of fractional flow functions. This is illustrated by the following example with fractional flow functions from Kok [12]:

In figure 2.1 we observe that the fractional flow function for water depends heavily on both S_w and S_g. This is *not* the case for gas. Looking at the fractional flow function for gas, in figure 2.2, we observe that the dependence on water is very weak. To investigate whether or not a three phase model may be approximated by a triangular model, it is useful to look at Taylor expansions of the gas flux function:

$$\begin{aligned} F_g(S_g, S_w) &= F_g(S_{g0}, S_{w0}) + \frac{\partial F_g}{\partial S_g}(S_{g0}, S_{w0})\Delta S_g + \frac{\partial F_g}{\partial S_w}(S_{g0}, S_{w0})\Delta S_w \\ &\quad + O(\Delta S_g \Delta S_w, {\Delta S_w}^2, {\Delta S_g}^2), \end{aligned} \tag{2.24}$$

where $\Delta S_l = S_l - S_{l0}$. In a neighbourhood of (S_{g0}, S_{w0}), terms of second order are negligible. Assuming that the gas phase is independent of the water phase is the same as assuming that the partial derivative of the fractional flow function for the gas phase with respect to the water phase is negligible.

So, if the partial derivative with respect to the water phase, is sufficiently small compared to the partial derivate with respect to the gas phase in some norm, then the approx-

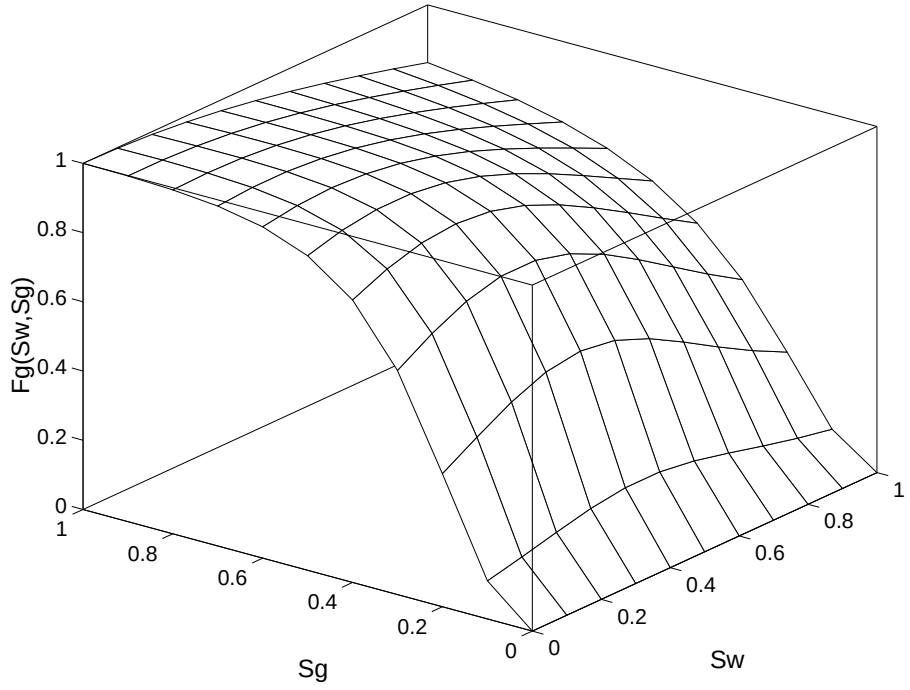

Figure 2.2: Fractional flow function for gas

imation is expected to be good. Let P be the phase plane, $P = \{(u, v) : u \geq 0, v \geq 0, u + v \leq 1\}$. We define the L_2-norm (on P) to be

$$||f|| = \left(\iint_P f^2 \right)^{1/2} = \left(\int_0^1 [\int_0^{1-u} f(u,v)^2 dv] du \right)^{1/2}. \tag{2.25}$$

Based on the previous reasoning we suggest the following condition:

Norm condition 1 *Let $f(u, v)$ be the gas flux function in a fully coupled 2×2 advection-diffusion system. If*

$$||f_v|| < k||f_u||$$

where $k \ll 1$, then the fully coupled system can be approximated reasonably well by a triangular system. The fully coupled system is made triangular by replacing $f(u, v)$ with $f(u, v_0)$, for some v_0.

Typically v_0 is chosen to be zero for the systems considered here, see [12]. The magnitude of k in the above statement is not determined, but it should obviously be much less than one. In Section 7.2 we investigate the Norm condition and try to decide the magnitude of k more accurately. It is of great interest to find the condition a system must satisfy to be approximated reasonably well by a triangular system.

Chapter 3

Corrected operator splitting

Our technique in solving the advection-diffusion equations will be operator splitting. It is a general way to simplify a problem. Operator splitting is fruitful when solving the whole problem in one operation is difficult, or when the problem consists of two parts that have different physics and therefore require different solution methods.

3.1 Operator splitting

We have to solve the system of advection-diffusion equations with initial data $\mathbf{s}_0$:

$$\begin{aligned} \mathbf{s}_t + \mathbf{f}(\mathbf{s})_x &= \epsilon\, D(\mathbf{s})_{xx}, \\ \mathbf{s}(x,o) &= \mathbf{s_0}, \end{aligned} \tag{3.1}$$

where ϵ is a small positive parameter,
$\mathbf{s} = \begin{pmatrix} u \\ v \end{pmatrix}$, $\mathbf{f}(\mathbf{s}) = \begin{pmatrix} f(u) \\ g(u,v) \end{pmatrix}$ and $D(\mathbf{s}) = \begin{pmatrix} d(u) & 0 \\ 0 & d(v) \end{pmatrix}$.

The method shortly described as follows:

First we solve the advection part of the system, a hyperbolic system. Let $\mathbf{v}(x,t) = \mathcal{S}(t)\mathbf{v}_0$ be the solution of the system

$$\begin{aligned} \mathbf{v}_t + \mathbf{f}(\mathbf{v})_x &= 0, \\ \mathbf{v}(x,0) &= \mathbf{v}_0. \end{aligned} \tag{3.2}$$

Then we solve the diffusion part of the system, a parabolic system. Let $\mathbf{w}(x,t) = \mathcal{H}(t)\mathbf{w}_0$ be the solution of the system

$$\begin{aligned} \mathbf{w}_t &= \epsilon D(\mathbf{w})_{xx}, \\ \mathbf{w}(x,0) &= \mathbf{w}(x,0). \end{aligned} \tag{3.3}$$

We then have a hyperbolic and parabolic solution operator, $\mathcal{S}$ and $\mathcal{H}$, correspondingly. With these two operators we are able to write an approximation to the solution of system

(3.1) as

$$\mathbf{s}(x, n\Delta t) \approx (\mathcal{H}(\Delta t)\mathcal{S}(\Delta t))^n \mathbf{s}_0(x). \tag{3.4}$$

For the scalar case the operator splitting solution converges to the correct solution of the advection-diffusion equation, see [17, Paper C]. Operator splitting for systems is yet not shown to converge.

It is well known that solutions of hyperbolic systems may develop shocks even for smooth initial data. Then the solutions are no longer differentiable. These solutions are called weak solutions, and they are generally not unique. Entropy conditions are needed to get uniqueness. See Section 4.1 for a thorough presentation of this matter.

If the solution of the hyperbolic system contains shocks only the envelope of the fractional flow functions is used. We then loose some vital information about the flux. Unfortunately this information is not recovered in the diffusion step, i.e., a splitting error is introduced. In Section 3.2 we present a method that reduces this error, corrected operator splitting.

3.1.1 Hyperbolic systems

A system of the form

$$p_t + Ap_x + Bp = F(x, t) \tag{3.5}$$

is hyperbolic if the matrix A is diagonalisable with real eigenvalues. If the eigenvalues in addition are different, the system is strictly hyperbolic. If, on the other hand, the eigenvalues are complex, the system is elliptic.

Equation (3.2) is of form (3.5) with B and F equal to zero. We write $\mathbf{f}(\mathbf{s})_x = A(\mathbf{s})\mathbf{s}_x$ where $A(\mathbf{s})$ is the Jacobian matrix of $\mathbf{f}(\mathbf{s})$. For a triangular system the Jacobian matrix is

$$A(\mathbf{s}) = \begin{bmatrix} f_u & 0 \\ g_u & g_v \end{bmatrix} \tag{3.6}$$

when $s = [u, v]$. This matrix clearly has real eigenvalues, $\lambda_1 = f_u$ and $\lambda_2 = g_v$ which at most points in the phase plane are different. Then our system is strictly hyperbolic with a finite number of points excepted. Since the eigenvalues are real, our system is never elliptic. Fully coupled systems generally may have some regions where they are elliptic, see [3] for further reading.

3.1.2 Parabolic systems

A system of the form

$$p_t = Bp_{xx} + Ap_x + Cp + F(x, t) \tag{3.7}$$

is parabolic if the eigenvalues of matrix B all have positive real parts. There are no restrictions placed on matrices A and C.

Equation (3.3) is of form (3.7) with C and F equal to zero. B is diagonal, $B_{ii} = \epsilon\ D'_{ii}$ for $i = 1, 2$, since the matrix D is diagonal. Then our system is parabolic as long as D'_{11} and D'_{22} are bounded away from zero (since ϵ is a positive number).

3.2 Corrected operator splitting

This is the method that will be used in this thesis. The presentation follows Natvig [18]. As noted in Section 3.1 some information about the flux may be lost in the advection step. We want to use this lost information in the diffusion step. In this way we hope to *correct* our solution.

Consider a scalar advection-diffusion equation,

$$u_t + f(u)_x = \epsilon d(u)_{xx}, \quad u_0 = u(x, 0), \tag{3.8}$$

and use operator splitting to solve it. First we solve the advection part, Equation (3.9), and then the diffusion part, Equation (3.10).

$$\begin{aligned} u_t + f(u)_x &= 0 && (3.9)\\ u_t &= \epsilon d(u)_{xx} && (3.10) \end{aligned}$$

If the solution of the advection equation develops shocks, it will in a neighbourhood of shock number i, the shock with left value u_i and right value u_{i+1}, satisfy

$$u_x + \sigma_i u_x = 0, \quad u_0 = \begin{cases} u_i & \text{for } x < x_i \\ u_{i+1} & \text{for } x > x_i \end{cases}. \tag{3.11}$$

For Equation (3.9) this means that the nonlinear flux function has been replaced by the linear flux term $\sigma_i u$. To reduce this splitting error we add a residual flux term,

$$f_{res,i}(u)_x = f(u)_x - \sigma_i u_x = f'(u)u_x - \sigma_i u_x, \tag{3.12}$$

to Equation (3.10). Using the chain rule we get:

$$f'_{res,i}(u)u_x = f'(u)u_x - \sigma_i u_x = (f'(u) - \sigma_i)u_x \Rightarrow f'_{res,i}(u) = f'(u) - \sigma_i. \tag{3.13}$$

Integrating and choosing constants equal to zero we get the residual flux,

$$f_{res,i} = f(u) - \sigma_i u. \tag{3.14}$$

This idea generalises to systems in the following way:

First, solve the hyperbolic conservation law as in Section 3.1. Let $\mathbf{s}(x, t) = \mathcal{H}(t)\mathbf{s}_0$ be the solution of the system

$$\begin{aligned} \mathbf{s}_t + \mathbf{f}(\mathbf{s})_x &= 0 \\ \mathbf{s}(x, 0) &= \mathbf{s}_0. \end{aligned} \tag{3.15}$$

For each shock in the solution of the advection equation, the solution will satisfy the linear transport equation

$$\mathbf{s}_t + \sigma_i \mathbf{s}_x = 0, \quad \mathbf{s}_0 = \begin{cases} \mathbf{s}_i & \text{for } x < x_i \\ \mathbf{s}_{i+1} & \text{for } x > x_i \end{cases} \tag{3.16}$$

locally (in time and space). We once again introduce a residual flux term to correct the error we make,

$$\mathbf{f}_{res,i} = \mathbf{f}(\mathbf{s}) - \sigma_i \mathbf{s}. \tag{3.17}$$

We define a region R_i,

$$R_i = (u_i, u_{i+1}) \times (v_i, v_{i+1}) \times (x_i - \delta, x_i + \delta), \tag{3.18}$$

where the residual flux exists. δ is a suitable restriction so that the residual flux is only used locally around the shock. We get a residual flux function for each shock and define the global residual flux function to be

$$\mathbf{f}_{res}(\mathbf{s}, x) = \sum_{i=1}^{n} \mathbf{f}_{res,i}(\mathbf{s}) \chi_{R_i}(\mathbf{s}, x) \tag{3.19}$$

where $\chi_{R_i}(\mathbf{s}, x) = \begin{cases} 1 & \text{if} \quad (\mathbf{s}, x) \in R_i \\ 0 & \text{else} \end{cases}$.

Then we solve the parabolic system with the residual flux term. Let $\mathbf{w}(x,t) = \mathcal{H}_{cos}(t)\mathbf{w}_0$ be the solution of the system

$$\begin{aligned} \mathbf{w}_t + \mathbf{f}_{res}(\mathbf{w}, x)_x &= \epsilon\, D(\mathbf{w})_{xx} \\ \mathbf{w}(x, o) &= \mathbf{w}(x, 0). \end{aligned} \tag{3.20}$$

We then have a hyperbolic and parabolic solution operator, $\mathcal{S}$ and $\mathcal{H}_{cos}$ correspondingly, for the corrected operator splitting approach. With these two operators we are able to write an approximation to the solution of system (3.1) as

$$\mathbf{s}(x, n\Delta t) \approx (\mathcal{H}_{cos}(\Delta t)\mathcal{S}(\Delta t))^n \mathbf{s}_0(x). \tag{3.21}$$

In Chapter 7 it is shown (numerically) that this approximation is better than the one in Section3.1. Note that the two methods coincide when $\mathbf{f}_{res} = 0$.

In Chapter 4 and 5 we construct a hyperbolic solution operator using front tracking and a Riemann solver. In Chapter 6 we construct two parabolic solution operators based upon explicit and implicit finite difference approximations.

Chapter 4

Riemann solver for the triangular system

In solving the advection equation the Riemann problem will be essential. The Riemann problem is a hyperbolic conservation law with piecewise constant initial data having only a single discontinuity located at $x = x_0$:

$$u_t + f(u)_x = 0 \quad \text{and} \quad u_0(x) = \begin{cases} u_L & \text{if} \quad x < x_0, \\ u_R & \text{if} \quad x > x_0. \end{cases} \tag{4.1}$$

In general u and f are vectors, and for convenience $x_0 = 0$ in this chapter.

Solutions of conservation laws are known to develop discontinuities. A more general solution concept is therefore needed. A differentiable function that satisfies the differential equation and the initial data is called a *classical* solution. The solutions of Equation (4.1) may develop shocks and are therefore no classical solution. A natural way to define a generalised solution of (4.1) that does not require differentiability, is to consider an integral form of the conservation law. Let $\phi \in C_0^1(\mathbf{R} \times \mathbf{R}^+)$, where $C_0^1(\mathbf{R} \times \mathbf{R}^+)$ is the space of functions that are continuously differentiable with compact support. If we multiply $u_t + f(u)_x = 0$ by $\phi(x,t)$ and then integrate over space and time, we obtain

$$\int_0^\infty \int_{-\infty}^\infty [\phi u_t + \phi f(u)_x] dx dt = 0. \tag{4.2}$$

Now integrating by parts yields

$$\int_0^\infty \int_{-\infty}^\infty [\phi_t u + \phi_x f(u)] dx dt + \int_{-\infty}^\infty \phi(x,0) u(x,0) dx = 0. \tag{4.3}$$

We are now in the position of defining a weak (or generalised) solution of 4.1.

Definition 1 (Weak solution) *The function $u(x,t)$ is called a weak solution of the conservation law (4.1) if for all $\phi \in C_0^1(\mathbf{R} \times \mathbf{R}^+)$ the equality (4.3) holds.*

This definition introduces a solution concept that allows discontinuous solutions, but not all kinds of discontinuities are accepted. One can show from the weak formulation

of the conservation law (4.2) that any discontinuity must satisfy what is called the Rankine-Hugoniot shock condition.

Theorem 1 (Rankine-Hugoniot shock condition) *u_L and u_R are the left and right values in the shock, and s is the shock speed. The shock is admissible if*

$$s = \frac{f(u_R) - f(u_L)}{u_R - u_L}, \tag{4.4}$$

where u and f in general are vectors.

The weak solution is generally not unique and an additional condition is required to pick out the correct physical solution. Hyperbolic conservation laws often arise in models where dispersive (diffusion) terms are ignored. For example, the parabolic equation

$$u_t + f(u)_x = \epsilon u_{xx}, \tag{4.5}$$

where ϵ is a small positive number, would often be a more exact description of the physics than the inviscid equation (4.1). Consistency of the models would then demand that solutions of the two equations are "close" in some sense, and in the limit as ϵ goes to zero, the solution of (4.5) should converge to the solution of (4.1). The requirement that the solution of (4.1) should be the limit solution to (4.5) is called the *entropy condition*. A weak solution satisfying the entropy solution is called an entropy (or entropy weak) solution. There are various forms of the entropy condition. The first to find an entropy condition for the scalar conservation law was Oleinik [19].

Theorem 2 (Oleinik's entropy condition) *The (piecewise smooth) weak solution is the entropy solution if all discontinuities (with shock speed s, and with left value u_L and right value u_R) satisfy the Rankine-Hugoniot shock condition, and in addition the entropy condition*

$$\frac{f(u) - f(u_L)}{u - u_L} \geq s \geq \frac{f(u) - f(u_R)}{u - u_R} \tag{4.6}$$

for all u between u_L and u_R.

4.1 Scalar Riemann problem

The scalar advection equation can be solved exactly for sufficiently simple flux functions. We will briefly investigate the nature of the solution using two different methods. The solutions are assumed to be classical, i.e., the derivates exist. However, the results carry over to non-classical solutions.

One approach is the method of characteristics. Using the chain rule the scalar conservation law is written as follows:

$$u_t + f(u)_x = \frac{\partial u}{\partial t} + \frac{\partial f}{\partial u}\frac{\partial u}{\partial x} = 0. \tag{4.7}$$

A characteristic is a curve in the x-t plane, $(x,t) = (x(\tau), t(\tau))$, that satisfies the following system of ordinary differential equations:

$$\frac{dt}{d\tau} = 1, \qquad \frac{dx}{d\tau} = f'(u). \tag{4.8}$$

Then using the chain rule to get

$$\frac{du}{d\tau} = \frac{\partial u}{\partial t}\frac{dt}{d\tau} + \frac{\partial u}{\partial x}\frac{dx}{d\tau} = \frac{\partial u}{\partial t} + \frac{\partial f}{\partial u}\frac{\partial u}{\partial x} = 0. \tag{4.9}$$

In other words, u is constant along the characteristic curve. The curve is given by:

$$x(\tau) = f'(u_0)\tau + x_0, \qquad t = \tau, \qquad \text{where } \; u_0 = u(x_0, 0). \tag{4.10}$$

Another approach is to search for self similar solutions to the Riemann problem. A solution is self similar if it only depends on the ratio x/t, i.e, $u(x,t) = u(x/t)$. Such solutions exist since if $t_1 = st$ and $x_1 = sx$, then

$$u_t + f(u)_x = s(u_{t_1} + f(u)_{x_1}) = 0. \tag{4.11}$$

Let $s = x/t$, and write $u(x,t) = u(s)$. Using the chain rule the scalar conservation law is rewritten as follows:

$$u'(s)\frac{\partial s}{\partial t} + f'(u)u'(s)\frac{\partial s}{\partial x} = u'(s)\frac{-x}{t^2} + f'(u)u'(s)\frac{1}{t} = 0. \tag{4.12}$$

Multiply with t and use that $x/t = s$ to get

$$(f'(u) - s)u'(s) = 0. \tag{4.13}$$

This equation is satisfied if $u(s)$ is constant or $f'(u) = s$. The last equality gives us $u(x,t) = (f')^{-1}(x/t)$. The solution is single valued only if $f'(u)$ is monotone, either increasing or decreasing. This is normally *not* the case. The lower and upper convex envelope of f , f_{cl} and f_{cu}, respectively, have monotone derivatives. Replacing f with a envelope will make the solution single valued.

There are two possible cases to consider:

1. $u_L < u_R$ and
2. $u_R < u_L$

We only look at case one. Case two is treated similarly.

We take the lower convex envelope, f_{cl}, of f. Looking carefully we see that taking this envelope, we satisfy the *entropy* condition. (We take the envelope between u_L and u_R.) In addition all shocks will satisfy the Rankine-Hugoniot condition.

In Figure 4.1 we see an upper envelope where $u_L = 1.0$ and $u_R = 0.0$, (a), and a lower envelope where $u_L = 0.0$ and $u_R = 0.4$, (b). The envelopes are dotted.

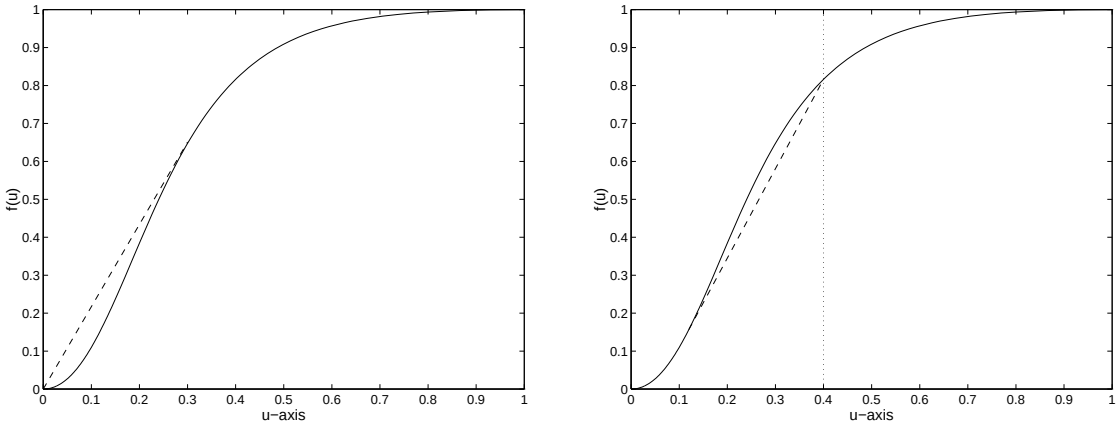

(a) Upper convex envelope of f

(b) Lower convex envelope of f

Figure 4.1: Convex envelopes for different Riemann problems.

Then we are able to write the solution for a general scalar Riemann problem as follows

$$u(x,t) = \begin{cases} u_L & \text{if} \quad x/t < s_L, \\ (f_c')^{-1}(x/t) & \text{if} \quad s_R < x/t < s_L, \\ u_R & \text{if} \quad x/t > s_R, \end{cases} \tag{4.14}$$

where we take the lower envelope if $u_L < u_R$ and the upper envelope if $u_R < u_L$. This is an entropy solution of the scalar Riemann problem since the solution satisfies Oleinik's entropy condition. If the solution is continuous, it is also a classical solution.

The solution will consist of *shocks* and *rarefraction waves*. (There will of course also be a constant state to the left and the right of the line $x/t = s_L$ and $x/t = s_R$, respectively, in the x-t plane.) Shocks are discontinuities in the solution. It arises when $f_c'(u)$ is constant on an interval. Rarefraction waves are continuous parts of the solution, and they arise when $f_c'(u)$ is not constant.

Usually it is not trivial to find $(f_c')^{-1}$. To do this we approximate f by a piecewise linear function f^Δ. Δ is the distance between node points where f is evaluated. Then $f_c^{\Delta\prime}$ is piecewise constant and $(f_c^{\Delta\prime})^{-1}$ easy to find. The solution of the Riemann problem with f^Δ instead of f consists of finitely many shocks. The shock speeds are increasing since the envelopes have derivatives that are monotone. Comparing the original solution with the solution from the linearised problem we see that the rarefraction waves are approximated with many small shocks. Approximating f gives us a solution that has the same form as the correct solution. Moreover, in the L^1-norm the solutions can be made arbitrary close, as stated in the theorem below. For further reading, see [20].

Theorem 3 (Lucier) *If f and h are Lipschitz continuous functions, u_0 and v_0 are of bounded variation, u and v are the solutions of*

$$\begin{array}{ll} u_t + f(u)_x = 0 \\ u(x,0) = u_0 \end{array} \qquad \textit{and} \qquad \begin{array}{ll} v_t + h(v)_x = 0 \\ v(x,0) = v_0, \end{array}$$

then for any $t > 0$*;*

$$\|u(t) - v(t)\|_{L^1} \leq \|u_0 - v_0\|_{L^1} + t\|f - h\|_{Lip} \min(\|u_0\|_{BV}, \|v_0\|_{BV})$$

u_0 and v_0 in the theorem are equal since we only consider the same Riemann problem with different flux functions f. It then follows from the theorem that we can get the solutions, u and v, as close as we want in the L^1-norm by making better approximations to f, see Figure 4.2. A result of this is that replacing f with a piecewise linear function is a reasonable approach when finding an approximative solution of the scalar Riemann problem. Notice that the linearised Riemann problem can be solved exactly.

The following example illustrates the linearising procedure. Let the Riemann problem be

$$f(u) = \frac{u^2}{(u^2 + (1-u)^2/10))} \quad \text{and} \quad u_0 = \begin{cases} 1 & \text{if } x < 0, \\ 0 & \text{if } x > 0. \end{cases} \tag{4.15}$$

Since $u_L > u_R$ we have to take the upper convex envelope to get the entropy solution.

In Figure 4.2 envelopes, flux functions and corresponding solutions for the Riemann problem (4.15) are shown. The envelopes are seen as dotted lines when they do not coincide with the flux functions, see Figure 4.2 (a),(c) and (e). In Figure 4.2 (b) we have the reference solution, computed using a forward-time backward-space finite difference scheme with small discretisation parameters. Then we linearised $f(u)$ using $\Delta u = 0.10$. The flux function and the solution are presented respectively in figure 4.2 (c) and (d). As expected the rarefraction waves are represented by small shocks and the original shock (in position $x \approx 0.85$) is preserved. If we linearise using $\Delta u = 0.25$, it is harder to recognise the original solution. In this case the flux function and the envelope coincide. In Figure 4.2 (e) and (f) we have the flux function and the solution.

4.2 Triangular Riemann problem

A triangular Riemann problem is a Riemann problem for a triangular system of hyperbolic conservation laws, see Section 2.4:

$$u_t + f(u)_x = 0 \tag{4.16}$$
$$v_t + g(u,v)_x = 0 \tag{4.17}$$

and

$$u_0 = \begin{cases} u_L & \text{if } x < x_0, \\ u_R & \text{if } x > x_0, \end{cases} \qquad v_0 = \begin{cases} v_L & \text{if } x < x_0, \\ v_R & \text{if } x > x_0. \end{cases} \tag{4.18}$$

To make the triangular Riemann problem easier to solve the class of functions considered is limited. Only flux functions f that are increasing in u with at most one inflection point are considered. Flux functions g are limited to functions that are increasing in v with at most one inflection point for each u, and that are strictly decreasing in u.

Motivated by the scalar Riemann problem, the flux functions are linearised. The resulting system is called a *linearised triangular Riemann problem*. The idea is that when making the approximation finer, linearising with more intervals, also the solution of the linearised system converges to the solution of the original system.

First we solve the scalar Riemann problem, Equation (4.16), with the flux function *linearised*. The solution consists, as shown in Figure 4.2 (c), of finitely many shocks u_i/u_{i+1} with shock speed s_i, $i = 1, \ldots, n$. ($u_1 = u_L$ and $u_{n+1} = u_R$.) All shock speeds are positive since only increasing flux functions are considered. In addition the shock speeds are finite since the flux function is continuous, and they form a strictly increasing sequence. (For convenience, let $s_0 = -\infty$ and $s_{n+1} = \infty$.)

Secondly Equation (4.17) is solved. There are two cases to consider:

1. $u_L < u_R$
2. $u_R < u_L$

We will only consider case 1. Case 2 is treated similarly.

Since $u_L < u_R$ and the solution of the scalar Riemann problem is monotone, we have $u_i < u_{i+1}$. We define $g_i(v) = g(u_i, v)$. Then $g_i(v) > g_{i+1}(v)$ since g is decreasing in u. In each region where u is constant ($u = u_i$, for some i), we consider only the scalar equations:

$$v_t + g(u_i, v) = v_t + g_i(v) = 0 \quad i = 1, \ldots, n \tag{4.19}$$

The equations are solved with the flux function linearised. In each region the solution is then found exactly. The global solution are found by linking the solutions from each region together. The state v_L must be connected with v_R, going through all the g-functions, i.e., all the u-regions. When we jump from g_k to g_{k+1}, i.e., from one region to

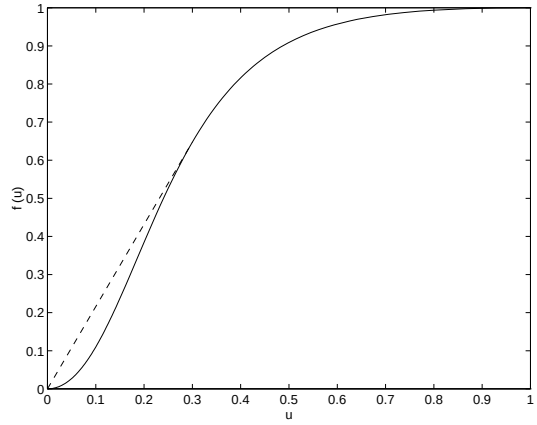

(a) Flux function

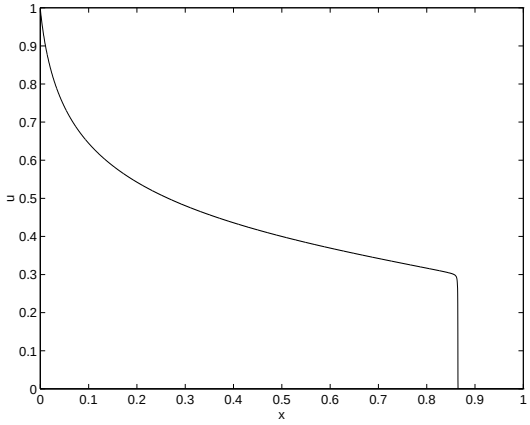

(b) Solution at t=0.4

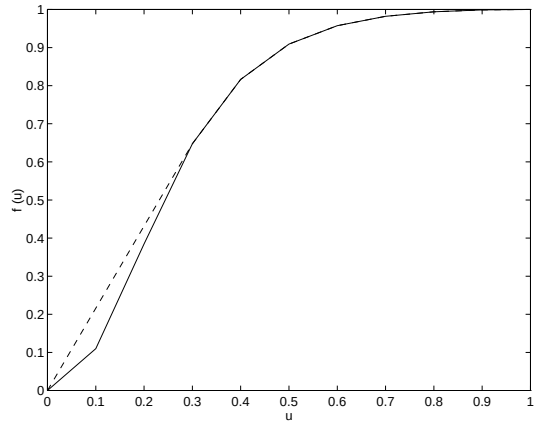

(c) Linearised flux function, Δu=0.10

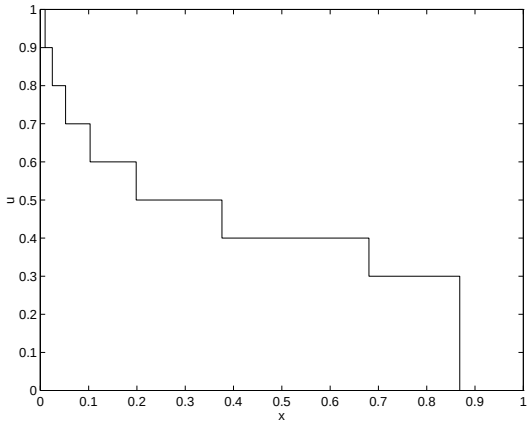

(d) Solution at t=0.4

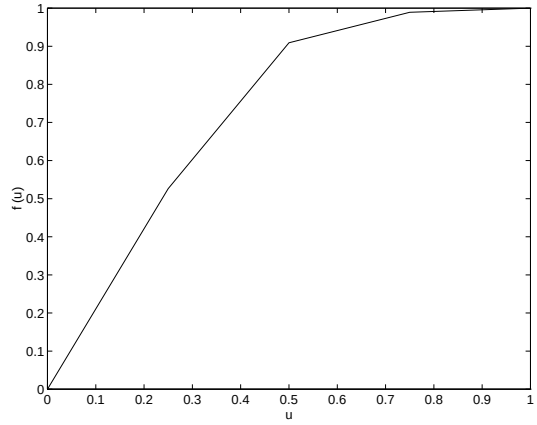

(e) Linearised flux function, Δu=0.25

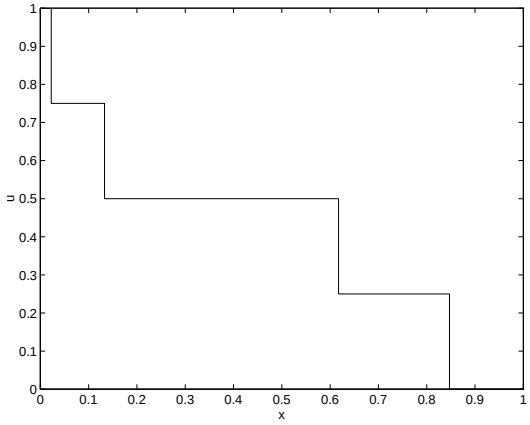

(f) Solution at t=0.4

Figure 4.2: Solutions of Riemann problem (4.15) with the original flux function and linearised flux functions.

the next, the only physical possibility is to have a shock with shock speed equal to s_i. If not, the solution will not be stable. In addition, the shocks from solving Equation (4.19) for some $i = k$ must have shock speeds s satisfying $s_{k-1} \leq s \leq s_k$ because the solution has to be in the correct region, i.e., $u = u_k$. This gives a restriction on possible v-values on each side of the u-shocks/discontinuities.

To keep track of admissible jumps *H-sets* are constructed, see Section 4.2.1.

The solution of the triangular Riemann problem may not exist even though the class of flux functions we consider already is limited. In [11] Gimse showed that:

Theorem 4 (Uniqueness and existence) *Let $f(u)$ be a piecewise linear Lipshitz continuous function and let $g(u, v)$ be a Lipshitz continuous function in v for each u with a uniformly bounded Lipshitz constant. Furthermore assume that*

$$f(0) = 0, \qquad f(1) = 1, \qquad g(u, 1-u) = 1 - f(u),$$

$$\frac{\partial g}{\partial v} \geq 0, \qquad \frac{\partial g}{\partial u} < 0, \qquad f'(u) \geq 0,$$

and that $f(\cdot)$ and $g(u, \cdot)$ have at most one inflection point. Then the solution of the triangular Riemann problem exists and is unique inside the phase plane $0 \leq u + v \leq 1$, $u \geq 0$ and $v \geq 0$.

g is piecewise linear and finite, and therefore Lipshitz continuous. The five last conditions are satisfied for the class of flux functions that we consider. If in addition the three first are satisfied, then the Riemann problem has a unique solution by Theorem 4. Moreover, the solution is exact since only linearised scalar Riemann problems are solved and they can be solved exactly.

We will now give the physical meaning of the conditions in the theorem. f has to be an increasing function of u with at most one inflection point. Thus the gravity part of the flux function f must be excluded. g has to be an increasing function of v with at most one inflection point for each u. Thus also the gravity part of the flux function g must be excluded. Then flux functions f and g only consist of advection terms. See Section 7.3 for treatment of the case where gravity terms are included in the flux functions. In addition g has to be a decreasing function in u. That is the water saturation decreasing if the gas saturation increases. Generally this is not the case since the flow of the third phase, oil, has to be taken into account. If the gas saturation increases, then either the water saturation or the oil saturation or both saturations decreases. Thus g being a decreasing function in u limits the class of functions that Theorem 4 is applicable to.

As stated above the flux functions must consist of the advection terms only, i.e., $f(u) = \lambda_g/\lambda_t$ and $g(u, v) = \lambda_w/\lambda_t$. Thus the two first conditions in the theorem is trivially satisfied because of the properties of the mobilities. The third condition is not straight forward. If the system originally was triangular, the properties of the mobilities insure us that the third condition always is satisfied. See Equation (4.20) with $f(u, v)$ replaced with $f(u)$ for justification. However, if the system is made triangular by modifying a fully coupled system, the condition is generally not satisfied. The system is modified by replacing $f(u, v)$ with $f(u, v_0)$ as suggested by the Norm condition, see Section 2.4.

($f(u, v_0)$ is set equal to $f(u)$ in the triangular system.) The following argument will illustrate the problem:

Let $f(u, v)$ be the fractional flow function from the fully coupled system. In addition let $w = S_o$ and $h(u, v) = \lambda_o/\lambda_t$ be the fractional flow function for the oil phase. The total fractional flow is one, i.e, $f(u, v) + g(u, v) + h(u, v) = 1$. If $v = 1 - u$, then $w = 1 - u - v = 0$. Thus $\lambda_o = 0$ and $h(u, 1 - u) = 0$. Then

$$1 - g(u, 1 - u) = f(u, 1 - u) + h(u, 1 - u) = f(u, 1 - u) \tag{4.20}$$

for all u in the phase plane. Now $f(u, v)$ is replaced with $f(u, v_0)$ making the model triangular. Let u_0 be the only u such that $v_0 = 1 - u = 1 - u_0$. Generally $f(u, 1 - u) \neq f(u, v_0)$ for all u in the phase plane except u_0. It follows that $1 - g(u, 1 - u) \neq f(u, v_0)$, and the condition in theorem 4 is not satisfied. The resulting triangular model will be in-physical. If $f(u, 1 - u) < f(u, v_0)$, then the total fractional flow for the triangular system is larger than one since

$$\begin{aligned} f(u, v_0) + g(u, 1 - u) + h(u, 1 - u) &> f(u, 1 - u) + g(u, 1 - u) + h(u, 1 - u) \\ &= f(u, 1 - u) + g(u, 1 - u) = 1. \end{aligned}$$

If $f(u, 1 - u) > f(u, v_0)$, then the fractional flow for the oil phase is greater than zero even though the oil saturation is zero. It follows from the fact that

$$h(u, 1 - u) = 1 - f(u, v_0) - g(u, 1 - u) > 1 - f(u, 1 - u) - g(u, 1 - u) = 0.$$

This ends the argument.

However, for some functions the third condition in Theorem 4 can be satisfied by choosing the right v_0, see section 7.2.

Altogether the class of functions that Theorem 4 is applicable to is very limited. However, this is no problem to us since in the construction of the H-set in Section 4.3 we will for simplicity only consider this class. The construction is possible for more general flux functions, but is then much more complicated. Osnes [13] has shown the same result as in Theorem 4 for a wider class of flux functions:

Theorem 5 (Uniqueness and existence) *Let $f(u)$ and $g(u, v)$ be continuous functions. Assume that*

$$f(1) = 1, \qquad f(0) = g(u, 0) = 0 \quad \textit{and} \quad g(u, 1 - u) = 1 - f(u).$$

Then the solution of the triangular Riemann problem exists and is unique inside the phase plane $0 \leq u + v \leq 1$, $u \geq 0$ and $v \geq 0$.

The major difference in the two theorems is that Osnes does not put any constraints on the derivatives of the flux functions. It follows that Theorem 4 is a special case of Theorem 5.

Holden and Høegh-Krohn [21] have shown existence and uniqueness (except for sets with zero measure), for $N \times N$ triangular Riemann problems with weaker conditions than Gimse. If $N < 3$ there is always uniqueness (as in Theorem 4).

4.2.1 H-sets

We define two kinds of H-sets:

1) $H_{i,in}$: The set of v-values in region $u = u_i$ that can be reached from $H_{i,out}$ or v_L for $i = 1$.

2) $H_{i+1,out}$: The set of v-values in region $u = u_{i+1}$ that can be reached from $H_{i,in}$ by a shock with speed s_i.

In the following a point $(v, g_i(v))$ on the graph of g_i, will be denoted by its abcisse-value, v.

The H-sets are constructed recursively on basis of this definition. The i and $i+1$ refer to the g-functions or regions. $H_{i,in}$ and $H_{i+1,in}$ is admissible v-values to the left and right, respectively, of the u_i/u_{i+1}-shock. An example is given in Figure 4.3 for the two first H-sets. The H-sets are marked with solid lines below the graph. We notice that the endpoints of g_1 and g_2 are connected with a line with slope equal to s_1.

The construction of the H-sets goes as follows:
First we construct $H_{1,in}$. We start on g_1 and find all the v-values that can reach v_L with shock speed(s) less than s_1. (There may be intermediate values, and they must also be reached with shock speed less than s_1.) These values form $H_{1,in}$. Then we can find the rest of the H-sets recursively. Next we find the v-values on g_2 where we may jump to the v-values in $H_{1,in}$ with shock speed s_1. These values form $H_{2,out}$. $H_{2,in}$ is the set of v-values that can be reached from $H_{2,out}$ with shock speed(s) less than s_2 and greater than s_1. We continue until we have found $H_{n+1,out}$. Then all the H-sets are constructed. To find the H-sets a *H-set finder* was implemented, see Section 4.3.

We notice that the H-sets depend on the solution from the scalar equation, the u_i's, and on v_L. The construction is independent of v_R. So Riemann problems where you change only v_R are solved using the same H-sets.

4.2.2 Construction of the solution

To construct the solution of the linearised triangular Riemann problem, start at v_R and go through the g-functions to v_L. There are two possibilities:

1. $v_R \in H_{n+1,out}$
2. $v_R \notin H_{n+1,out}$

In Case 1 we may go straight ahead to track the solution. In Case 2 v_R must be connected to $H_{n+1,out}$ with shock speeds greater than s_n.

We are now in $H_{n+1,out}$ and may, by definition, jump to $H_{n,in}$. Then we can reach $H_{n,out}$ with an admissible jump, by the definition of the H-sets. We continue like this until we reach $H_{1,in}$. There are two possibilities:

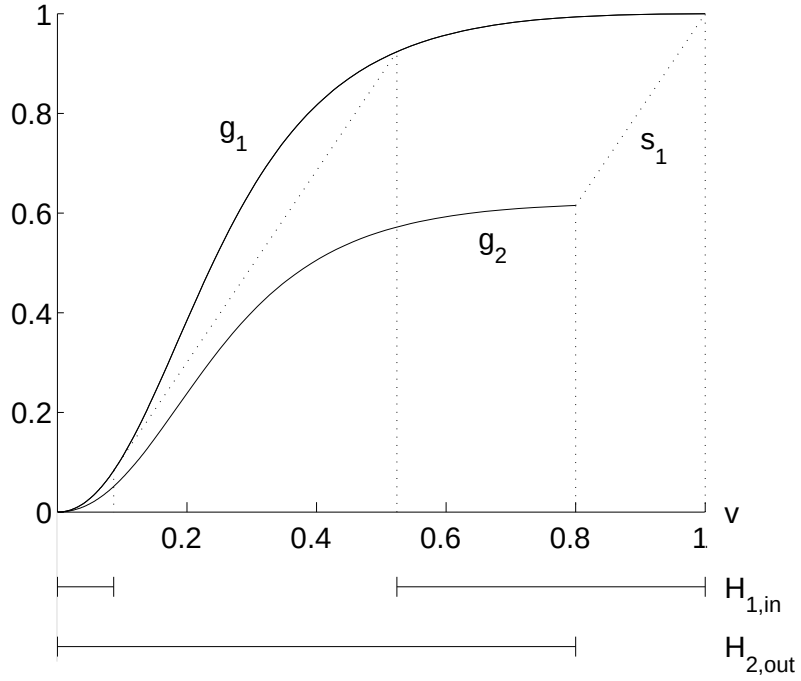

Figure 4.3: $H_{1,in}$ and $H_{2,out}$ when $u_1 = 0.0$, $u_2 = 0.175$, $s_1 = 1.92$ and $v_L = 0.0$

1. We have landed on v_L
2. We have not landed on v_L

In Case 1 the construction is finished. In Case 2 we can reach v_L with an admissible jump, once again by the definition of the H-sets, and the construction is finished. The general solution can be be written as follows:

$$(u_L, v_L) \xrightarrow{s_{1*}} (u_L, v_2) \xrightarrow{s_1} (u_2, v_3) \ldots \xrightarrow{s_{(n-1)*}} (u_{n-1}, v_{m-2}) \xrightarrow{s_n} (u_R, v_{m-1}) \xrightarrow{s_{n*}} (u_R, v_R)$$

where $m \geq n$, $v_R = v_m$ and s_{i*} denotes a possible front, shock or approximated rarefraction wave, in region i, i.e., a solution of Equation (4.19). The solution is an entropy solution. In addition the solution is exact for the linearised triangular Riemann problem.

The following example illustrates the procedure. As flux functions we use $f(u)$ from Section 4.1 and

$$g(u, v) = \frac{((1-u)^2 + u^2/10)v^2}{(10u^2 + (1-u)^2)(v^2 + (1-v)^2/10)} \tag{4.21}$$

Initial condition: $u_0 = v_0 = \begin{cases} 0.4 & \text{if } x < 4 \\ 0.2 & \text{if } x > 4 \end{cases}$

To solve the scalar equation we linearise using $\Delta u = 0.1$. The solution then is two shocks with shock speed s_1 and s_2:

$$u_L \quad \xrightarrow{s_1=1.69} \quad u_2 = 0.3 \quad \xrightarrow{s_1=2.63} \quad u_R \tag{4.22}$$

We then solve the coupled equation using the H-sets and get the solution (symbolically):

$$\begin{aligned}(0.4, 0.4) \quad &\xrightarrow{0.32} \quad (0.4, 0.30) \quad \xrightarrow{0.50} \quad (0.4, 0.20) \quad \xrightarrow{0.54} \quad (0.4, 0.11) \\ &\xrightarrow{s_1=1.69} \quad (0.3, 0.14) \quad \xrightarrow{s_2=2.63} \quad (0.2, 0.2)\end{aligned} \tag{4.23}$$

It is worth noticing that s_{1*} in this example denotes the three shocks with shock speed $0.32, 0.50$ and 0.54.

In Figure 4.4 flux functions g_1, g_2 and g_3 are shown. From the figure it follows that all points on g_i have slope less than s_i $(i = 1, 2)$ and all points on g_3 have slope less than s_2. Thus the H_{out}-sets for this Riemann problem are

$$H_{2,out} = [0, 1 - u_2] = [0, 0.7] \quad \text{and} \quad H_{3,out} = [0, 1 - u_3] = [0, 0.8].$$

Then all v_R is in $H_{3,out}$, especially $v_R = 0.4$, and the next v-value, v', in the solution is found jumping down from g_3 to g_2 with slope s_2. All v' are in $H_{2,out}$ and the next v-value, v'', is found jumping down from g_2 to g_1 with slope s_1. v'' is in $H_{1,in}$ by definition of the H-set, and the rest of the solution is found taking an upper envelope between v'' and v_L (since $v'' < v_L$). The construction is shown in Figure 4.4. We see that the endpoints of the flux functions g_i and g_{i+1} are connected with a line having shock speed s_i as slope $(i = 1, 2)$, as required by Theorem 4.

Having constructed this solution we can find the solution at any time just multiplying the shock speeds with the given time and adding this number to the position of the Riemann problem. In Figure 4.5 below we see the solution at $t = 0.4$ in the $u/v - x$ plane. It is apparent how we had to solve a scalar equation for v in each region; in region 1 (u_L) the solution is "continuous" solution, in region 2 and 3 (u_2 and u_R correspondingly) the solution is a shock.

In Figure 4.6 we see the same solution in the $x-t$ plane. u- and v-regions divided by solid and dotted lines, respectively. There are three regions where u is constant. In the first region we once again see that the solution in v contains several shocks, approximating a rarefraction wave.

4.3 H-set finder

In this section we will assume that the flux function $g(u, \cdot)$ always has one inflection point in the phase plane despite the fact that Theorem 4 only requires the function to have *at most* one inflection point. Assuming this, all functions $g(u, \cdot)$ will be S-shaped. We will also require that $g_{vv} > 0$ to the left of the inflection point, v_{ip}. In Figure 4.7 a typical flux function is illustrated together with $H_{1,in}$. See Appendix B for the case when the inflection point does not exist.

A H-set consist of two or less intervals and a possible midpoint and is written as follows:

$$H_{i,x} = [0, v_{i,x,l}] \cup v_{i,x,m} \cup [v_{i,x,r}, 1 - u_i],$$

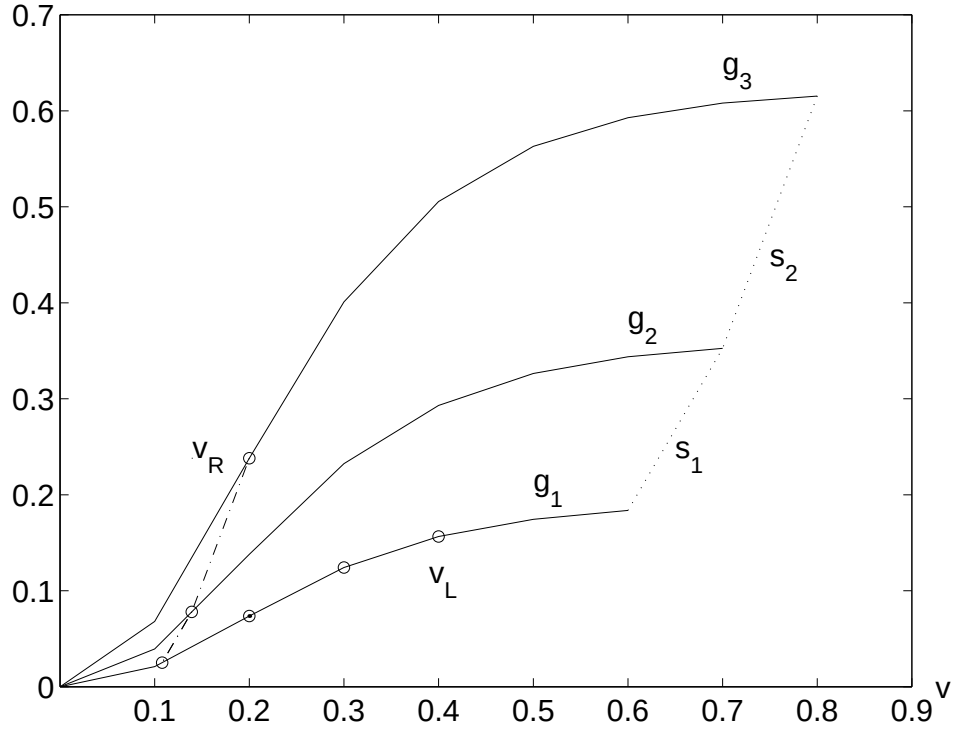

Figure 4.4: Solution for v in the triangular Riemann problem constructed using H-sets with $u_1 = 0.4$, $u_2 = 0.3$ and $u_3 = 0.2$.

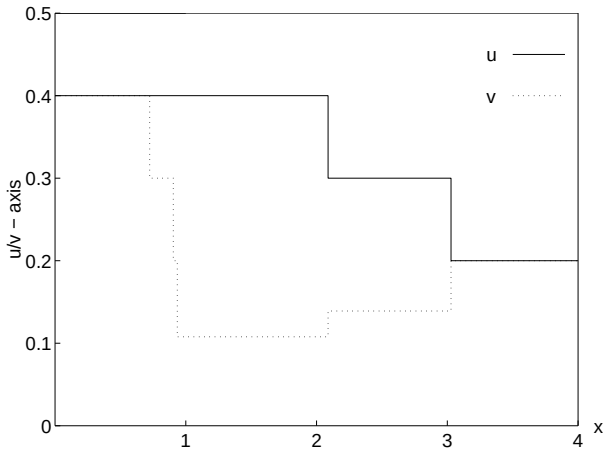

Figure 4.5: Solution of the triangular Riemann problem at time $t = 0.4$

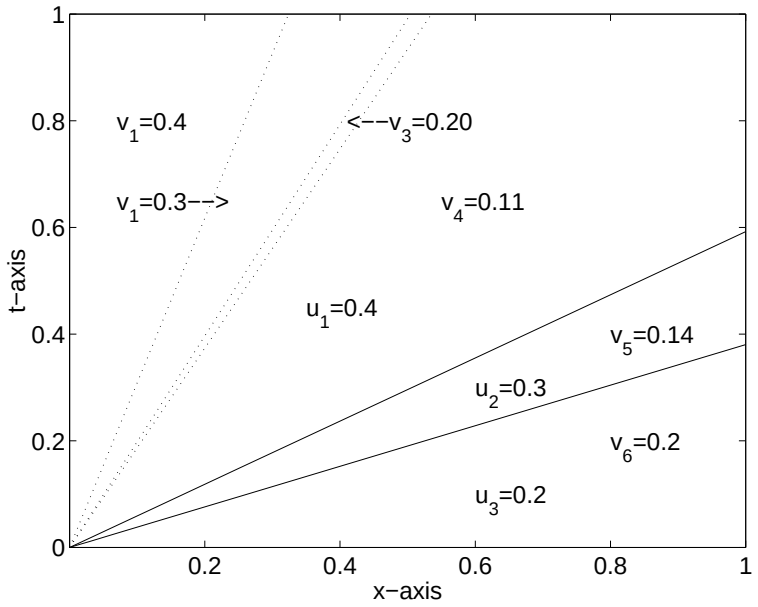

Figure 4.6: Solution in the x-t plane

where $v_{i,x,l}$, $v_{i,x,m}$ and $v_{i,x,r}$ determine the set uniquely. x is either *out* or *in*. The right interval goes only to $1-u_i$ since we have to be inside the phase plane. If $H_{i,x} = [1-u_i]$, then we set $v_{i,x,l}$ equal to $(1-u_i)$ and $v_{i,x,r}$ equal to 0.

In Figure 4.7 $H_{1,in}$ is illustrated together with a typical flux function. $H_{1,in}$. The solid line below the v-axis is $H_{1,in}$, and we see that $v_{1,in,l}$ and $v_{1,in,r}$ determine the set uniquely.

In all figures the dotted vertical lines connect the actual points on the graph with the values on the v-axis. The dotted secant lines illustrate how the sets are constructed . Since the triangular Riemann problem is linearised, it is possible to find all H-sets exact. However, to make the illustrations clearer the flux functions are not linearised in the figures. Except for Figure 4.7 we will not draw the H-sets as solid lines below the v-axis, but only mark the endpoints and possible midpoints of the sets on the v-axis.

In the following a point $(v, g_i(v))$ on the graph of g_i, will be denoted by its abcisse-value, v. In addition we must keep in mind that all values have to be in the phase plane: $u+v \leq 1, u \geq 0, v \geq 0$. *So when a point is said to not exist, either it does not exist or it is outside the phase plane.*

In the implementation of the H-set finder there are two important procedures:

1. Slope$(i, s, bool)$
The procedure takes three inputs: An index i to indicate which g-function we are on, a shock speed s and a boolean variable[1] which tells what direction to seek along. **Slope** seeks for a point on the flux function g_i with tangent equal to s. It returns the v-value if such a point exist, otherwise it returns -1.

[1]A boolean variable is a variable taking only two values, namely 0 and 1.

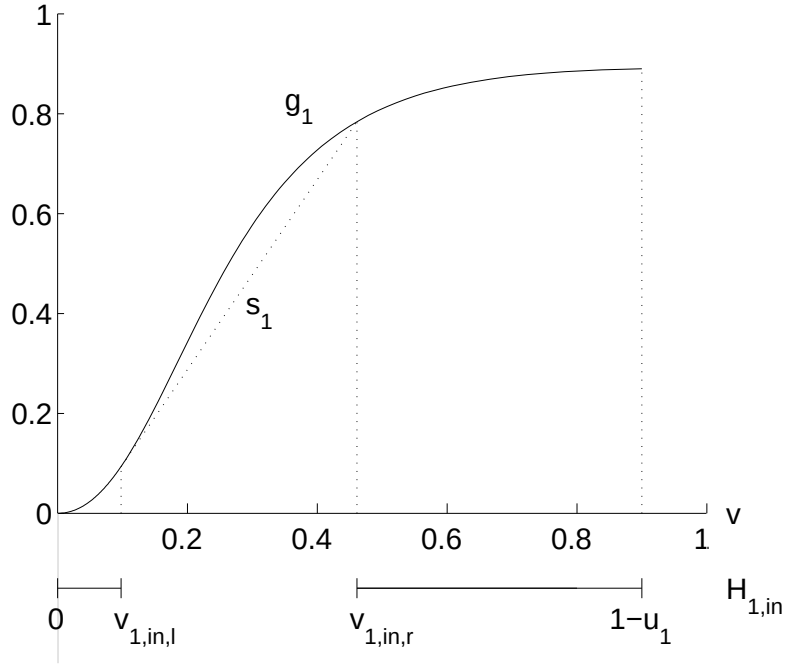

Figure 4.7: Illustration of $H_{1,in}$ in the case $u_1 = 0.1$, $v_L = 0.0$ and $s_1 = 1.9$.

2. Cut$(fr, to, v_0, s, bool)$
The procedure takes five inputs: An index fr to indicate which g-function we are jumping from, an index to to indicate which g-function we are landing on, a point v_0 to start from, a shock speed s and a boolean variable to tell what direction to seek along. **Cut** searches for an intersection between the line $s(v-v_0)+G$, where $G = g_{fr}(v_0)$, and the flux function g_{to}.**Cut** returns the point if it exists, otherwise it returns -1. The line $s(v - v_0) + G$, is the line from the point v_0 on g_{fr} with slope s.

Each time a cutting point or a point with a certain tangent is to be found, these procedures are invoked. Since the flux functions are linearised, the procedures provide an exact answer in reasonable time (if the linearisation is not too fine).

Remark 1:

In the program that solves the advection equations the flux function f is stored as a vector and g is stored as matrix. The vector contains the value of f at each node u_i and therefore defines the linearised flux function f. The matrix contains the node values of the linearised g_i's in each row, where $g_i = g(u_i, v)$. This data is static through the program to minimise runtime. It follows that the linearisation is chosen independent of the initial value problem. We will in the following assume that u_L and u_R are node points. If they were not we could just add the needed node values in the f-vector and the corresponding rows in the g-matrix. See Remark 2 in the end of Section 7.1 for further

discussion of this matter.

4.3.1 Finding $H_{1,in}$

$H_{1,in}$ consists of all the points that can be reached from v_L with a jump with shock speed less than (or equal to) s_1. First **Slope** is used to find all points on g_1 with tangent equal to s_1. There are three possibilities:

1. There are two tangent point, t_l and t_r.
2. There is one tangent point, t.
3. There are no tangent points, and the tangents are everywhere less than the shock speed.

Case 1: Two tangent points

In this case there are once again three possibilities:

1.1 v_L is less than or equal to the left tangent point, t_l.

1.2 v_L is larger than or equal to the right point of tangency, t_r.
Treated similarly as case 1.1.

1.3 v_L is in the interval defined by the two tangent points.

Subcase 1.1: $v_L \leq t_l$
All points to the left of t_l can be reached from v_L with speed less than s and are part of $H_{1,in}$. Thus, $v_{1,in,l}$ is equal to t_l. Then the cutting point c on g_1 is found by cutting from t_l to the right with slope s_1. Points to the right of the cutting point c has shock speed less than s_1 and are part of $H_{1,in}$, see Figure 4.8 (a). Thus, $v_{1,in,r}$ is equal to c. On the other hand, if c does not exist,i.e., the line does not cut, $v_{1,in,r}$ does not exist either, see Figure 4.8 (b).

In Figure 4.8 (a) and (b) v_L is equal. Despite this $v_{1,in,l}$ (equal to t_l) is different since the shock speeds are different. Furthermore, the cutting point and then also $v_{1,in,r}$, does not exist in Figure 4.8 (b) because the shock speed is too small. This illustrates the dependence on the shock speed s_1.

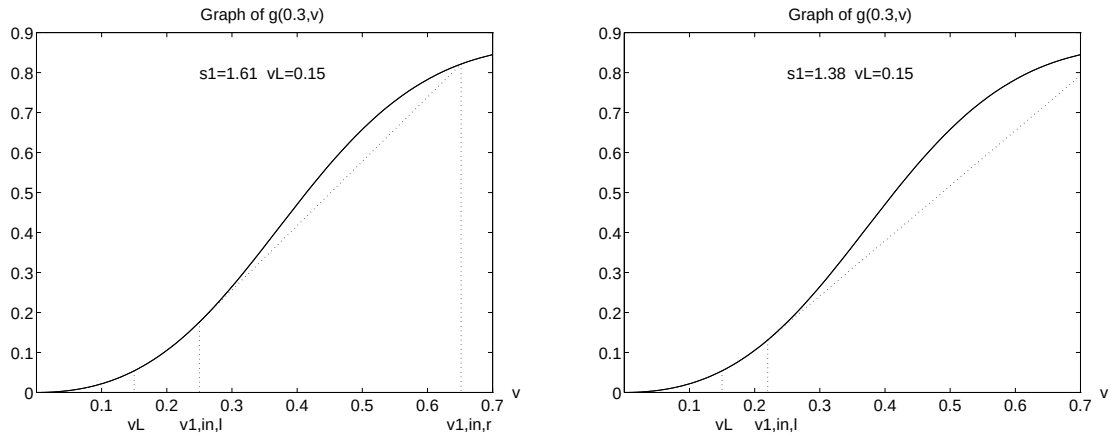

(a) $v_{1,in,r}$ exists.

(b) $v_{1,in,r}$ does not exist.

Figure 4.8: Finding $H_{1,in}$ in Subcase 1.1.

Subcase 1.3: $v_L \in (t_l, t_r)$
First, the left and the right cutting point, c_l and c_r, is found by cutting from v_L both to the left and right with s_1 on g_1. If the cutting points exist, $v_{1,in,l}$ and $v_{1,in,r}$ is equal to c_l and c_r, correspondingly, see Figure 4.9 (a). Sometimes only one or even none of the cutting points exist, see Figure 4.9 (b). In this case we always get a midpoint, $v_{1,in,m}$, equal to v_L.

Figure 4.9 illustrates the construction of $H_{1,in}$ when v_L is between the two tangent points. $v_{1,in,l}$ and $v_{1,in,r}$ is found by cutting to the left and right from v_L with s_1. As Figure 4.9 (b) shows, one (or even both) the cutting points might not exist if s_1 is too small.

Case 2: One tangent point

There are two possibilities:

2.1 The tangent point, t, is equal to the inflection point, v_{ip}.

2.2 The tangent point, t, is equal to the left point of tangency, t_l.

Subcase 2.1: t equal to v_{ip}.
If t is equal to v_{ip}, then all points can be reached with shock speeds less than s_1 since all points except v_{ip} has tangent less than s_1. Thus $H_{1,in} = [0, (1 - u_1)]$. There is no midpoint.

Subcase 2.2: t equal to t_l.
If t is equal to t_l, then the right point of tangency is not found because it is outside the phase plane. This case is treated as Case 1 with t_r equal to infinity.

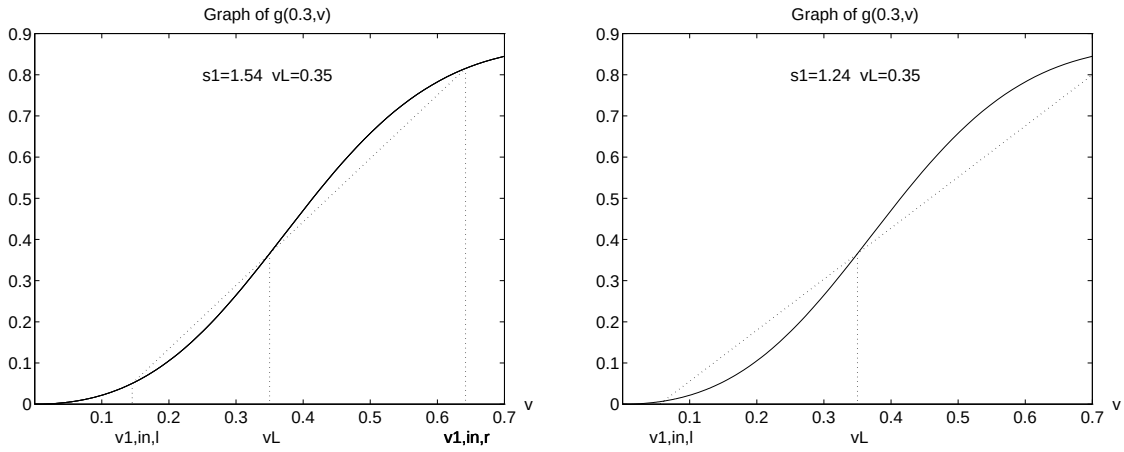

(a) Both $v_{1,in,l}$ and $v_{1,in,r}$ exist.

(b) Only $v_{1,in,l}$ (and $v_{1,in,m}$) exist.

Figure 4.9: Finding $H_{1,in}$ in Subcase 1.3.

Case 3: No tangent points

In case 3 all points can be reached with shock speeds less than s_1, and $H_{1,in} = [0, (1-u_1)]$. Then we set $v_{1,in,l}$ equal to $(1 - u_L)$ and $v_{1,in,r}$ equal to 0. There is no midpoint.

Decreasing and increasing sequences of u-shocks.

When finding all H-sets, except for $H_{1,in}$, there are two general cases:

1. $u_i < u_{i+1}$, u-shocks form an increasing sequence.
2. $u_i > u_{i+1}$, u-shocks form a decreasing sequence.

In the next subsections we will only consider Case 1, an increasing sequence.
Case 2 can be treated similarly.

From the conditions we put on $g(u, v)$ it follows that $u_i < u_{i+1} \Rightarrow g_i(v) > g_{i+1}(v)$. Geometrically this is g_i lying above g_{i+1}.

Observation 1

We have that $g_i(0) = 0$ for $i = 1, \ldots, n+1$, i.e., the flux functions are connected in the origin. This implies that if $v_{i,in,l}$ exists then $v_{i+1,out,l}$ also exists. This is the case since we always can do null-jumps[2]. The opposite is not always true.

The endpoints of g_i and g_{i+1} are connected with a straight line with slope s_i.
Proof:
Let $g_i(v) = g(u_i, v)$ as earlier defined. In addition g satisfies
$g(u, 1-u) = 1 - f(u)$. *Then*

$$\frac{g_{i+1}(1-u_{i+1}) - g_i(1-u_i)}{(1-u_{i+1}) - (1-u_i)} = \frac{(1-f(u_{i+1})) - (1-f(u_i))}{u_i - u_{i+1}} = \frac{f(u_i) - f(u_{i+1})}{u_i - u_{i+1}} = s_i.$$

■

This implies that if $v_{i,in,r}$ exists then $v_{i+1,out,r}$ also exists. The point $(1-u_{i+1})$ can always be reached from $(1-u_i)$ with shock speed s_i, and $(1-u_i)$ must be in $H_{i,in}$ since $v_{i,in,r}$ exists.

4.3.2 Finding $H_{i+1,out}$

Assume that $H_{i,in}$ is known, consisting of two or less intervals and possibly a midpoint. $H_{i+1,out}$ is the points on g_{i+1} that can be reached with a jump with speed s_i from $H_{i,in}$. There are three cases:

1. $v_{i,in,r}$ exists.
2. $v_{i,in,r}$ does not exist, but $v_{i,in,l}$ does.
3. Only $v_{i,in,m}$ exists.

Case 1: $v_{i,in,r}$ exists.

First the right point on g_{i+1} with tangent s_i is found, that is t_r. If t_r does not exist, we may jump from all points on $g_{i+1} \Rightarrow v_{i+1,out,l} = 1 - u_{i+1}$ and $v_{i+1,out,l} = 0$. Then the cutting point c between the line starting at $v_{i,in,r}$ with slope s_i and g_{i+1}, cutting down (to the left) is found. There are two possibilities:

1.1 $c < t_r$ or c does not exist.

1.2 $c > t_r$.

[2] A jump from zero to zero.

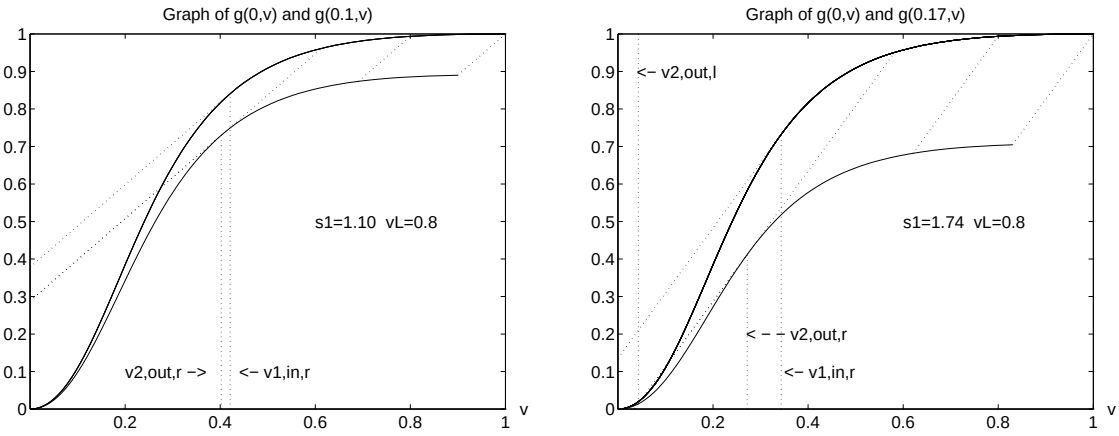

(a) Neither c nor c' exists.

(b) c' exists when c does not.

Figure 4.10: Finding $H_{2,out}$ in Subcase 1.1. Jumping down from g_1 to g_2.

Subcase 1.1: $c < t_r$ or c does not exist.
Then $v_{i+1,out,r}$ is equal to t_r, and $v_{i+1,out,l}$ is equal to the cutting point, c', between the line starting at t_r with slope s_i and g_{i+1}, cutting down. The construction is independent of the existence of $v_{i+1,out,l}$.

In Figure 4.10 (a) and (b) the cutting point c found by cutting from $v_{1,in,r}$ down to g_2 with s_1 does not exist. $v_{1,in,l}$ does not exist either, but this does not matter since the construction in this case is independent of $v_{1,in,l}$. The right tangent point on g_2 is equal to $v_{2,out,r}$. Cutting from $v_{2,out,r}$ to the left (on g_2) with s_1 we find c' which is equal to $v_{2,out,l}$ when it exists. In Figure 4.10 (a) $v_{2,out,l}$ does not exist and in (b) it exists.

Subcase 1.2: $c > t_r$.
In this case $v_{i+1,out,r}$ is equal to c. If $v_{i,in,l}$ exists (and possibly $v_{i,in,m}$), then $v_{i+1,out,l}$ and $v_{i+1,out,m}$ is equal to the cutting point between the line starting at $v_{i,in,l}$ with slope s_i and g_{i+1}, cutting down and up, respectively. If only $v_{i,in,m}$ exists, then $v_{i+1,out,m}$ is equal to the cutting point between the line starting at $v_{i,in,m}$ with slope s_i and g_{i+1}, cutting up. $v_{i+1,out,l}$ does not exist. Examples with $i = 1$, are shown in Figure 4.11 and 4.12.

Figure 4.11 and 4.12 are almost similar. They illustrate the important point that as long as $v_{1,in,l}$ exists the construction of $H_{2,out}$ is independent of $v_{1,in,m}$. The points are found just by cutting with s_1 down *and* up from $v_{1,in,l}$, and down from $v_{1,in,r}$. Notice that to simplify the figure the points $v_{1,in,l}$ and $v_{2,out,l}$ are excluded from Figure 4.12 (a). The two points are shown in the enlarged Figure 4.12 (b).

Case 2: $v_{i,in,r}$ **does not exist, but** $v_{i,in,l}$ **does.**

We know that $v_{i+1,out,r}$ does not exist, by Observation 1, since $v_{i,in,r}$ does not exist . $v_{i+1,out,l}$ and $v_{i+1,out,m}$ are equal to the cutting points between the line starting at $v_{i,in,l}$ with slope s_i, and g_{i+1}, cutting down and up, respectively. This is independent of the

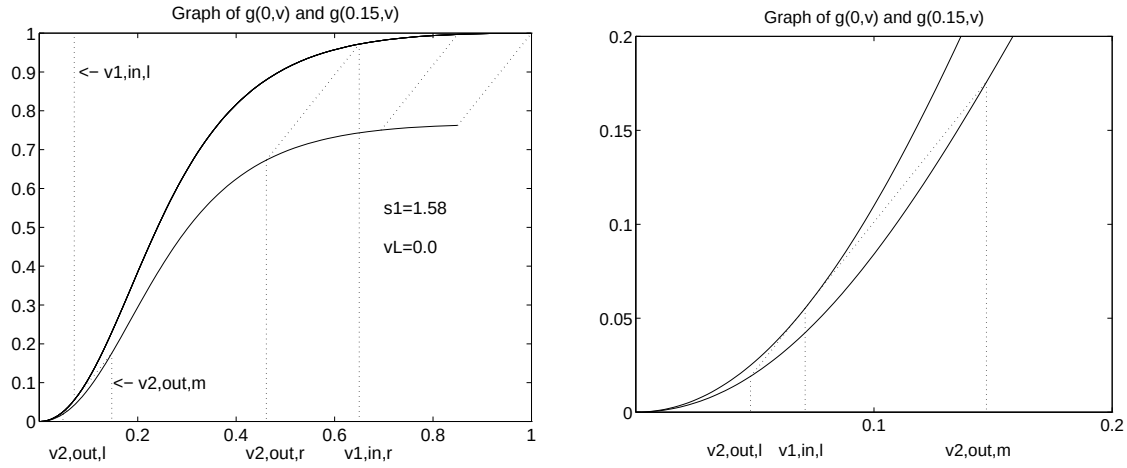

(a) $v_{1,in,m}$ does not exist.

(b) Figure 4.11 (a) enlarged.

Figure 4.11: Finding $H_{2,out}$ in Subcase 1.2. Jumping down from g_1 to g_2.

existence of $v_{i,in,m}$ since $v_{i,in,m}$ and $v_{i,in,l}$ lie on a line with slope s_i when they exist, see Observation 2. An example for $i = 1$ is shown in Figure 4.13 (a).

Case 3: Only $v_{i,in,m}$ exists

It is obvious that we get $v_{i+1,out,m}$ equal to the cutting point between the line starting at $v_{i,in,m}$ with slope s_i and g_{i+1}, cutting up (to the right). No other points exist. See Figure 4.13 (b) for illustration, $i = 1$.

In Figure 4.13 (a) $v_{2,out,l}$ and $v_{2,out,m}$ are found simply by cutting up and down from $v_{1,in,l}$ with s_1. To make the figure readable the axes had to be scaled. In Figure 4.13 (b) only $v_{1,in,m}$ exists and $v_{2,out,m}$ is found by cutting up from $v_{1,in,m}$ with s_1.

Observation 2

Assume that the points $v_{i,in,l}$, $v_{i,in,m}$ and $v_{i,in,r}$, when they exist, lie on a line with slope s_i. This is certainly the case for $i = 1$, and we will in the next section see that it is always true. When we construct $H_{i+1,out}$, we just cut from these points with the same slope (s_i) as when we constructed $H_{i,in}$, thus, the points $v_{i,out,l}$, $v_{i,out,m}$ and $v_{i,out,r}$ also lie on a line with slope s_i, when they exist.

4.3.3 Finding $H_{i+1,in}$

Assume that $H_{i+1,out}$ is known. To construct $H_{i+1,in}$, we have to find the points on g_{i+1} that can be reached with a jump from $H_{i+1,out}$ with shock speed s less than s_{i+1} and greater than s_i. In [11] it is shown that $H_{i+1,out} \subset H_{i+1,in}$ which implies that

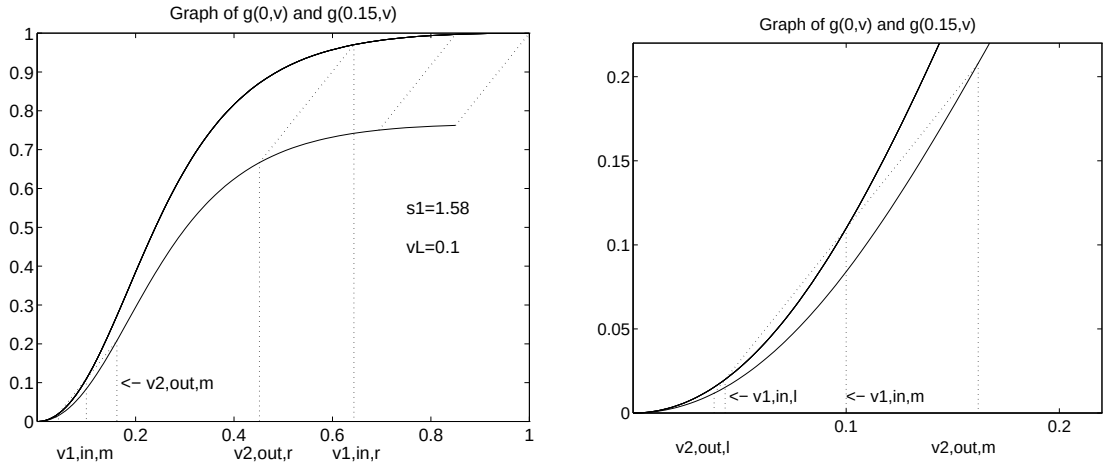

(a) Both $v_{1,in,l}$ and $v_{1,in,m}$ exist.

(b) Figure 4.12 (a) enlarged.

Figure 4.12: Finding $H_{2,out}$ in Subcase 1.2. Jumping down from g_1 to g_2.

$v_{i+1,in,l} > v_{i+1,out,l}$ and $v_{i+1,in,r} < v_{i+1,out,r}$, when the points exist. First we use **Slope** to find the two points where the tangent has slope s_{i+1}, $t_{i+1,l}$ and $t_{i+1,r}$. Then we use **Slope** to find the two points where the tangent has slope s_i, $t_{i,l}$ and $t_{i,r}$. These tangent points do not necessarily exist.

Looking away from the trivial case $H_{i+1,out} = [0, 1 - u_{i+1}] = H_{i+1,in}$ there are two cases to consider:

1. $v_{i+1,out,m}$ exists.
2. $v_{i+1,out,m}$ does not exist.

Case 1: $v_{i+1,out,m}$ exists.

When $v_{i+1,out,m}$ exists, there are three possibilities:

1.1 $t_{i+1,l}$, $t_{i+1,r}$ exist and $v_{i+1,out,m} \in (t_{i+1,l}, t_{i+1,r})$

1.2 $t_{i+1,l}$, $t_{i+1,r}$ exist and $v_{i+1,out,m} \in [t_{i,l}, t_{i+1,l}] \cup [t_{i+1,r}, t_{i,r}]$

1.3 $t_{i+1,l}$, $t_{i+1,r}$ do not exist and $v_{i+1,out,m} \in [t_{i,l}, t_{i,r}]$

Subcase 1.1: $t_{i+1,l}$, $t_{i+1,r}$ exist and $v_{i+1,out,m} \in (t_{i+1,l}, t_{i+1,r})$
In this case it is obvious that $v_{i+1,in,m} = v_{i+1,out,m}$. It follows since it is impossible to jump from any point in small neighbourhood of $v_{i+1,out,m}$ with admissible speed. The line between $v_{i+1,out,l}$, $v_{i+1,out,m}$ and $v_{i+1,out,r}$ have slope s_i, by Observation 2. Then it is clear that $v_{i+1,in,l}$ and $v_{i+1,in,r}$ is equal to the cutting points between g_{i+1} and the line with slope s_{i+1} starting at $v_{i+1,out,m}$, cutting to the left and right, respectively. None of these points have to exist, but if they do we will find them in the way described above.

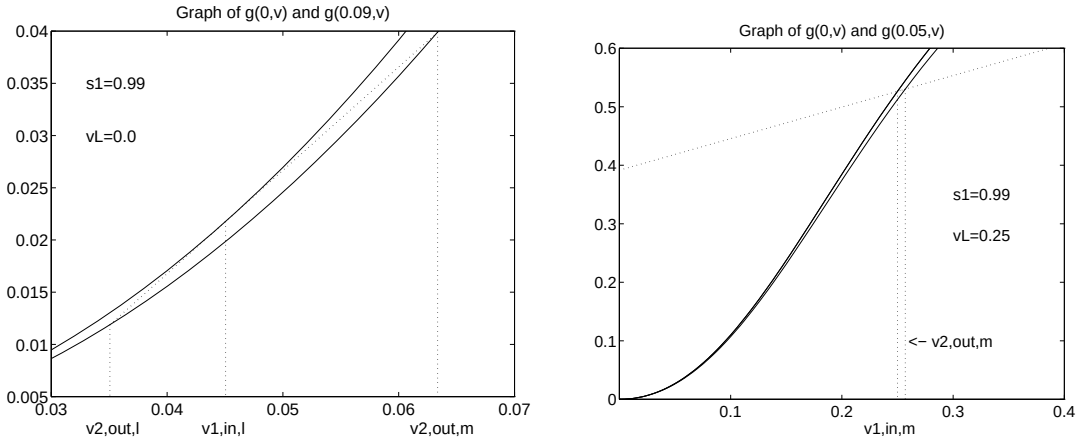

(a) $v_{1,in,m}$ does not exist.

(b) Only $v_{1,in,m}$ exists.

Figure 4.13: Finding $H_{2,out}$ in Case 2 and 3. Jumping down from g_1 to g_2.

The construction of $H_{2,in}$ when $v_{2,out,m}$ is between the two points with tangent s_2, is illustrated in Figure 4.14 (on the next side). The points $v_{2,in,l}$ and $v_{2,in,r}$ are found simply by cutting up and down from $v_{2,out,m}$. In Figure 4.14 (a) $v_{2,in,l}$ exists even though $v_{2,out,l}$ does not exist, and in Figure 4.14 (b) $v_{2,in,r}$ exists even though $v_{2,out,l}$ and $v_{2,out,r}$ do not exist. The construction depends on $v_{2,out,m}$ only.

Subcase 1.2: $t_{i+1,l}$, $t_{i+1,r}$ exist and $v_{i+1,out,m} \in [t_{i,l}, t_{i+1,l}] \cup [t_{i+1,r}, t_{i,r}]$
In this case the midpoint will disappear since the intervals will cover it. There are of course two cases depending on which of the tangent intervals contains the midpoint. Assume that the right interval contains the midpoint. The other case is treated similarly.

By observation 2 the line between $v_{i+1,out,m}$ and $v_{i+1,out,r}$ have slope s_i. Then all points between the midpoint and $v_{i+1,out,r}$ can be reached from the midpoint with speed greater than s_i (and less than s_{i+1} since the midpoint is to the right of $t_{i+1,r}$). All points between the midpoint and $t_{i+1,r}$ can be reached from the midpoint with speed less than s_{i+1} by definition of $t_{i+1,r}$. Thus $v_{i+1,out,r}$ is found equal to $t_{i+1,r}$. We find the cutting point c between the line starting at $t_{i+1,r}$ with slope s_{i+1} and g_{i+1}, cutting to the left. By observation 2 the line between $v_{i+1,out,m}$ and $v_{i+1,out,l}$ have slope s_i. All points between $v_{i+1,out,l}$ and c can be reached from $v_{i+1,out,m}$ with admissible shock speeds since we take the upper convex envelope. Thus $v_{i+1,in,l}$ is equal to c, and as proposed the midpoint no longer exists.

In Figure 4.15 we see an example where $v_{2,out,l}$ does not exist since the dotted line between $v_{2,out,r}$ and $v_{2,out,m}$ does not cut the graph. We see that $v_{2,out,m}$ is to the left of $t_{1,r}$ and to the right of $t_{2,r}$, and thus $v_{2,in,r} = t_{2,r}$. $v_{2,in,l}$ is found as the cutting point between the line starting at $v_{2,in,r}$ with slope $s_2 = 0.9$.

Subcase 1.3: $t_{i+1,l}$, $t_{i+1,r}$ do not exist and$v_{i+1,out,m} \in [t_{i,l}, t_{i,r}]$.
All points on g_{i+1} between $v_{i+1,out,l}$ and $v_{i+1,out,m}$, and between $v_{i+1,out,m}$ and $v_{i+1,out,r}$ can be reached with shock speeds less than s_{i+1} and greater than s_i, since the three points lie on a line with slope s_i. Thus $H_{i+1} = [0, (1 - u_{i+1})]$. If $v_{i+1,out,l}$ or $v_{i+1,out,r}$, or both

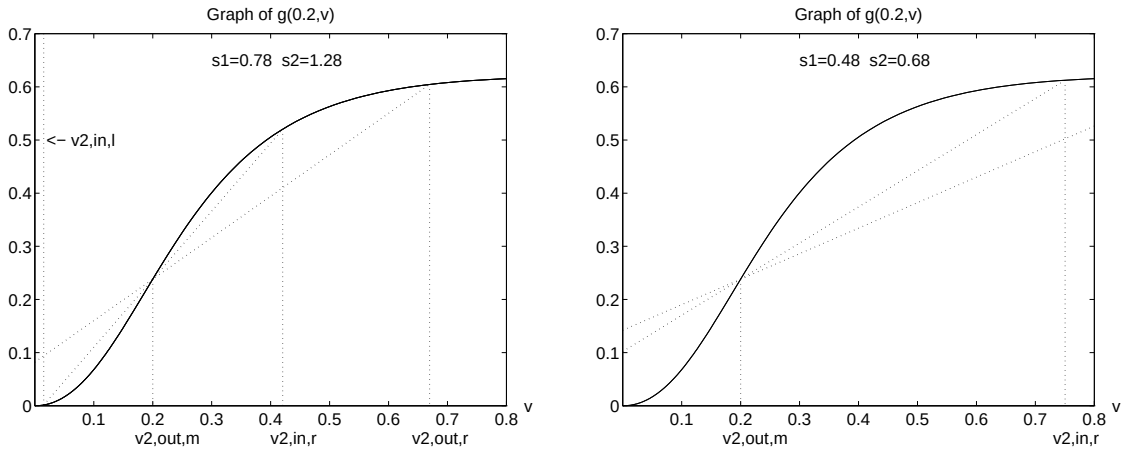

(a) $v_{2,out,l}$ does not exist.

(b) $v_{2,out,l}$ and $v_{2,out,r}$ do not exist.

Figure 4.14: Finding $H_{2,in}$ in Subcase 1.1.

do not exist, the conclusion still holds.

Case 2: $v_{i+1,out,m}$ does not exist.

If $v_{i+1,out,m}$ does not exist, it is easier to find $H_{i+1,in}$. We know that $v_{i+1,out,l}$ and $v_{i+1,out,r}$ lie on a line with slope s_i, and that $v_{i+1,out,r}$ is equal to $t_{i,r}$. Reasoning as we did in case 1.2 it is apparent that $v_{i+1,in,r}$ is equal to $t_{i+1,r}$, and that $v_{i+1,in,l}$ is the cutting point between the line starting at $t_{i+1,r}$ with slope s_{i+1}, and g_{i+1}, cutting to the left. Neither $v_{i+1,out,l}$ nor $v_{i+1,in,l}$ have to exist, and we observe that $v_{i+1,in,l}$ may exist without $v_{i+1,out,l}$ existing. If $t_{i+1,r}$ does not exist, all points between $v_{i+1,out,l}$ and $v_{i+1,out,r}$ can be reached with shock speeds less than s_{i+1} and greater than s_i. Thus $H_{i+1} = [0, (1 - u_{i+1})]$. If $v_{i+1,out,l}$ does not exist, the conclusion still holds.

In Figure 4.16 we see an example where $v_{2,out,l}$ does not exist since the dotted line from $v_{2,out,r}$ with slope $s_1 = 0.28$, does not cut the graph inside the phase plane. $v_{2,out,r}$ is of course equal to $t_{1,r}$. $v_{2,in,r}$ is equal to $t_{2,r}$ since all points between $t_{1,r}$ and $t_{2,r}$ can be reached from $v_{2,out,r}$ with admissible shock speeds, that is speeds between s_1 and s_2. (Remember that we take the upper envelope since the right value is less than the left value.) $v_{2,in,l}$ is the cutting point between the line starting at $v_{2,in,r} = t_{2,r}$ with slope $s_2 = 0.52$. This is correct since all points between 0.0 and $v_{2,in,l}$ can be reached from $v_{2,out,r}$ with admissible shock speeds, taking upper envelopes. (Actually it should be between $v_{2,out,l}$ and $v_{2,in,l}$, but since $v_{2,out,l}$ does not exist we must use 0.0 instead.)

As predicted in observation 2 the points $v_{i+1,in,l}$, $v_{i+1,in,m}$ and $v_{i+1,in,r}$ lie on a line with slope s_{i+1} by construction (when they exist).

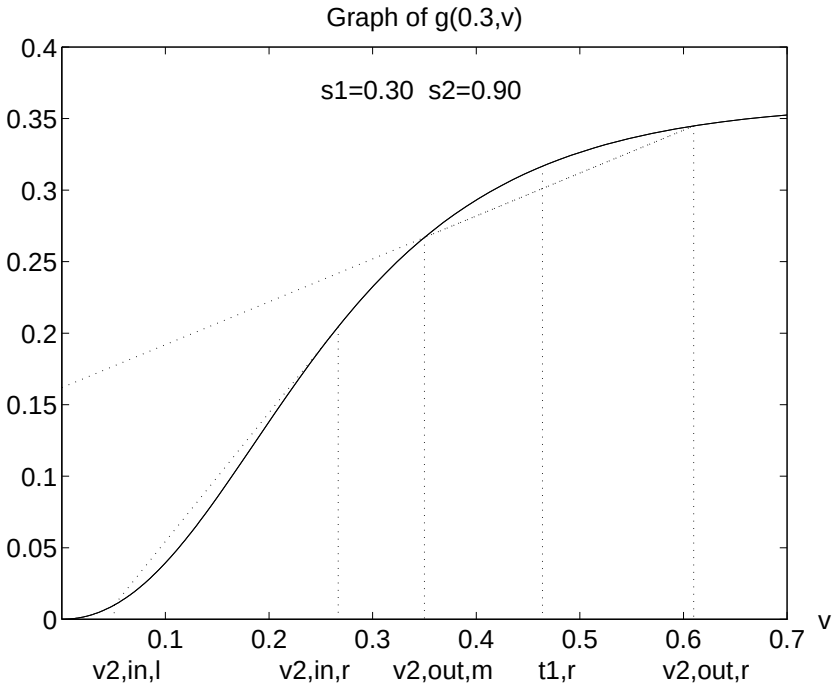

Figure 4.15: Finding $H_{2,in}$ in Subcase 1.2.

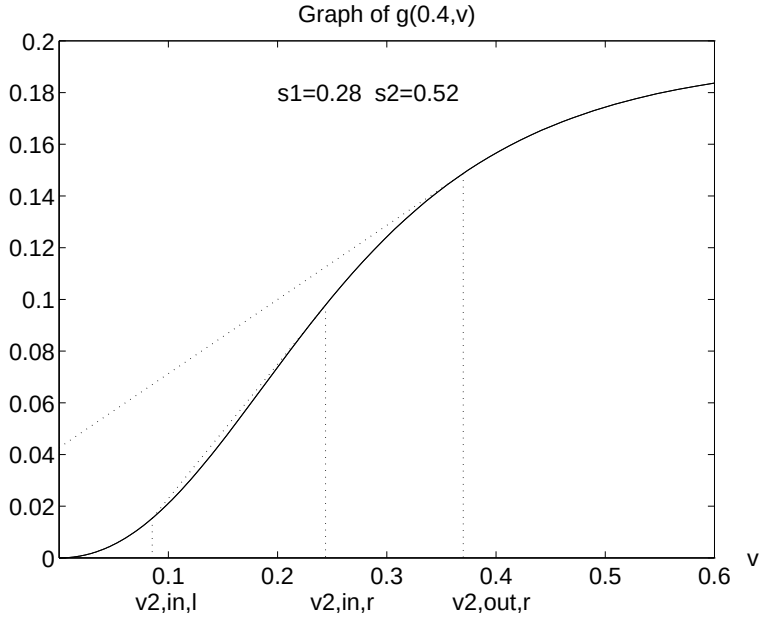

Figure 4.16: Finding $H_{2,in}$ when $v_{2,out,m}$ does not exist.

Treatment of a decreasing sequence of u-shocks.

Earlier in this section we have only considered the case where $u_i < u_{i+1}$ and claimed that we could treat a decreasing sequence, $u_i > u_{i+1}$, similarly. This may not always be obvious, so some comments are necessary:

1 Finding $H_{1,in}$.
This is independent of decreasing or increasing sequence.

2 Finding $H_{i+1,out}$.
We now jump up from g_i to g_{i+1} instead of down. Then the three cases to consider are:

   1. $v_{i,in,l}$ exists.
   2. $v_{i,in,l}$ does not exist, but $v_{i,in,r}$ exists.
   3. Only $v_{i,in,m}$ exist.

   We observe that $v_{i,in,l}$ and $v_{i,in,r}$ has changed roles. Generally speaking the angle of attack is changed from right to left in the construct of $H_{i+1,out}$.

3 Finding $H_{i+1,in}$.
The cases to consider are the same. In the construction the angle of attack is left instead of right.

Chapter 5

Front tracking

In this chapter we are going to solve the hyperbolic part of triangular system of conservations laws that we found in Section 2.4), with general initial conditions. There are several methods for solving 2×2 systems of conservation laws: Method of characteristics, finite difference (implicit /explicit) and so on. For a brief introduction to solution procedures for hyperbolic equations see [22].Our approach in solving this system will be front tracking. The most important part of the front tracker is the (triangular) Riemann solver found in chapter 4. We will present the method and some quasi-code.

5.1 Tracking

As for the Riemann problem we linearise the flux functions. Furthermore the initial functions are made piecewise constant.

To do so, the x-axis has to be discretised into a finite number of grid cells or blocks and we use some kind of averaging to find the u- and v-value in each grid cell. In

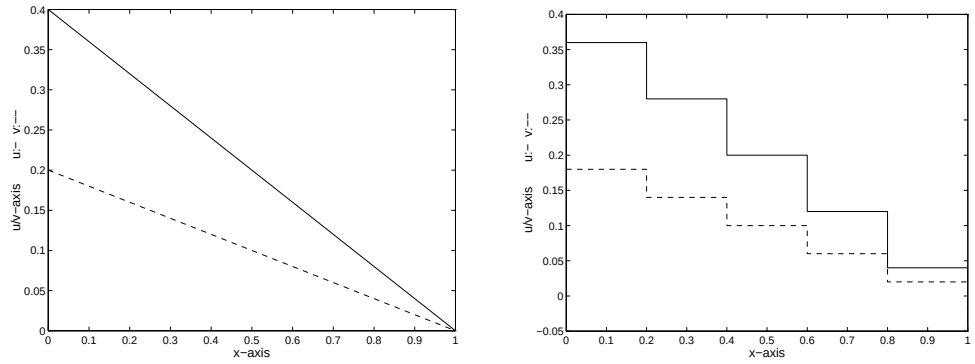

(a) (b)

Figure 5.1: Initial functions and their piecewise constant approximations.

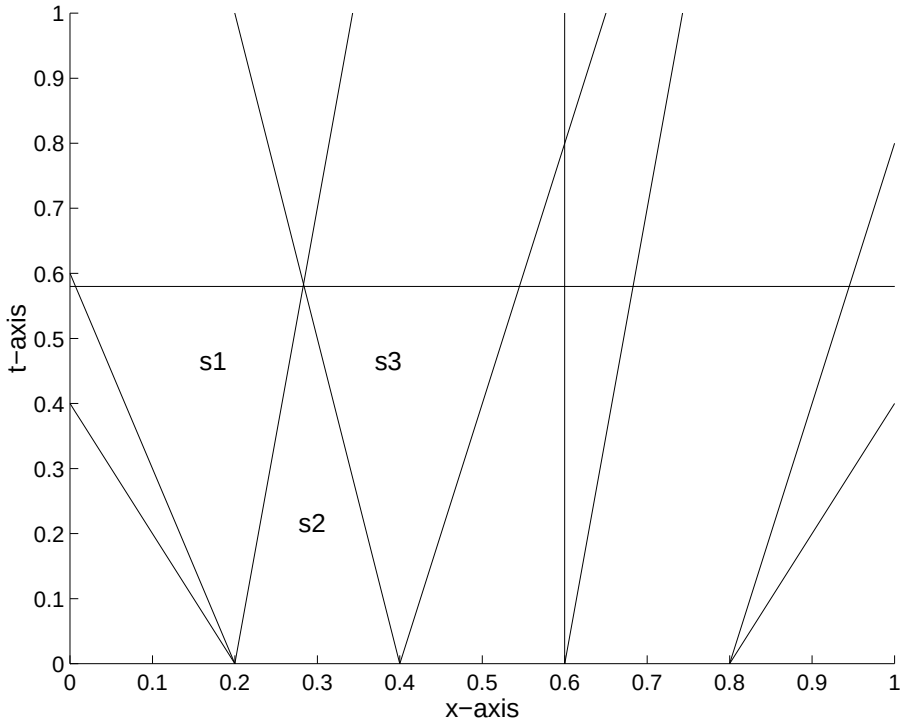

Figure 5.2: Solution of the Riemann problems in Figure 5.1 in the x-t plane.

Figure 5.1 (a) and (b) above we see an example of initial functions and their piecewise constant approximations, correspondingly. In each node (except the endpoints) we have a (triangular) Riemann problem to solve. The solutions contains only shocks/fronts, and the idea is to keep track of these fronts until they collide and define a new Riemann problem.

In Figure 5.2 we see a possible solution in the $x-t$ plane of the triangular system with piecewise constant initial functions like in Figure 5.1 (b). The first shock collision will be at $t = 0.58$ and $x = 0.28$, and this defines a new Riemann problem with $s1$ and $s2$ as left and right state, respectively, located at $x_0 = 0.28$. The new Riemann problem is solved. The fronts that collided are removed from the $x-t$ plane, and the fronts from the solution of the new Riemann problem are added at $t = 0.58$, $x = 0.28$. The fronts that did not collide at $t = 0.58$ and the new fronts are tracked until they collide. The shock collision defines a new Riemann problem. We continue tracking the fronts until we have reached a final time or no more fronts will collide.

In Figure 5.3 we see an example of front tracking with two Riemann problems initially located at $x = 0.4$ and $x = 0.8$. The first shock collision takes place at $t = 0.80$, $x = 0.67$. We then solve the new Riemann problem (which gives only one front) and continue the tracking. The second collision takes place at $t = 1.12$,$x = 0.97$. The collision is between the new front and a front from the initial Riemann problem located $x = 0.8$. After solving this Riemann problem we see in the $x-t$ plane that no more fronts will collide. The front tracking algorithm stops.

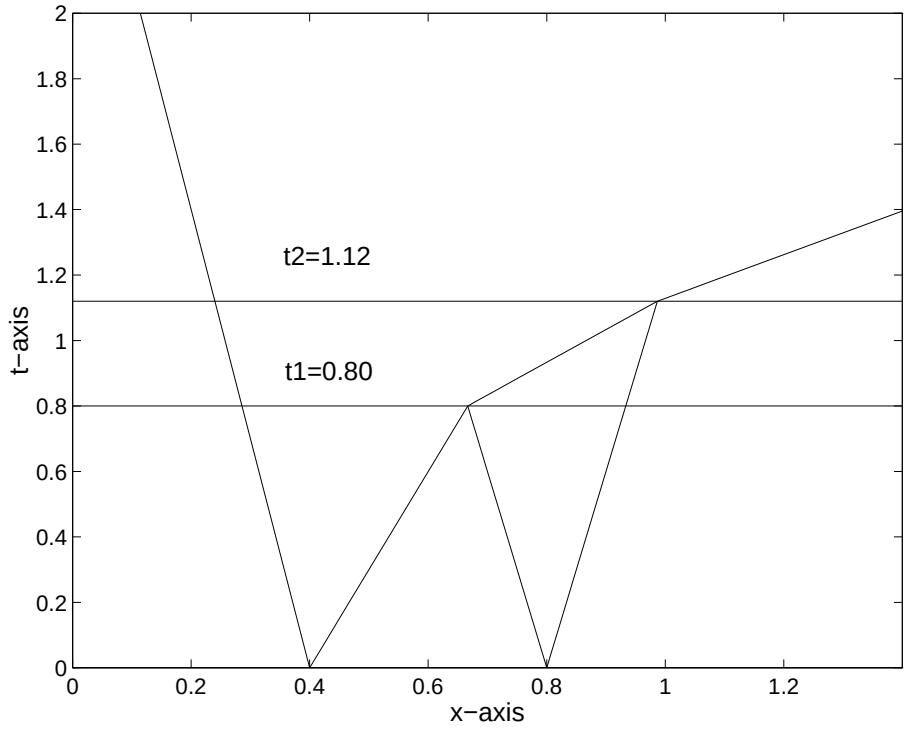

Figure 5.3: Front tracker solution in x-t plane.

5.2 Implementation

We want to solve the problem on a interval $[a, b]$ of the x-axis. This interval is divided into $n + 1$ blocks with nodes x_i $(i = 0, \ldots, n + 1)$ where $x_0 = a$ and $x_{n+1} = b$. We make the initial functions constant on each block by some averaging process. This gives us n Riemann problems to solve. To keep track of the fronts we make a `front-list` where we put all the fronts (shocks) from the n Riemann problems together with their (x, t)-position and their speed. The fronts are listed from left to right. Then the (x, t)-locations of the first $n - 1$ (or less) collisions are calculated. The first collisions are the ones between the rightmost front from the Riemann problem located at x_i and the leftmost front from the Riemann problem located at x_{i+1} $(1 \leq i \leq n - 1)$. To keep track of the collisions a `collision-list` is made. The fronts are sorted chronologically after when they collide. A `collisionpointer` is made to point at the first collision in the `collision-list`. Each front is an object with pointers to the `front-list` and (possibly) to the `collision-list`. The following quasi code describes the method:

```
Generate step function approximation for the initial functions;
Solve Riemann problems;
Make front-list and collision-list;

WHILE (collisionpointer != NULL)
  time=collisionpointer->time;
  IF (time < endtime)
    Find all the fronts that take part in Riemann problem;
```

```
    Remove them from the front-list;
    Solve Riemann problem defined by collisionpointer;
    Put new fronts in front-list;
    Remove collision from collision-list;
    Update collision-list;
    collisionpointer=first_collision;
  ELSE return;
```

In this algorithm, `endtime` is the time when we wish to end the simulations. If the `collisionpointer` points to `NULL` at time t', then there are no more collisions in the `collision-list`. This means that no lines cross each other in the $x - t$ plane over the horizontal line $t = t'$. At `endtime` the solution is in the `front-list`. Even though the algorithm is easy to understand, it is not trivial to implement.

Chapter 6

Diffusion solver

In this chapter we are going to solve the diffusion equation by difference methods. Explicit difference methods have several advantages; they are easy to understand and easy to implement. The drawback is that they are slow because of stability constraints. Implicit difference methods are unconditionally stable, but their implementation is generally not straight forward.

The diffusion equation, $u_t = \epsilon\, d(u)_{xx}$, is in general a non-linear heat equation. Choosing $d(u) = u$ and $\epsilon = k$ gives the heat equation $u_t = k u_{xx}$. The diffusion equation *with* the residual flux included will be solved since this is the diffusion step in the corrected operator splitting:

$$u_t + f_{res}(u)_x = \epsilon\, d(u)_{xx}. \tag{6.1}$$

6.1 Difference approximations

Selecting a mesh size $h > 0$ and a time step $\tau > 0$, the value of the approximation at $(x_j, t_m) = (jh, m\tau)$ will be denoted v_j^m. Let the solution time $T = K\tau$ and the x-range be $x_{max} = Nh$. The forward-time difference approximation is

$$u(x_j, t_m)_t \approx \frac{v_j^{m+1} - v_j^m}{\tau}.$$

The second order term $d(u)_{xx}$ will be discretised by a central difference:

$$d(u(x_j, t_m))_{xx} \approx \frac{d(v_{j+1}^{m+1}) - 2d(v_j^{m+1}) + d(v_{j-1}^{m+1})}{h^2}.$$

The first order term $f_{res}(u)_x$ will also be discretised by a central difference:

$$f_{res}(u(x_j, t_m))_x \approx \frac{f_{res}(v_{j+1}^m) - f_{res}(v_{j-1}^m)}{2h}$$

The forward-time central-space difference scheme then is as follows:

$$v_j^{m+1} = v_j^m - k_1[f_{res}(v_{j+1}^m) - f_{res}(v_{j-1}^m)] + k_2[d(v_{j+1}^m) - 2d(v_j^m) + d(v_{j-1}^m)],$$

where $k_1 = \tau/2h$ and $k_2 = \epsilon\ \tau/h^2$.

Let $d'(u) = D(u)$, as in Section 2.4. To ensure stability we must choose h and k so that

$$h \max_u |f'(u)| \leq 2\epsilon \qquad \text{and} \qquad 2\epsilon\ \frac{\tau}{h^2} \max_u |D(u)| \leq 1,$$

see Appendix A. In our model we have chosen $D(u) = 4u(1-u) + \delta$ which has a maximum at $u = 1/2$. The reason for the δ-parameter is to avoid the advection-diffusion to degenerate for $u = 0, 1$, where $D(u)$ would be equal to zero if δ was not introduced. Let $\delta = 0.01$. Then $\max_u |D(u)| \approx 1$ and the stability constraints implies that $\tau < \frac{h^2}{2\epsilon}$. If the time steps in the operator splitting are Δt, the number of (local) time steps in the diffusion solver is $N = \Delta t/\tau$. N is generally a large number and together with the fine grid this makes the procedure slow.

To avoid the stability constraints we could make the scheme implicit by evaluate all variables at time $t = (m+1)\tau$ and using backward-time in stead of forward-time. The backward-time difference approximation is

$$u(x_j, t_{m+1})_t \approx \frac{v_j^{m+1} - v_j^m}{\tau},$$

and the following implicit scheme is

$$v_j^{m+1} = v_j^m - k_1[f_{res}(v_{j+1}^{m+1}) - f_{res}(v_{j-1}^{m+1})] + k_2[d(v_{j+1}^{m+1}) - 2d(v_j^{m+1}) + d(v_{j-1}^{m+1})],$$

where k_1 and k_2 is as earlier defined.

Solving this scheme at each node gives us a system of N coupled equations to solve for each time step. Since d and f_{res} is non-linear, Newton linearisation is used on the system. The resulting matrix is tridiagonal and the system is easily solved. Picard iterations is used until the desired accuracy is achieved on each time step. Since we have no stability constraints we may choose the local time steps equal to the splitting time steps, and in that way make it faster than the explicit scheme even though there is more work on each time step. A possible modification of the scheme is to evaluate f_{res} at time $t = m\tau$ avoiding the linearisation of the residual flux function.

We have used both methods, and in Chapter 7 we will make a comparison of accuracy and runtime for the methods.

6.2 Super time stepping acceleration

Super time stepping (STS) is an efficient way to speed up explicit schemes for parabolic problems. The STS procedure relaxes the restrictive stability condition associated with

the explicit scheme so that the resulting diffusion solver runs at least as fast and is of comparable or better accuracy than the corresponding implicit diffusion solver. Although the method can only be justified theoretically for linear problems, it appears to be applicable to non-linear problems as well, see [23]. In order to relax the restrictive stability conditions for explicit scheme we do not require stability at the end of each time step τ, but rather at the end of a cycle of N time steps. Introducing a *super step* Δt_s consisting of N time step $\tau_1, \tau_2, \ldots, \tau_N$, the idea is to ensure stability over the super step, while trying to maximise its duration $\Delta t_s = \sum_{j=1}^{N} \tau_j$. The computed values after each τ_j are not approximations to the solution only intermediate calculations. Only the values at the end of each super step Δt_s approximate the solution. The τ_j are easily found as

$$\tau_j = \Delta t_{expt} \left((-1+\nu) \cos\left(\frac{2j-1}{N} \frac{\pi}{2} \right) + 1 + \nu \right)^{-1} \qquad j = 1, \ldots, N,$$

where $0 < \nu < \lambda_{min}/\lambda_{max}, \Delta t_{expt} = 2/\lambda_{max}$. λ_{max} is the largest eigenvalue of the matrix associated with the difference scheme and Δt_{expt} is the maximum time step for the explicit scheme. Letting $\nu \to 0$, shows that super stepping is (up to) N times faster than the standard explicit scheme, at almost the same cost. The only extra computations is finding the τ_j's. The length of the super step is determined by λ_{max}, and the choice of N and ν. Choosing ν too small can make the method sensitive to round-off errors.

Super time stepping acceleration is easily implemented in already existing explicit schemes for parabolic problems.

Chapter 7

Numerical results

We are going to study some test cases and compare our results with the reference solutions. Runtime for some initial value problems will be measured. Ordinary operator splitting versus corrected operator splitting are discussed in Section 7.1. In Section 7.2 we will compare the triangular model with a fully coupled model, and flux function with gravity is treated in section 7.3.

7.1 Operator splitting

In this section we have solved the triangular system

$$u_t + f(u)_x = \epsilon d(u)_{xx}, \tag{7.1}$$
$$v_t + g(u,v)_x = \epsilon d(v)_{xx}, \tag{7.2}$$

with initial data

$$u_0 = \begin{cases} 0.4 & \text{if } x < 0.4, \\ 0.0 & \text{if } x > 0.4, \end{cases} \quad \text{and } v_0 = \begin{cases} 0.6 & \text{if } x < 0.4, \\ 0.0 & \text{if } x > 0.4. \end{cases} \tag{7.3}$$

The flux functions,

$$f(u) = \frac{u^2}{u^2 + (1-u)^2/10},$$
$$g(u,v) = \frac{(1-u)^2 + u^2/10}{10u^2 + (1-u)^2} \cdot \frac{v^2}{v^2 + (1-v)^2/10},$$

used in the triangular system were found in [12].

The solutions are computed using ordinary and corrected operator splitting with one or more time steps. The advection step is always solved with the front tracker. The diffusion step is solved with an explicit finite difference scheme if nothing else is stated. The reference solution is always computed with an explicit upwind finite difference scheme.

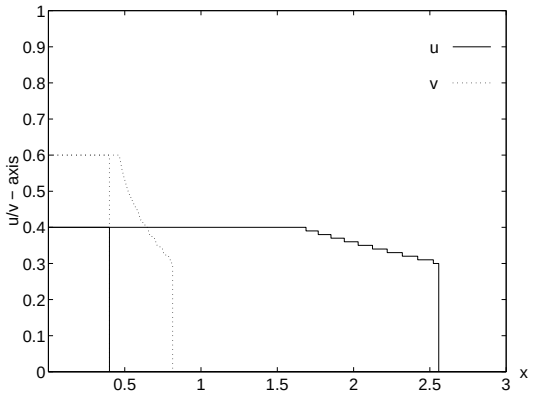

(a) $\epsilon = 0.0$, $\Delta u = 0.01$, $\Delta t = 1.0$, $Cu_{ff} = 500$.

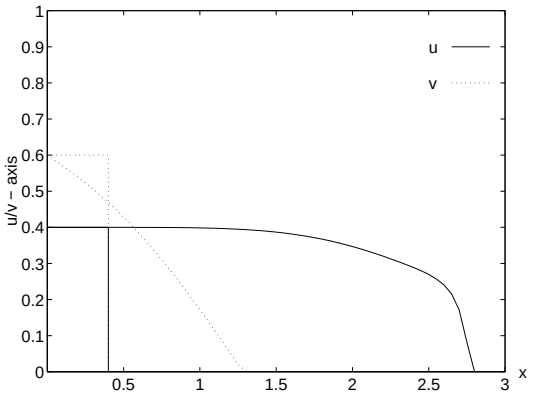

(b) $\epsilon = 0.1$, $\Delta u = 0.01$, $\Delta t = 1.0$, $Cu_{ff} = 500$.

Figure 7.1: Solutions of the triangular problem at time $t = 0.0, 1.0$ computed using the corrected operator splitting method.

The spatial mesh parameter Δx is chosen. The time mesh parameter Δt is then given implicitly through the stability constraints for the finite difference scheme:

$$Cu \leq 1 \qquad \text{and} \qquad \Delta t \leq \max ||d'|| \ \frac{\Delta x^2}{2\epsilon}, \tag{7.4}$$

where the CFL-number, Cu, is defined by

$$Cu = \max ||f'|| \ \frac{\Delta t}{\Delta x}.$$

The CFL-number for the front tracker, denoted Cu_{ff}, will also be calculated.

In Figure 7.1 (a) and (b) the solution of the linearised triangular system with $\Delta u = 0.01$ is shown for $\epsilon = 0.0$ and $\epsilon = 1.0$, correspondingly. The solutions are computed using corrected operator splitting from now on denoted COS. When $\epsilon = 0.0$ a triangular Riemann problem is solved, and the solution actually is found using the Riemann solver. The diffusion step does not alter the solution since $\epsilon = 0.0$. When $\epsilon = 0.1$, the diffusion step smoothes out the structures of the front tracker solution.

In Figure 7.2 the reference solution is compared to the COS solution at time $t = 1.0$. The reference solution is computed using an explicit upwind finite difference scheme. Since ϵ is equal to zero the COS solution coincide with the Riemann solver solution. Even when Δu is as large as 0.01 the approximation is very good. Runtime for the Riemann solver was 0.01 seconds and for the difference scheme it was 22.05 seconds. The exceptional runtime for the Riemann solver is easily explained since there was a single Riemann problem in this case and therefore no interacting waves. With general initial data the Riemann solver (front tracker) is slowed down.

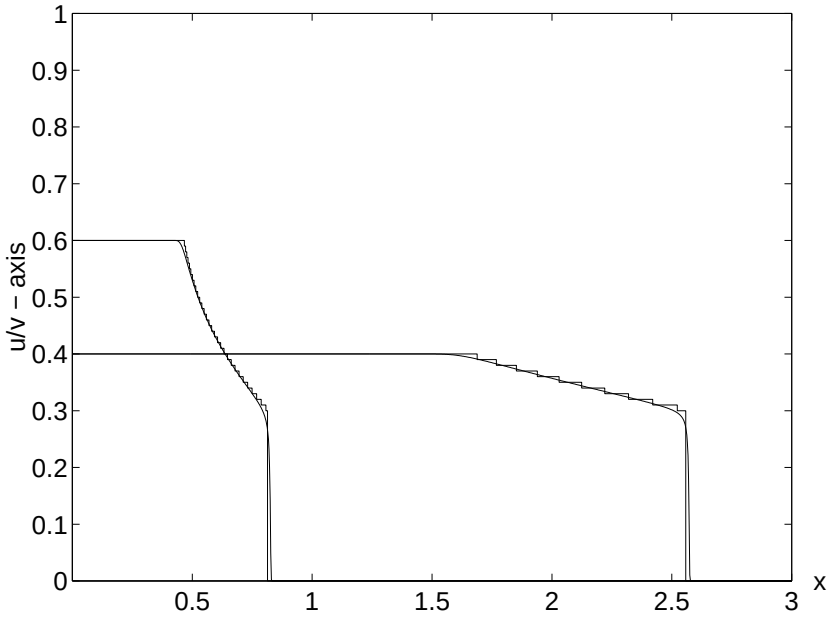

Figure 7.2: Comparison of reference and corrected operator splitting solution at time $t = 1.0$, $\epsilon = 0.0$, $\Delta u = 0.01$, $\Delta t = 1.0$, $Cu_{ff} = 500$, $\Delta x = 0.0025$, $Cu = 0.5$.

General initial data

The triangular system is solved with the following general initial data:

$$u_0 = v_0 = \begin{cases} 0.4 - x & \text{if } x \leq 0.4, \\ 0.0 & \text{if } x > 0.4. \end{cases} \tag{7.5}$$

ϵ is equal to 0.05, and the mesh parameter for the initial data is 0.02. The flux functions are linearised with $\Delta u = 0.01$

In Figure 7.3 the COS solution and the reference solution at time $t = 1.0$ is seen together with the piecewise constant initial data. Four time steps are used. The COS solution is a good approximation to the reference solution. Even now the front tracker is very fast, using only 0.28 seconds. In comparison the explicit diffusion solver uses 10.94 seconds on the four diffusion steps. It follows that some effort should be used on reducing the runtime for the diffusion solver. Then this operator splitting method would be more complete.

Effect of varying ϵ

The magnitude of ϵ decides how diffusive the system is. Typically, larger ϵ leads to more smooth solutions with less structure. In Figure 7.4 the COS solutions of the triangular system with initial data (7.3) for ϵ equal to 0.1 and 0.01 are compared at time $t = 1.0$. The COS solution is computed using four time steps, $\Delta u = 0.01$ and $Cu_{ff} = 125$. The

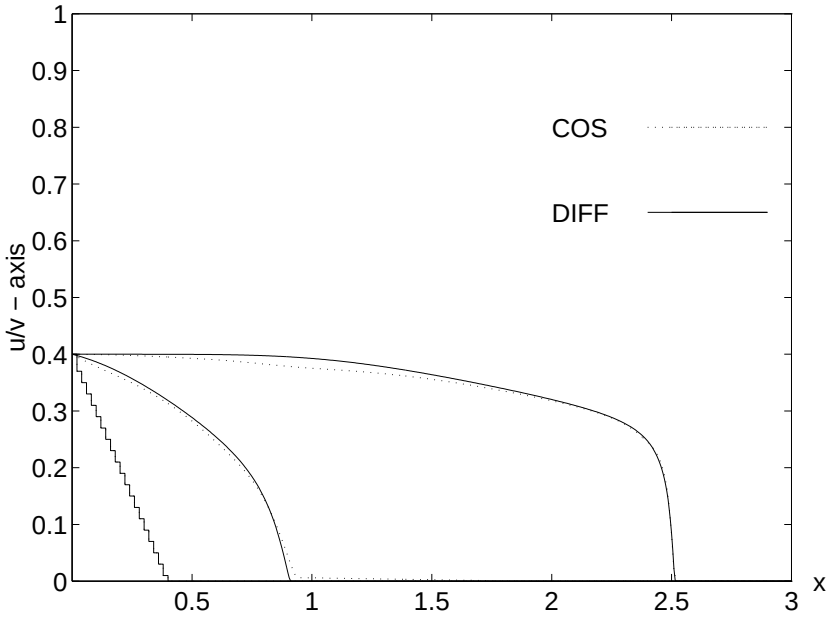

Figure 7.3: The corrected operator splitting (COS) solution and the reference solution (DIFF) at time $t = 0.0, 1.0$ with initial data (7.5), $\epsilon = 0.05$, $\Delta u = 0.01$, $\Delta t = 0.25$, $Cu_{ff} = 125$, $\Delta x = 0.005$, $Cu = 0.25$

figure illustrates how solutions of advection-diffusion equations depend on ϵ. The limit case where ϵ is equal to zero is shown in Figure 7.2.

Looking carefully at Figure 7.4, a slight error in the transport for the water phase is discovered in the case ϵ equal to 0.1. The error is located around $x = 1.75$. No such error is seen in the water phase when ϵ equal to 0.01. This behaviour is explained by Remark 2 in Subsection 7.1.2.

Implicit diffusion solver

The triangular system with initial data (7.3) will now be solved with ordinary operator splitting. Three time steps will be used. The diffusion step will be solved with both the implicit and explicit difference scheme. Comparing the solutions will then tell us about the qualities of the implicit diffusion solver versus the explicit diffusion solver.

In Figure 7.5 the two solutions are shown. They are equal except for a small area around $x = 1$. The difference is most likely introduced by the Riemann solver, see Remark 2 in Subsection 7.1.2, and not by the explicit diffusion solver. The runtime for the three diffusion steps was 0.01 seconds for the implicit solver and 0.16 seconds for the explicit solver. This was expected since the implicit solver uses a local time step equal to the splitting step. However, we experienced that if the ratio $\Delta t/\Delta x^2$ became too large, the solution from the implicit solver started to oscillate. Doing Picard iterations in those cases did not improve the result. We therefore used the explicit solver, where the stability restrictions are known. Moreover, the runtime for the explicit solver can be dramatically reduced by using Super time stepping acceleration, see Section 6.2.

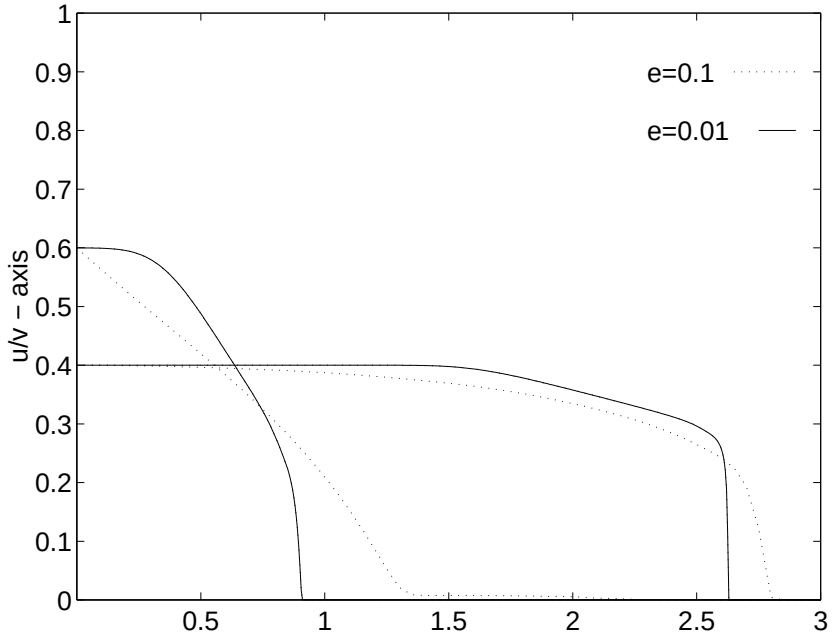

Figure 7.4: Solution of the system with ϵ equal to 0.1 and 0.01, at time $t = 1.0$. Solutions computed with corrected operator splitting with $\Delta u = 0.01$, $\Delta t = 0.25$, $Cu_{ff} = 125$.

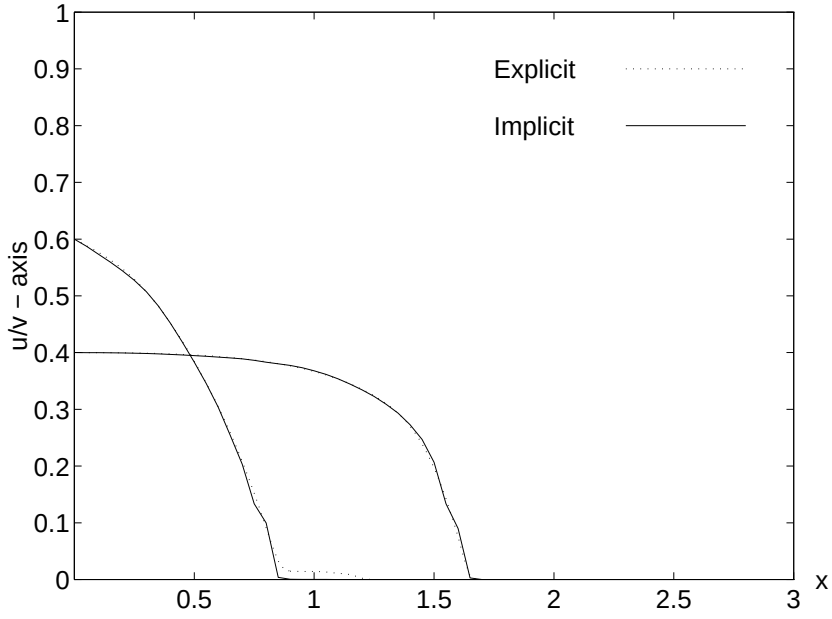

Figure 7.5: Solution of the triangular system with ϵ equal to 0.05 at time $t = 0.5$ computed using ordinary operator splitting with $\Delta u = 0.01$, $\Delta t = 0.167$, $Cu_{ff} = 83.5$. The diffusion step is solved with both the explicit and the implicit difference scheme.

7.1.1 Splitting with and without correction

In Section 3.2 the corrected operator splitting method was introduced to improve the solutions from the operator splitting method from now on denoted OS. If there are shocks in the solution after the advection step, the COS method uses a residual flux term to reduce the splitting error. If there are no shocks, the methods coincide.

Because the COS method did not give the predicted improvement in the numerical experiments, it became clear that the global residual flux defined in Section 3.2 had to be modified. The global flux was defined as follows:

$$\mathbf{f}_{res}(\mathbf{s}, x) = \sum_{i=1}^{n} \mathbf{f}_{res,i}(\mathbf{s}) \chi_{R_i}(\mathbf{s}, x)$$

where $\chi_{R_i}(\mathbf{s}, x) = \begin{cases} 1 & \text{if} \quad (\mathbf{s}, x) \in R_i \\ 0 & \text{else} \end{cases}$ and $\mathbf{f}_{res,i}$ is the residual flux function associated with shock i. The definition of the (local) residual flux function is in order, but the function that tells where the global flux should live, $\chi_{R_i}(\mathbf{s}, x)$, had to be modified. The problem is the definition of R_i: $R_i = (u_i, u_{i+1}) \times (v_i, v_{i+1}) \times (x_i - \delta, x_i + \delta)$, where u_i and v_i is the left values in the shock and u_{i+1} and v_{i+1} is the right values. After the advection step the solution consists of finitely many shocks. The diffusion solver uses a uniform grid[1] and therefore the advection solution has to be projected onto that grid. The projection consists of an averaging process of the solution onto the uniform grid. When the shock is in both phases the definition of R_i is in order, but when one phase is constant in the shock the definition is not sufficient since the advection solution is altered by the projection. If one phase, for example u, is constant in the shock we have $R_i = u_i \times (v_i, v_{i+1}) \times (x_i - \delta, x_i + \delta)$. Let (u, v, x) be the advection solution and (u', v', x) be the projection onto a uniform grid. Then $(u', v', x) \notin R_i$ even though $(u, v, x) \in R_i$. Similarly if v is the constant case. The problem is resolved by redefining R_i:

$$R_i \stackrel{def}{=} (u_i + c_u \Delta u, u_{i+1} - c_u \Delta u) \times (v_i + c_v \Delta u, v_{i+1} - c_v \Delta u) \times (x_i - \delta, x_i + \delta),$$

where $|c_u| = |c_v| = c$ and c_w is positive if $w_i \geq w_{i+1}$ and negative if not (s=u,v). Δu is the linearising parameter (for the flux functions) and c is typically larger than 2.

After this modification the corrected operator splitting gave very good results. All figures show solution of the triangular system with initial data (7.3).

In Figure 7.6 the COS solution is compared with the OS solution for $\epsilon = 0.1$. One splitting step is used. In the gas phase, u, the front is sharpened up. The water phase, v, has basically a smooth solution and therefore no correction or sharpening of the front is seen. As will be seen in Figure 7.8, the COS solution is very accurate. Runtime for the ordinary operator splitting is 0.08 seconds and for the corrected operator splitting 0.18 seconds. The extra time used by the COS method is due to the construction of the residual flux.

In Figure 7.7 the COS solution is compared with the OS solution once again. This time ϵ is equal to 0.01. One time step is used. The u-front is once again sharpened nicely

[1] Both the explicit and implicit diffusion solver uses uniform grids.

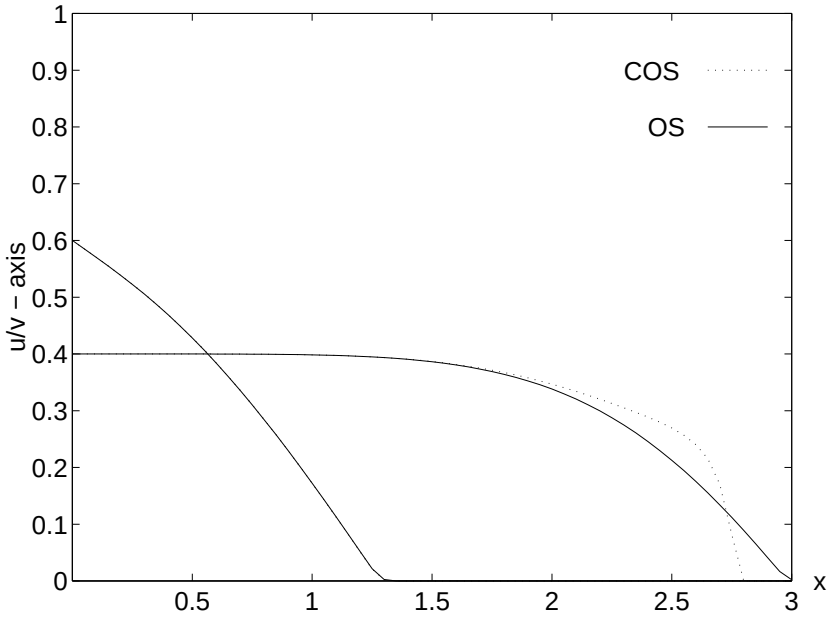

Figure 7.6: Comparison of ordinary operator splitting (OS) and corrected operator splitting (COS) at time $t = 1.0$, $\epsilon = 0.1$, $\Delta u = 0.01$, $\Delta t = 1.0$, $Cu_{ff} = 500$.

up. In addition there is some sharpening in the v-front. This follows since the solution for the water phase is less smooth than it was when ϵ was equal 0.1. Runtime in this case was 2.01 seconds and 5.28 seconds for OS and COS respectively. Still the corrected operator splitting solution is considerably better than the ordinary operator splitting.

7.1.2 Number of time steps

The number of (splitting) time steps used depends on the magnitude of ϵ. The trivial case is ϵ equal to zero, where only one step should be used, as seen earlier in this section. The idea is to use as few steps as possible to achieve acceptable accuracy. The optimal number of time steps is expected to be proportional to ϵ. When the diffusion, ϵ, is small, the error made using long time steps is also small. When ϵ is increased the error grows, and shorter time steps must be used. The following examples will illustrate this. Note that when the fronts in the solution are established, the solution will be translated along the x-axis without changing shape. Thus few time steps can be used even if ϵ is large. In addition the correspondence between number of steps and ϵ does not necessarily carry over to two or three dimensions.

The triangular system is solved with initial data (7.3) and ϵ equal to 0.1 and 0.01. The solution is found using COS with various number of time steps. The reference solution is computed using a finite difference scheme with small mesh parameters.

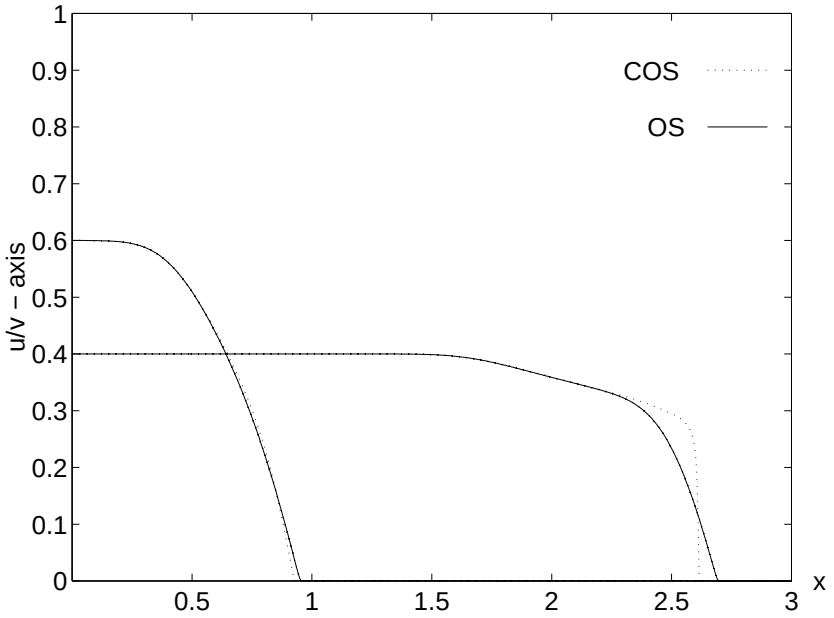

Figure 7.7: Comparison of ordinary operator splitting (OS) and corrected operator splitting (COS) at time $t = 1.0$, $\epsilon = 0.01$, $\Delta u = 0.01$, $\Delta t = 1.0$, $Cu_{ff} = 500$.

ϵ equal to 0.1

In Figure 7.8 (a) and (b) the reference solution and the COS solution is compared using one and four time steps, correspondingly, with ϵ equal to 0.1. In Figure 7.8 (a) the error is large in both phases. This illustrates what happens if too few steps are used when ϵ is large. Increasing the number of time steps to four, significantly reduces the error made by the COS method, as seen in Figure 7.8 (b). Using more time steps did not improve the accuracy since the Riemann solver then introduces an error, see Remark 2 below.

ϵ equal to 0.01

In Figure 7.9 (a) and (b) the reference solution and the COS solution is compared using one and two time steps, correspondingly, with ϵ equal to 0.01. Using only one time step the error is already small, as seen in Figure 7.9 (a). Increasing the number of time steps to two improves the solution some, as seen in Figure 7.9 (b). The same accuracy as when using four time steps in the case ϵ equal to 0.1, is achieved using only two steps.

Remark 2:

In several of the examples the number of (splitting) time steps had to be limited because of errors introduced by the Riemann solver. The problem arises when the solution from the diffusion solver is given to the Riemann solver as initial data. In each node of the grid

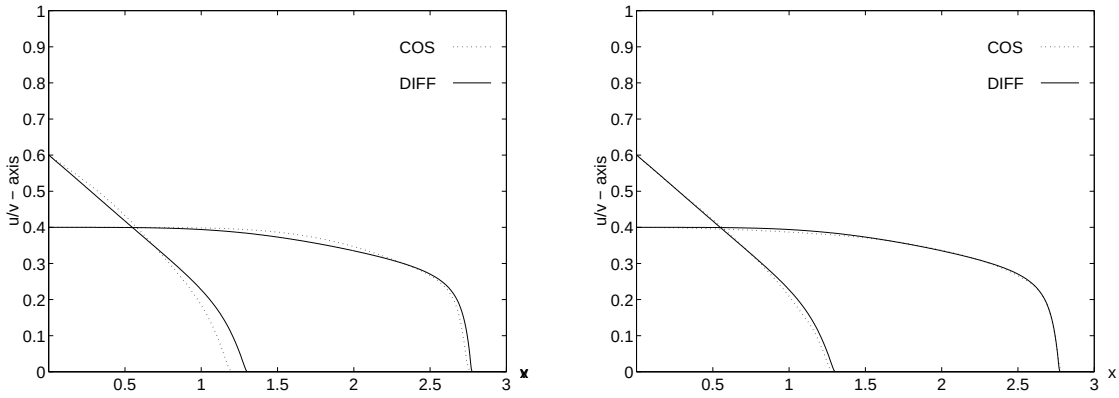

(a) COS $\Delta u = 0.01$, $\Delta t = 1.0$, $Cu_{ff} = 500$; DIFF $\Delta x = 0.005$, $Cu = 0.125$

(b) COS $\Delta u = 0.01$, $\Delta t = 0.25$, $Cu_{ff} = 125$; DIFF $\Delta x = 0.005$, $Cu = 0.125$

Figure 7.8: Comparison of the reference solution (DIFF) and the corrected operator solution (COS) solution at time $t = 1.0$, using one and four time steps.

from the diffusion solution, a Riemann problem is defined. Since this grid is very fine the differences between the left and right states in the Riemann problem generally are very small. Let u_L, u_R, v_L and v_R be defined in an obvious way. The u_i's are the nodes in the linearised flux function f, and $g_i = g(u_i, v)$, see Remark 1 in Section 4.2. There must be finitely many u_i's and g_i's since we have the memory available is limited. The number of g_i's is equal to the number of nodes in the linearisation of the flux function f.

First, assume that the right and left states for both phases are not equal. First the scalar Riemann problem defined by u_L and u_R is solved. Secondly the coupled Riemann problem is solved. Since u_L and u_R are close by assumption, they will define the same flux function g_i, i.e, $g_i(v) \approx g(u_L, v) \approx g(u_R, v)$. Since there is only one g_i available, it is impossible to construct the H-sets. Then the only possibility is to find an approximative solution of the coupled Riemann problem, where u is set equal to the average of u_L and u_R. This may not seem very drastic, but the result is that the shock speeds will be wrong. When this happens in very many Riemann problems, the approximation is no longer accurate.

Secondly, assume that one of the phases has (almost) equal right and left states. If v_L is (almost) equal to v_R, then there is no problem. Only the scalar Riemann for the gas phase has to be solved, and no approximations are made. On the other hand, if u_L is (almost) equal to u_R, then we are forced to do an approximation since there normally is no i such that $u_L = u_R$ is exactly equal to u_i. The approximative solution is found by using the best possible g_i in the scalar Riemann problem for v. Once again the result may be that the shock speeds are wrong.

There are two ways to improve the Riemann solver. The easiest and fastest way to resolve the problem measured in runtime, is to project the diffusion solution onto a coarser grid. Then the differences between the left and right states would be larger, and fewer Riemann problems have to be approximated. However, this may not be the most

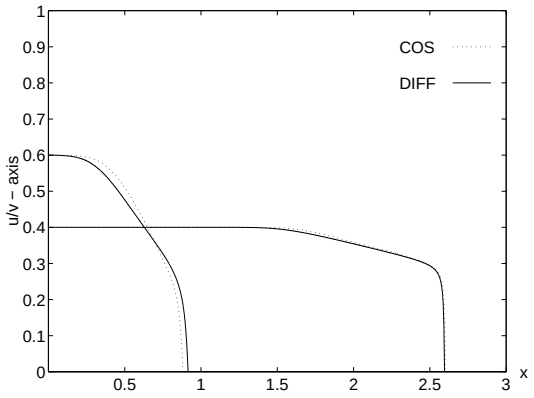

(a) COS $\Delta u = 0.01$, $\Delta t = 1.0$, $Cu_{ff} = 500$; DIFF $\Delta x = 0.0005$, $Cu = 0.125$

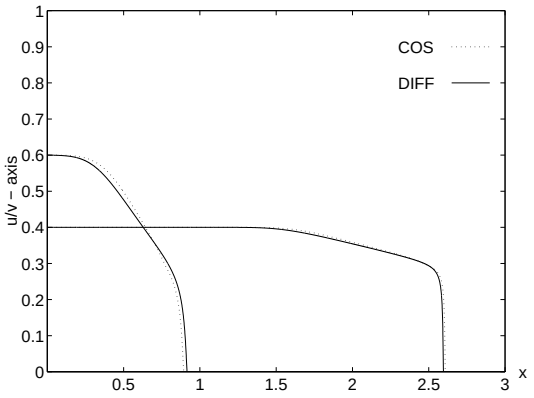

(b) COS $\Delta u = 0.01$, $\Delta t = 0.5$, $Cu_{ff} = 250$; DIFF $\Delta x = 0.0005$, $Cu = 0.125$

Figure 7.9: Comparison of reference solution (DIFF) and the corrected operator splitting solution (COS) at time $t = 1.0$, using one and two time steps.

accurate way to do it. Adding new node points for u_L and u_R on the flux function f, when they are needed, gives two different flux functions g_i for the water phase. It follows that the solution of the Riemann problem is exact. Despite this fact, this method is probably not prefered because doing this for each Riemann problem would result in very many nodes slowing the Riemann solver dramatically down.

7.2 Triangular versus fully coupled

In Section 2.4 we suggested to approximate the fully coupled model

$$u_t + f(u,v)_x = \epsilon\ d(u)_{xx}, \tag{7.6}$$
$$v_t + g(u,v)_x = \epsilon\ d(v)_{xx}, \tag{7.7}$$

with the triangular model

$$u_t + f(u)_x = \epsilon\ d(u)_{xx}, \tag{7.8}$$
$$v_t + g(u,v)_x = \epsilon\ d(v)_{xx}, \tag{7.9}$$

where $f(u)$ is equal to $f(u, v_0)$. v_0 is an arbitrary chosen constant. From the Norm condition in Section 2.4 it follows that if $||f_v|| < k\ ||f_u||$, where $k \ll 1$, then the approximation is expected to be reasonably well. The fully coupled systems are solved by an explicit forward-time central-space finite difference scheme, see Appendix A.

Example 1:

The flux functions for the fully coupled system are taken from [12]:

$$f(u,v) = \frac{u^2}{u^2 + v^2/10 + (1-u-v)^2/10}, \tag{7.10}$$

$$g(u,v) = \frac{v^2}{10u^2 + v^2 + (1-u-v)^2}. \tag{7.11}$$

$f(u)$ and $g(u,v)$ in the corresponding triangular system must satisfy the conditions in Theorem 4 in Section 4.2. The conditions are:

f1. $f(0) = 0$ and $f(1) = 1$.

f2. $f'(u) > 0$, increasing in u.

f3. f has at most one inflection point.

g1. $g(u, 1-u) = 1 - f(u)$

g2. $g_v \geq 0$, increasing in v.

g3. $g_u < 0$, decreasing in u.

g4. g has at most one inflection point.

The flux function for the gas phase, $f(u)$, is found just by setting v_0 equal to zero in $f(u, v_0)$. Then f satisfies conditions f1, f2 and f3. In Section 4.2 we showed that condition g1 is generally not satisfied. However, choosing v_0 equal to zero makes $g(u,v)$ satisfy the condition in this case. In addition $g(u,v)$ satisfies the conditions g2 and g4. $g(u,v)$ does not satisfy condition g3. It follows that g_i and g_{i+1} may cross each other for some (or all) i making the construction of the H-sets impossible. To insure that the construction is possible, $g(u,v)$ has to be reshaped so that $g_u < 0$. The endpoints are fixed since condition g1 still has to be satisfied. The reshaped flux function is an approximation to the original flux function and introduces an error in the solution. Hopefully this error is of the same order as the other approximations made[2] and therefore does not alter the accuracy of the solution. The reshaped flux function g was not renamed.

The following flux functions are used in the triangular system:

$$f(u) = \frac{u^2}{u^2 + (1-u)^2/10} \tag{7.12}$$

$$g(u,v) = \frac{(1-u)^2 + u^2/10}{10u^2 + (1-u)^2} \cdot \frac{v^2}{v^2 + (1-v)^2/10} \tag{7.13}$$

Several other choices of reshaping are possible. More effort could have been used in finding the optimal reshaped flux function. This flux function would have to satisfy condition g3 (and g1, g2 ,g4) and differ least from the original flux function in some norm. Since the flux functions are linearised in the solution procedure, a possible way

[2]The major approximations are: replacing $f(u,v)$ with $f(u)$, making the initial data piecewise constant, and linearising the flux functions.

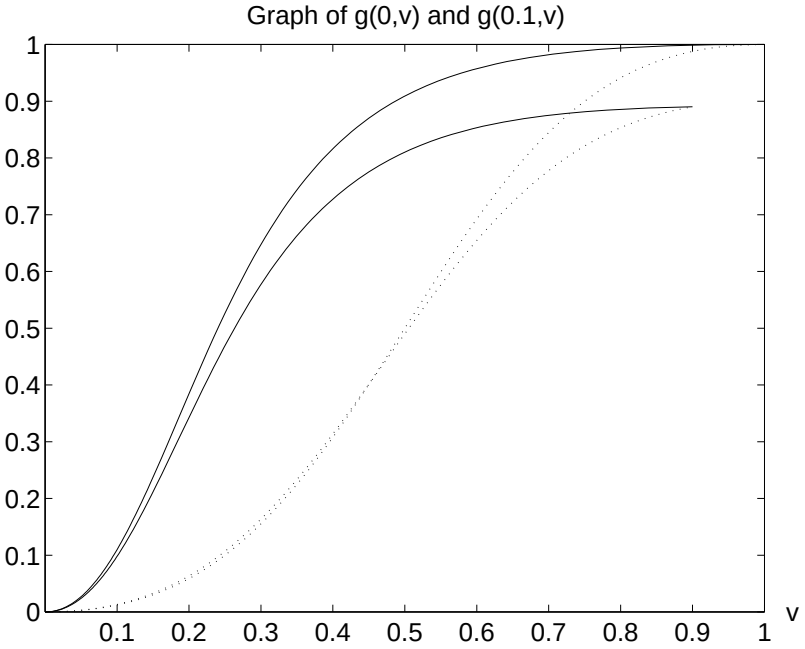

Figure 7.10: The original flux function g (dotted line) compared to the reshaped flux function g (solid line).

to minimise the difference is to just tabulate the values of the flux function in each node in stead of finding a functional form for the flux function.

In Figure 7.10 the original and reshaped flux functions $g(u, v)$ are compared for two values of u. The original flux functions cross each other for the two u-values. The reshaped functions do not cross each other, but the derivatives are different from the derivatives for the original flux function. This is a non-trivial observation because changing the derivatives may change the transport in the system.

In Section 2.4 we defined an L^2-norm on the phase plane. In this norm

$$||f_v|| = 0.208, \quad ||f_u|| = 1.325 \;\Rightarrow\; ||f_v|| < k\ ||f_u|| \text{ satisfied for } k = 1/6. \tag{7.14}$$

This suggests that the solution of (7.12-7.13) is a reasonably good approximation to the solution of (7.10-7.11). The systems are compared for ϵ equal to 0.01 and with initial data

$$u_0 = \begin{cases} 0.6 & \text{if } x < 0.4, \\ 0.2 & \text{if } x > 0.4, \end{cases} \quad \text{and } v_0 = \begin{cases} 0.3 & \text{if } x < 0.4, \\ 0.7 & \text{if } x > 0.4. \end{cases} \tag{7.15}$$

In Figure 7.11 (a) the reference solution for the fully coupled system is shown . The solution is computed with a finite difference scheme with $\Delta x = 0.0005$ and $Cu = 0.125$. The solution of the triangular system shown in Figure 7.11 (b), is found by the COS method with $\Delta u = 0.01$, $\Delta t = 0.25$, i.e., two time steps are used, and $Cu_{ff} = 125$.

In Figure 7.12 the solutions of the fully coupled system and the triangular system are compared. The transport is slightly different, but the structures of the solutions are

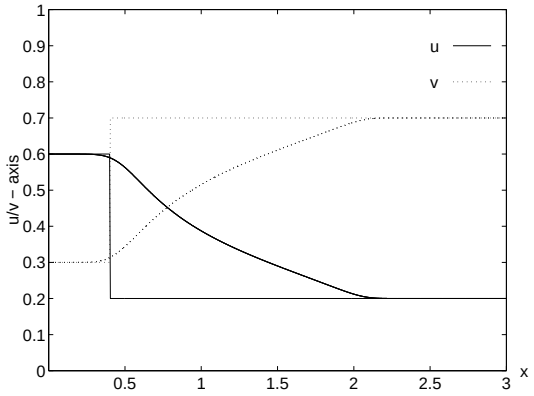

(a) The reference solution of the fully coupled system.

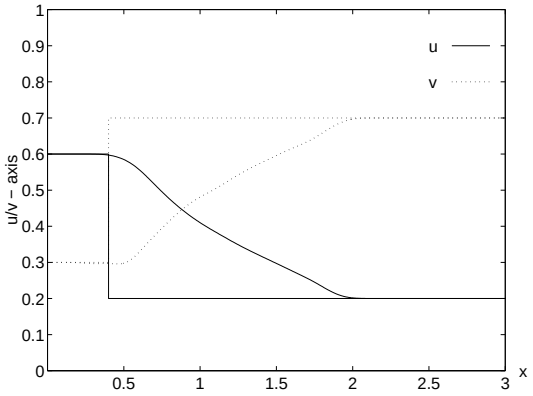

(b) The COS solution of the triangular system.

Figure 7.11: Solutions of the Riemann problem (7.15) at time $t = 0.0$ and $t = 0.5$.

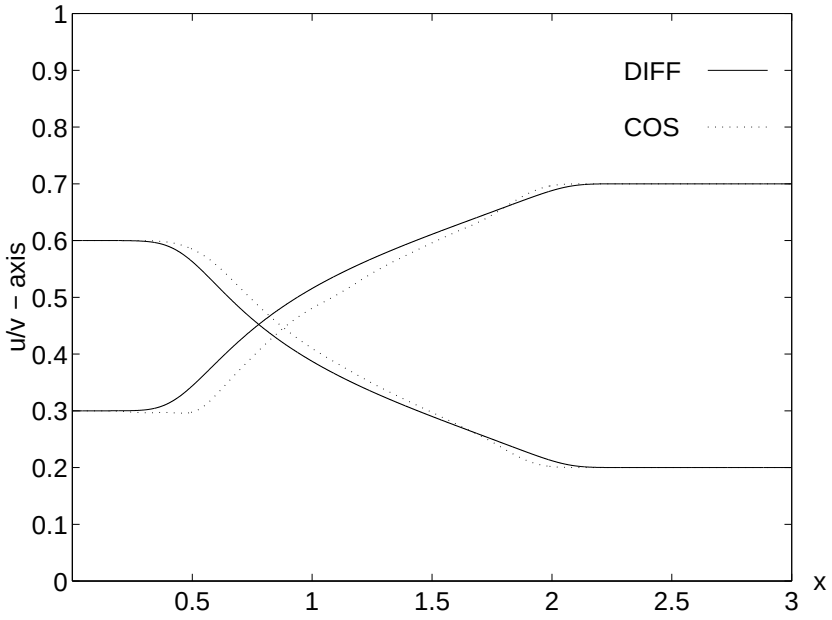

Figure 7.12: Comparison between the reference solution (DIFF) in Figure 7.11 (a) and the COS solution in Figure 7.11 (b) of Riemann problem (7.15) at time $t = 0.5$.

equal. Some difference in the transport is expected since the flux functions are modified, altering the derivates, as noted earlier. This example suggests that approximating fully coupled systems by triangular systems is a good approach when they satisfy the norm condition.

Example 2:

The flux functions for the fully coupled system are taken from [3]:

$$f(u,v) = \frac{50u}{v^3 + 3.14(1-u-v)(1-u)^2(1-v)^2 + 50u}, \tag{7.16}$$

$$g(u,v) = \frac{v^3}{v^3 + 3.14(1-u-v)(1-u)^2(1-v)^2 + 50u}. \tag{7.17}$$

$f(u)$ and $g(u,v)$ in the corresponding triangular system must satisfy the same conditions as in Example 1. Once again $f(u)$ is found by setting v_0 equal to zero in $f(u,v_0)$. Then f satisfies conditions f1, f2 and f3. g satisfies conditions g2, g3 and g4, but not condition g1. Thus, existence of a solution is not guaranteed. In fact, there exist initial value problems that have no solution. Neither Theorem 4 nor the more general Theorem 5 is applicable to this function. In Section 4.2 we showed that g not satisfying condition g1, introduces in-physical behaviour. In this case the contradiction is that the oil flux is larger than zero even though the oil saturation is zero. This follows from the fact that $f(u)$ is less than $f(u,1-u)$. In this example no choice of v_0 makes $f(u)$ equal to $f(u,1-u)$. However, minimising the distance between the two functions in some norm on the interval from 0 to 1 will give an optimal choice of v_0. The optimal value of v_0 in the L^∞-norm is approximately 0.3211. Then $||f(u) - f(u,1-u)||_L^\infty \approx 0.00315$. But, no matter what choice of v_0 we make, we are not insured that the solution exists, so for simplicity, v_0 is set equal to zero. Even though condition g1 is not satisfied we will solve the triangular system since the construction gives the correct solution if it exists.

It follows that the flux functions used for the triangular system are:

$$f(u) = \frac{50u}{3.14(1-u)^3 + 50u}, \tag{7.18}$$

$$g(u,v) = \frac{v^3}{v^3 + 3.14(1-u-v)(1-u)^2(1-v)^2 + 50u}. \tag{7.19}$$

We use the same norm as in Example 1. In this norm

$$||f_v|| = 0.205, \quad ||f_u|| = 4.868 \;\Rightarrow\; ||f_v|| < k\ ||f_u|| \text{ satisfied for } k = 1/20. \tag{7.20}$$

In this example k is equal to 1/20. In the light of Example 1 where k was equal 1/6, we expect the solution of (7.18-7.19) to be a good approximation to the solution of (7.16-7.17).

The systems are compared for ϵ equal to 0.1 and with initial data

$$u_0 = \begin{cases} 0.25 & \text{if } x < 0.4, \\ 0.1 & \text{if } x > 0.4, \end{cases} \quad \text{and } v_0 = \begin{cases} 0.75 & \text{if } x < 0.4, \\ 0.0 & \text{if } x > 0.4. \end{cases} \tag{7.21}$$

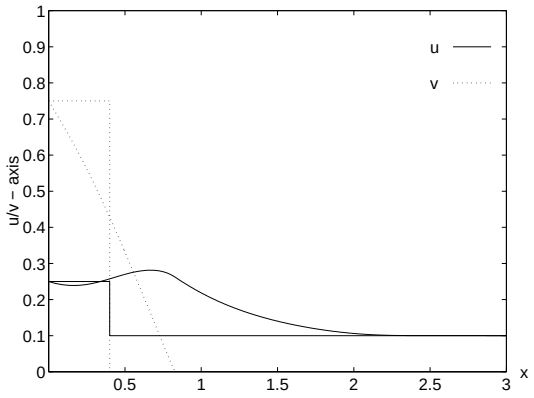

(a) The reference solution of the fully coupled system.

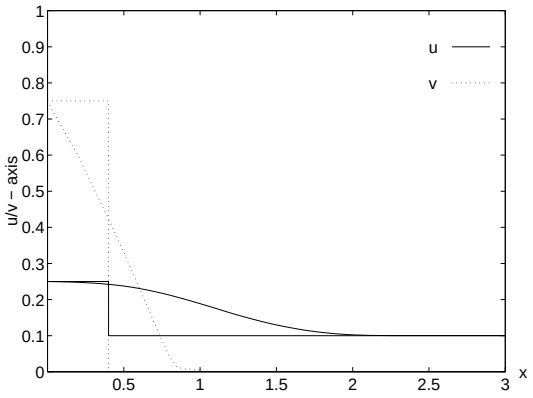

(b) The COS solution of the triangular system.

Figure 7.13: Solutions of Riemann problem (7.21) at time $t = 0.0, 0.5$.

In Figure 7.13 the solutions of the fully coupled and the triangular system is shown time at $t = 0.0$ and $t = 0.5$. The reference solution for the fully coupled system is shown in Figure 7.13 (a). The solution is found by a finite difference scheme with $\Delta x = 0.0005$ and $Cu = 0.125$. The solution of the triangular system shown in Figure 7.13 (b), is found by corrected operator splitting with $\Delta u = 0.01$, $\Delta t = 0.25$, i.e., two time steps are used, and $Cu_{ff} = 125$. Even though condition 1 is not satisfied, the solution exist for this choice of initial data.

In Figure 7.14 the solutions of the fully coupled system and the triangular system are compared. In this case the approximation is not as good as in the first case even though we expected it to be better since the norm condition is satisfied with a smaller k. It may seem that the norm condition has failed. The triangular model does not show the additional wave structure structure in the gas phase. This should not be a surprise since the gas phase equation is decoupled and the solution therefore is monotone, see Section 4.1. However, the triangular model at least captures the transport very accurately. In fact the transport is more accurate in this example than in example 1. This should be expected since only flux function f is modified now as opposed to example 1 where both flux functions were modified.

In Figure 7.15 the solutions for the gas phase are compared at time $t = 0.5$ and $t = 1.0$. The additional wave structure in the gas phase is enhanced with time and is not seen in the solution from the triangular system. However, the transport is still very accurate and it seems that the error in the transport does not increase with time.

The solutions were also computed with ϵ equal to 0.01 just to see if this changed the conclusion above. In Figure 7.16 the solutions for the gas phase are compared at time $t = 0.5$ and $t = 1.0$. The additional wave structure is even larger, but the transport is still very accurate. The error in transport does not seem to increase with ϵ which is as expected since the advection part of the equation dominates when ϵ gets small.

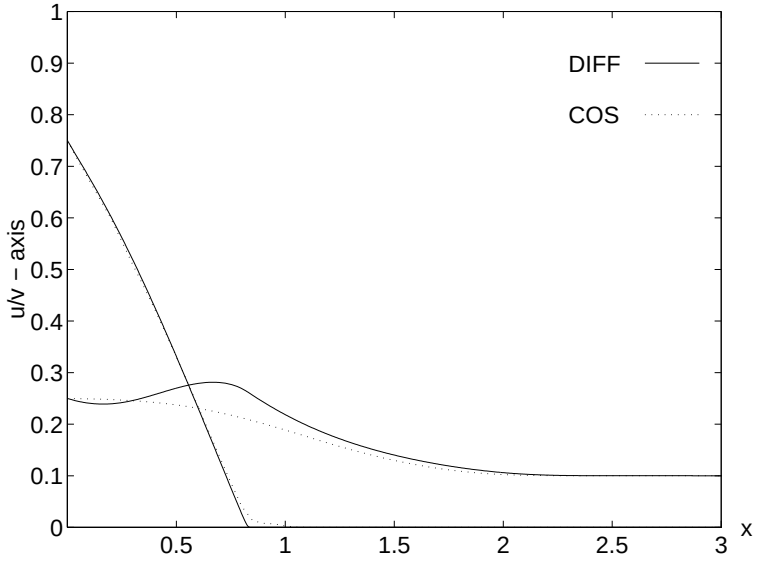

Figure 7.14: Comparison between the reference solution (DIFF) in Figure 7.13 (a) and the COS solution in Figure 7.13 (b) of Riemann problem (7.21) at time $t = 0.5$.

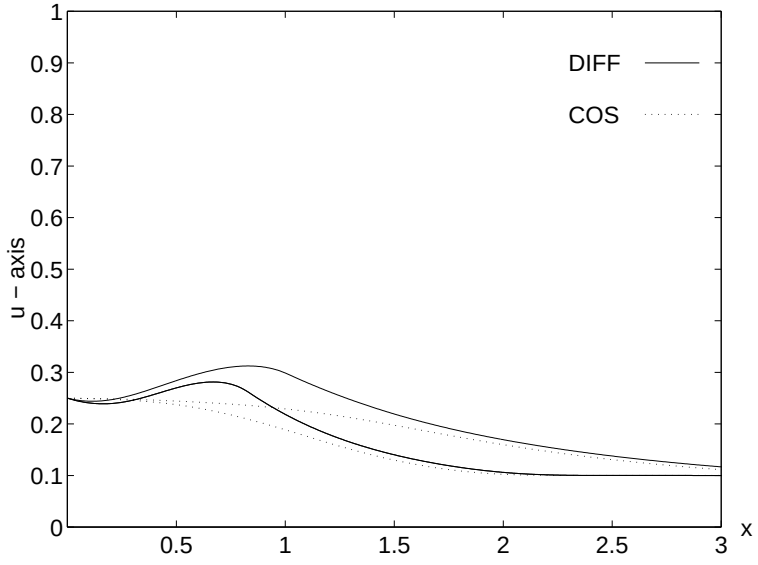

Figure 7.15: Comparison of u for the reference solution (DIFF) and the COS solution of Riemann problem (7.21) at time $t = 0.5$ and $t = 1.0$, $\epsilon = 0.1$.

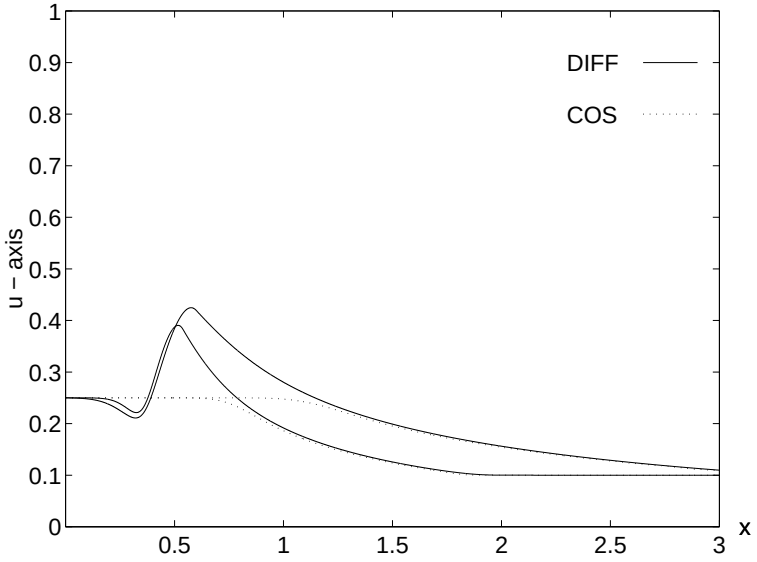

Figure 7.16: Comparison of u for the reference solution (DIFF) and the COS solution of Riemann problem (7.21) at time $t = 0.5$ and $t = 1.0$, $\epsilon = 0.01$.

This suggests the following modification to the Norm condition:

Norm condition 2 (modified) *Let $f(u, v)$ be the gas flux function in a fully coupled 2×2 advection-diffusion system. If*

$$||f_v|| < k||f_u||$$

where $k \ll 1$, then the transport in the fully coupled system can be approximated reasonably well by the transport in a triangular system. The fully coupled system is made triangular by replacing $f(u, v)$ with $f(u, v_0)$, for some v_0.

It seems like approximating the fully coupled system with a triangular system is fruitful. However, the last example demonstrates some limitations for this approximation. Further work should be done to verify the (modified) norm condition analytically.

The most important concern is the restrictions on the flux function $g(u, v)$. In the cases where $g_u < 0$ and all other conditions are satisfied, it seems like we just have to reshape the flux function. The approximation is still good as example 1 showed. In the cases where $g(u, 1 - u) \neq 1 - f(u)$ there are two possibilities. One possibility is to ignore the fact that the condition is not satisfied, but then the solution of some initial value problems do not exist and the triangular model is in-physical. Another possibility is to reshape the flux function, but that may change the physics of the system because the derivatives of the flux function may increase or decrease. The major problem may be that after the system has been made triangular many flux functions do not satisfy the condition $g(u, 1 - u) = 1 - f(u)$. Further investigation of these problems is of great importance for the usefulness of the triangular method.

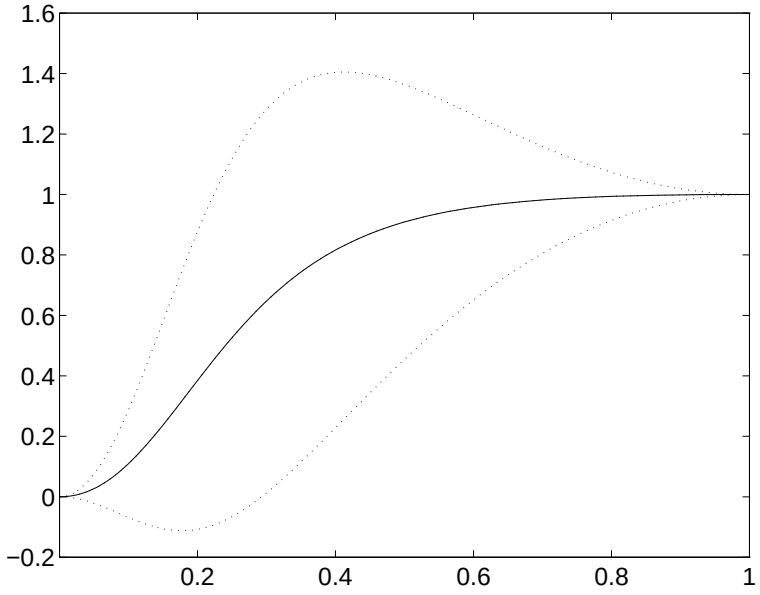

Figure 7.17: Flux function with (dotted lines) and without gravity (solid line).

7.3 Flux functions with gravity

In all the preceding sections the gravity effects have been neglected. This is a consequence of Theorem 4 in Section 4.2 which requires the flux functions $f(u)$ and $g(u,v)$ to satisfy $f_u(u) \geq 0$ and $g_v(u,v) \geq 0$.

In Figure 7.17 a flux function with a gravity term is shown. The solid line shows the flux function when the direction of flow is horizontal, i.e, the gravity term is equal to zero. The dashed lines show two possible flux functions when the direction of the flow is not horizontal, either downwards or upwards.

Let $f(u,v) = f_f(u,v) + f_g(u,v)$ and $g(u,v) = g_f(u,v) + g_g(u,v)$ where $f_f(u,v)$ is the advection part of the fractional flow function and $f_g(u,v)$ is the gravity part, correspondingly for $g(u,v)$. From Equation (2.10) and (2.11) in Section 2.3 we may express the gravity terms as

$$f_g(u,v) = c\left(c_1\frac{\lambda_g\lambda_w}{\lambda_t} + c_2\frac{\lambda_o\lambda_g}{\lambda_t}\right) \tag{7.22}$$

and

$$g_g(u,v) = c\left(c_3\frac{\lambda_g\lambda_w}{\lambda_t} + c_4\frac{\lambda_o\lambda_g}{\lambda_t}\right), \tag{7.23}$$

where $c = \frac{K}{u_t}\cos\theta$ and $c_1 - c_4$ is constants depending on the specific gravities of the phases, $c_1, c_2 > 0, c_3, c_4 < 0$. θ is the angle between the (positive) vertical and direction of flow. Thus the sign of c depends on the flow being up- or downwards. In addition if the total velocity u_t is large or if the absolute permeability is small, then the gravity term is small.

Using mobilities from [12] and setting $c = -1/100$, $c_1 = 950$ $c_2 = 860$, $c_3 = -950$, $c_4 = -270$, and v equal to zero in $f_g(u, v)$ since the system should be triangular, the gravity terms become

$$f_g(u) = -\frac{1}{100}\left(\frac{860(1-u)^2u^2}{10u^2 + (1-u)^2}\right)$$

and

$$g_g(u,v) = -\frac{1}{100}\left(\frac{-950u^2v^2}{10u^2 + v^2 + (1-u-v)^2} + \frac{-27(1-u-v)^2v^2}{10u^2 + v^2 + (1-u-v)^2}\right).$$

The triangular system is now

$$\begin{aligned} \mathbf{s}_t + \mathbf{f}_f(\mathbf{s})_x + \mathbf{f}_g(\mathbf{s})_x &= \epsilon\, D(\mathbf{s})_{xx} \\ \mathbf{s}(x,o) &= \mathbf{s_0} \end{aligned} \tag{7.24}$$

The system will be solved by (corrected) operator splitting. Since the conditions in Theorem 4 is violated if the gravity terms are included in the hyperbolic step, the gravity terms have to be included in the parabolic step. Terminology from Chapter 3 is adapted in an obvious way.

First the advection part of the triangular system is solved. Let $\mathbf{v}(x,t) = \mathcal{S}(t)\mathbf{v}_0$ be the solution of the system

$$\begin{aligned} \mathbf{v}_t + \mathbf{f}_f(\mathbf{v})_x &= 0 \\ \mathbf{v}(x,o) &= \mathbf{v}_0. \end{aligned} \tag{7.25}$$

Secondly the diffusion part of the triangular system is solved. Let $\mathbf{w}(x,t) = \mathcal{H}(t)\mathbf{w}_0$ be the solution of the system

$$\begin{aligned} \mathbf{w}_t + \mathbf{f}_{fres}(\mathbf{v})_x + \mathbf{f}_g(\mathbf{s})_x &= \epsilon D(\mathbf{w})_{xx} \\ \mathbf{w}(x,o) &= \mathbf{w}(x,0). \end{aligned} \tag{7.26}$$

The approximation to the solution of system (7.24) then is

$$\mathbf{s}(x, n\Delta t) \approx (\mathcal{H}(\Delta t)\mathcal{S}(\Delta t))^n \mathbf{s}_0(x). \tag{7.27}$$

The system is solved with ϵ equal to 0.1 and with the same initial data as in Section 7.2, example 2,

$$u_0 = \begin{cases} 0.25 & \text{if } x < 0.4 \\ 0.1 & \text{if } x > 0.4 \end{cases} \quad \text{and } v_0 = \begin{cases} 0.75 & \text{if } x < 0.4 \\ 0.0 & \text{if } x > 0.4 \end{cases} \tag{7.28}$$

In Figure 7.18 (a) and (b) the COS solution of the system is shown for one and two time steps, respectively. When using only one step the gravity introduces some "oscillations", see Figure 7.18 (a). These oscillations disappear when two time steps are used, see Figure 7.18 (b). The solution does not improve when more steps are used.

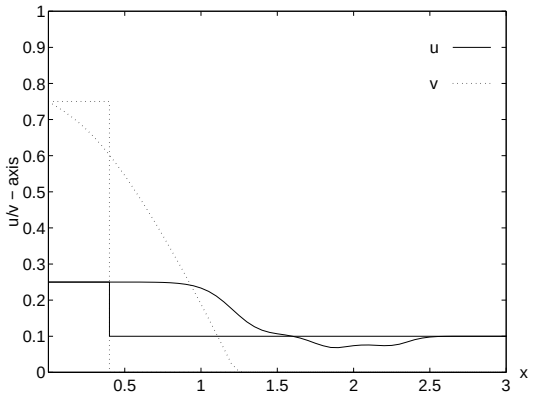

(a) $\Delta u = 0.01$, $\Delta t = 0.5$ and $Cu_{ff} = 250$.

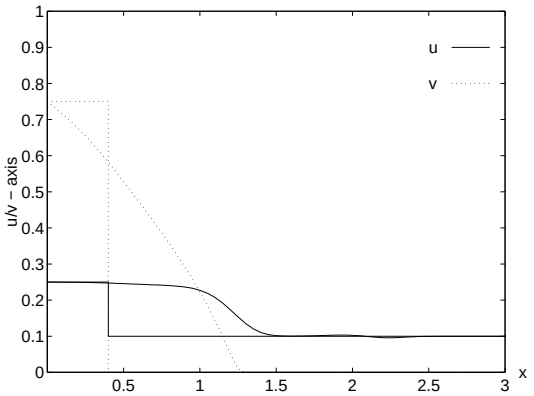

(b) $\Delta u = 0.01$, $\Delta t = 0.25$ and $Cu_{ff} = 125$.

Figure 7.18: COS solutions of Riemann problem (7.28) with gravity at time $t = 0.0$ and $t = 0.5$.

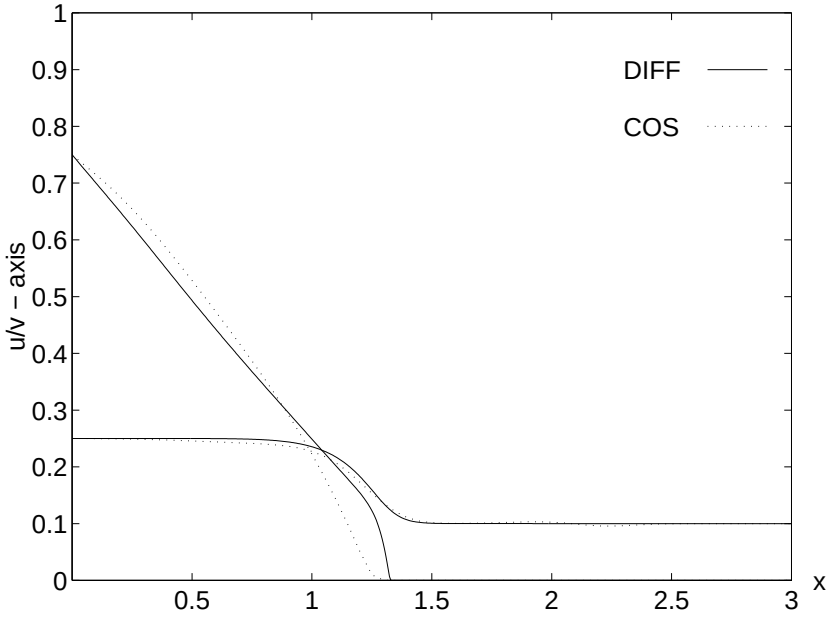

Figure 7.19: The reference and COS solution of the Riemann problem (7.28) compared at time $t = 0.5$

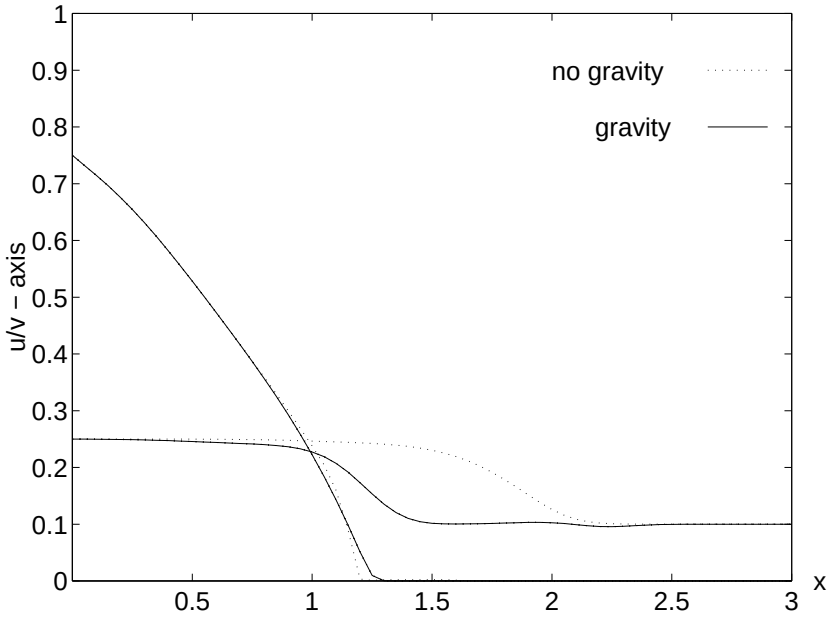

Figure 7.20: Comparison of the COS solutions from the triangular system with and without gravity at time $t = 0.5$.

In Figure 7.19 the reference and COS solution is compared. The reference solution was computed using a finite difference scheme with $\Delta x = 0.005$ and $Cu = 0.125$. The COS solution was computed using $\Delta u = 0.01$, $\Delta t = 0.25$ and $Cu_{ff} = 125$. For the gas phase the COS solution is very accurate. In the water phase some inaccuracy is introduced, but it is most likely from the Riemann solver and not the splitting. Handling flux functions with gravity seems to be no great problem.

In a similar manner to the "gravity splitting", we may treat flux functions that do not satisfy the conditions in Theorem 4. Rather than making a more complex Riemann solver, using the theory from Osnes [13], we split the flux functions into one part that satisfies the conditions and one that does not. The difficult part is then handled together with the diffusion term. This may broaden the class of problems that the triangular method is applicable to. Further work should go into investigating such splittings to determine when they are useful and how well they approximate the correct solution.

To end this section we look at the physics of systems having flux functions with gravity:

Figure 7.20 illustrates what introducing gravity in the flux functions does to the solution. The solutions are found using corrected operator splitting with and without gravity, $\Delta u = 0.01, \Delta t = 0.25$ and $Cu_{ff} = 125$. One phase is accelerated and the other is decelerated. In this example the gas phase is decelerated, and the water phase is accelerated. (The acceleration of the water phase is hard to see because of the inaccurate solution of the system with gravity, see above.)

Chapter 8

Summary and conclusions

In this thesis a triangular model for three phase flow with capillary forces has been investigated. The basis for the model is the assumption that the fractional flow function for the gas phase is independent of the water and the oil phase. The system of advection-diffusion equations was solved using a corrected operator splitting method. The hyperbolic part was solved by a front tracking algorithm. The essential part of the front tracker is the Riemann solver, which is constructed using H-sets. The flux functions are linearised in the solution procedure giving finitely many shocks u_i/u_{i+1} in the gas phase and finitely many corresponding flux functions g_i for the water phase. An introduction to the construction of H-set was given, and the Riemann solver was implemented. The diffusion part was solved by finite difference schemes.

Earlier works, [11, 12, 13], on the triangular model have neglected the capillary forces and therefore only solved the hyperbolic equation. Including capillary forces in the model and operator splitting, introduces new problems that have to be addressed.

Most important, using the grid from the solution of the diffusion equation as grid for the front tracker, results in many Riemann problems with almost equal right and left states. The approximations that have to be done to solve these Riemann problems give a solution that has slightly wrong transport compared to the correct solution when the time step goes to zero. One possible way to resolve this problem is to project the solution from the diffusion solver onto a coarser grid. The resulting Riemann problems would then have right and left states that differ more.

The corrected operator splitting (COS) method was taken from [18]. The correction was achieved solving the diffusion equation with residual flux terms. We had to modify the definition of the residual flux terms in [18] because of the averaging process used to project the front tracker solution onto the uniform diffusion grid. After this modification the COS method gave good results. The runtime for the front tracker is very good, so implementing a faster diffusion solver, for example super time step acceleration, would make the COS method very fast.

The triangular model was compared with the fully coupled model. Based on Taylor expansions of the flux function for the gas phase a *Norm condition* was introduced. The Norm condition suggests that if the L^2-norm of the partial derivative of the gas

flux function with respect to the water phase is much less than the partial derivative with respect to the gas phase, then the transport in the fully coupled model can be approximated reasonably well by the triangular model. The fully coupled system is made triangular by setting the water saturation in the gas flux function constant. The numerical experiments support the Norm condition, but it should be verified analytically. The solution, however, is not well approximated by the triangular model. Since the gas phase is decoupled in the triangular model, the solution for the gas phase is monotone. Thus, the triangular model can not show any additional wave structures in the gas phase.

The solution of the hyperbolic part of the triangular system was essentially computed by the Riemann solver. The front tracker only tracks the fronts from the solution of each Riemann problem. In [13] a uniqueness and existence theorem is given for the (hyperbolic) triangular model with general flux functions. However, constructing the H-sets in the general case is very hard, and we therefore considered only a restricted class of flux functions. This class was defined by the conditions taken from the more restrictive uniqueness and existence theorem in [11]. The major restrictions on the flux functions follow:

The condition that the flux functions should be increasing implied that no gravity terms could be included in the functions. This restriction can be avoided by splitting the flux functions into a advection part and a gravity part, and solving the gravity part in the diffusion step, as demonstrated by the numerical experiments.

The condition that the water flux should decrease when the gas saturation increases was generally not satisfied. Thus, the water flux function had to be reshaped, i.e., approximated by a function satisfying this condition. This approximation is critical since it alters the derivatives of the flux function giving errors in the transport of the system. An optimalisation procedure for this approximation should possibly be developed.

The condition that the endpoints of g_i and g_{i+1} should be connected by a line with slope s_i, i.e., the shock speed of the i'th shock, is always satisfied for a system that is originally triangular. However, for triangular systems that are derived from fully coupled systems, this condition is generally not satisfied. It is possible to choose an optimal constant for the water phase in the gas flux function that minimises the error. If the condition is not satisfied, there exist initial value problems that have no solution. In addition the triangular model will be in-physical. Approximating the water flux function with a function that satisfies the condition resolves the problems, but then the transport may be wrong since the approximation will alter the derivatives.

It follows that it is not straightforward to approximate a fully coupled system with a triangular system. However, since the numerical results are promising, future work should be used on analysing the problems mentioned above.

Appendix A

Finite difference scheme for a class of nonlinear parabolic systems

In Chapter 7 a finite difference scheme was used to find the solution of the advection-diffusion equation

$$u_t + f(u)_x = \epsilon\, D(u)_{xx}, \quad (x,t) \in \mathbf{R} \times \mathbf{R}^+, \tag{A.1}$$

with initial data

$$u(x,0) = u_0(x), \quad x \in \mathbf{R}. \tag{A.2}$$

Here $u \in \mathbf{R}^n$, $f, D \in C^2$, ϵ is a positive constant, and v_0 is of bounded variation. Thus discontinues initial data is allowed, e.g. Riemann problems.

Let $x_k = k\Delta x$ and $t_n = n\Delta t$. The approximation to $u(x_k, t_n)$ is denoted v_k^n. Then the (forward-time central-space) finite difference scheme is

$$\frac{v_m^{n+1} - v_m^n}{\Delta t} = \epsilon \frac{v_{m+1}^n - 2v_m^n + v_{m-1}^n}{\Delta x^2} - \frac{f(v_{m+1}^n) - f(v_{m-1}^n)}{2\Delta x}. \tag{A.3}$$

Nishida and Smoller [24] have shown that v_k^n does converge to the classical solution of advection-diffusion equation. In [25], Hoff and Smoller established a more precise result by obtaining the error bound

$$\sup_k |v_k^n - u(x_k, t_n)| \le \frac{C}{\sqrt{t_n}} \left[\Delta x \sum_k |v_k^0 - u_0(x_k)| + \Delta x |\ln \Delta x| \right] \tag{A.4}$$

for $0 < t_n \le T$, where C only depends on T, ϵ and f.

The mesh parameters must satisfy

$$\epsilon \max_u |D'(u)| \Delta t / \Delta x^2 \le 1/2 \tag{A.5}$$

and

$$\Delta x \max_u |f'(u)| \le 2\epsilon \tag{A.6}$$

to make the difference scheme stable and to make the error bound hold.

Appendix B

Finding H-sets when the flux function has no inflection point

In this appendix we only consider flux functions $g(u,\cdot)$ that has no inflection point. Generally, there are two intervals, I_1 and I_2, such that

$$u \in I_1 \Rightarrow g_{vv} \neq 0 \ \ \forall v \in [0,1] \qquad \text{and} \qquad u \in I_2 \Rightarrow \exists v! \ \ g_{vv} = 0,$$

where one of the intervals possibly is empty. For all u where $g(u,\cdot)$ has one inflection point the construction follows Section 4.3.

We assume that g_{vv} is positive, i.e., g_v is strictly increasing. This follows from the assumption in Section 4.3 setting the inflection point equal to infinity. In Figure B.1 a typical flux function with no inflection point (and $g_{vv} > 0$) is shown. The flux function is taken from Example 2 in Section 7.2.

Constructing H-sets when the flux function has no inflection point, is really a special case that could be treated with the machinery in Section 4.3 assuming the inflection point to be outside the phase plane, e.g. in infinity. Even though we will go briefly through the construction just for clarification.

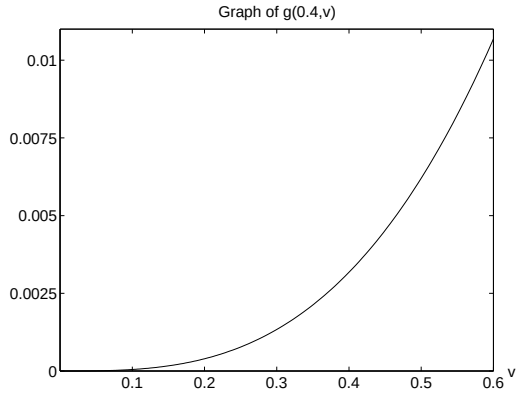

Figure B.1: Flux function without inflection point.

The definition of the H-sets are found in Section 4.2. A H-set consist of two or less intervals and a possible midpoint and is written as

$$H_{i,x} = [0, v_{i,x,l}] \cup v_{i,x,m} \cup [v_{i,x,r}, 1 - u_i],$$

where $v_{i,x,l}$, $v_{i,x,m}$ and $v_{i,x,r}$ determine the set uniquely. x is either *out* or *in*.

When finding H-sets there are two general cases:
1. $u_i < u_{i+1}$, u-shocks form an increasing sequence.
2. $u_i > u_{i+1}$, u-shocks form a decreasing sequence.

In this appendix the two cases will be treated one at the time. We use the same structure as in Section 4.3.

In the construction of each $H_{k,x}$ only g_k is assumed to have no inflection point. g_{k-1} has at most one inflection point as assumed in Section 4.2.

B.1 Increasing sequences

In this section only increasing sequences of u-shocks are considered.

Finding $H_{1,in}$

$H_{1,in}$ consists of all the points that can be reached from v_L with a jump with shock speed less than (or equal to) s_1. The construction goes as in Section 4.3 except that there is no case with two tangent points since $g_{vv} > 0$. Thus there are two possibilities:

1. There is one tangent point.
2. There are no tangent points, and the tangents are everywhere less than the shock speed.

The only difference from Section 4.3 is in case 1 where $v_{1,in,r}$ never exists since the inflection point is in infinity. The only exception from that being when $v_{1,in,m} = v_{1,in,r} = 1 - u_1$.

Finding $H_{i+1,out}$

Assume that $H_{i,in}$ is found, consisting of two or less intervals and possibly a midpoint. $H_{i+1,out}$ consist of find the points on g_{i+1} that are reachable with a jump with speed s_i from $H_{i,in}$. There are three cases:

1. $v_{i,in,r}$ exists.
2. $v_{i,in,r}$ does not exist, but $v_{i,in,l}$ does.
3. Only $v_{i,in,m}$ exists.

From Section 4.3 we have that $v_{i,in,l}$, $v_{i,in,m}$ and $v_{i,in,r}$ lie on a line with slope s_i when they exist.

1. $v_{i,in,r}$ exists

From Section 4.3 we have that if $v_{i,in,r}$ exists, then $v_{i+1,out,r}$ always exists.

If there is no points on g_{i+1} with tangent equal to s_i, it is obvious that all points on g_{i+1} can be reached from g_i with shock speed s_i since $g_{vv} > 0$.

If there is a tangent point, $v_{i+1,out,r}$ is equal to $(1 - u_{i+1})$ and $v_{i+1,out,l}$ is equal to the cutting point between the line with slope s_i starting at $v_{i+1,out,r}$, and g_{i+1}, cutting down. $v_{i+1,out,m}$ does not exist.

2. $v_{i,in,r}$ does not exist, but $v_{i,in,l}$ does

Since $v_{i,in,r}$ does not exist, we know that $v_{i+1,out,r}$ does not exist either. $v_{i+1,out,m}$ and $v_{i+1,out,l}$ are found cutting up and down, respectively, with slope s_i from $v_{i,in,l}$. The construction is independent of the existence of $v_{i,in,m}$.

3. Only $v_{i,in,m}$ exists

It is obvious that we get $v_{i+1,out,m}$ equal to the cutting point between the line starting at $v_{i,in,m}$ with slope s_i and g_{i+1}, cutting up (to the right). $v_{i+1,out,m}$ and $v_{i+1,out,m}$ do not exist.

Finding $H_{i+1,in}$

We now assume that we $H_{i+1,out}$ is known and want to construct $H_{i+1,in}$. Looking away from the trivial case $H_{i+1,out} = [0, 1 - u_{i+1}] = H_{i+1,in}$, there are two cases to consider:

1. $v_{i+1,out,m}$ exists.
2. $v_{i+1,out,m}$ does not exist.

1. $v_{i+1,out,m}$ exists

If $v_{i+1,out,m}$ exists, then $v_{i+1,out,r}$ does not exist. This is evident since in the construction of $H_{i+1,out}$ (in the increasing case) both points can not exist at the same time. However, one of them always exists. $v_{i+1,in,m}$ is obviously equal to $v_{i+1,out,m}$, and $v_{i+1,in,l}$ is found cutting down from $v_{i+1,out,m}$ with slope s_{i+1}.

2. $v_{i+1,out,m}$ **does not exist**

Since $v_{i+1,out,m}$ does not exist, $v_{i+1,out,r}$ must exist, refer above. Thus $v_{i+1,in,r} = v_{i+1,out,r} = 1 - u_{i+1}$, and $v_{i+1,in,l}$ is equal to the cutting point between the line starting at $1 - u_{i+1}$ with slope s_{i+1}, cutting down.

B.2 Decreasing sequences

In this section only decreasing sequences of u-shocks are considered.

Finding $H_{1,in}$

Same as for the increasing sequence, see above.

Finding $H_{i+1,out}$

Assume that $H_{i,in}$ is known, consisting of two or less intervals and possibly a midpoint. $H_{i+1,out}$ consist of the points on g_{i+1} that can be reached with a jump with speed s_i from $H_{i,in}$. From Section 4.3 we have that $v_{i,in,l}$, $v_{i,in,m}$ and $v_{i,in,r}$ lie on a line with slope s_i when they exist.

Since g_i is lying below g_{i+1} and g_{i+1} is convex for $0 \leq v \leq (1 - u_{i+1})$, s_i must be larger than $S = g_{i+1}(1 - u_{i+1})/(1 - u_{i+1})$, i.e., the slope of the straight line from origin to the endpoint of g_{i+1} is less than s_i. No straight line cutting down, to the left, from a given point on g_i will cut g_i outside the phase plane since g_i is lying below the straight line, see Figure B.2 below. Then it is impossible for $H_{i,in}$ to consist only of the midpoint, $v_{i,in,m}$, since a line with slope s_i starting at $v_{i,in,m}$ would cut g_i inside the phase plane and give $v_{i,in,l}$. And if $v_{i,in,r}$ exists, then $v_{i,in,l}$ also has to exist because of the same cutting property. Thus there is only one case to consider:

$v_{i,in,l}$ **exists**

Since $v_{i,in,l}$ exists, $v_{i+1,out,l}$ also exists.

If there is no points on g_{i+1} with tangent equal to s_i, it is obvious that all points on g_{i+1} can be reached from g_i with shock speed s_i since $g_{vv} > 0$. This is independent of the existence of $v_{i,in,m}$ and $v_{i,in,r}$.

If there is a tangent point, t, then let c be the cutting point between the line starting at $1 - u_i$ with slope s_i, and g_{i+1}. If $v_{i,in,r}$ exists, then $v_{i+1,out,r}$ is equal to $1 - u_{i+1}$ and $v_{i+1,out,l}$ is equal to c. If $v_{i,in,r}$ does not exist, then $v_{i+1,out,r}$ does not exist either and $v_{i+1,out,l}$ is equal to t.

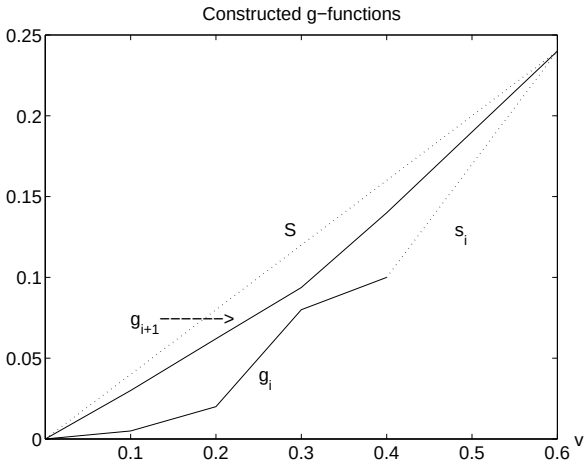

Figure B.2: Illustration of g_i and g_{i+1} when g_{i+1} has no inflection point and the sequence of u-shocks is decreasing. The functions are constructed (and linearised).

Finding $H_{i+1,in}$

We now assume that we $H_{i+1,out}$ is known and want to construct $H_{i+1,in}$. Looking away from the trivial case $H_{i+1,out} = [0, 1 - u_{i+1}] = H_{i+1,in}$, there is only one case to consider:

$v_{i+1,out,m}$ does not exist

Since $v_{i+1,out,m}$ does not exist, $v_{i+1,in,m}$ does not exist either.

If only $v_{i+1,out,l}$ exists, then $v_{i+1,in,l}$ is equal to the point with tangent s_{i+1}. $v_{i+1,in,r}$ do not exist.

If $v_{i+1,out,r}$ exists, then $v_{i+1,in,r} = v_{i+1,out,r} = 1 - u_{i+1}$ and $v_{i+1,in,l}$ is equal to the cutting point between the line starting at $1 - u_{i+1}$ with slope s_{i+1}, cutting down.

Bibliography

[1] K. W. Morton. *Numerical Solution of Convection-Diffusion Problems.* Chapman & Hall, 1996.

[2] M. Eikemo. Operatorsplittings-teknikker for tre-fase tre-komponent modeller. Cand. Scient. thesis, Dept. of Mathematics, Univ. of Bergen, 1993.

[3] H. Reme. Matematisk og numerisk studie av en inkompressibel modell som inkluderer kapillarkrefter. Cand. Scient. thesis, Dept. of Mathematics, Univ. of Bergen, 1996.

[4] L. Løvstakken. Numerisk og analytisk studie av en tre-fase modell for strøm i porøse medier. Cand. Scient. thesis, Dept. of Mathematics, Univ. of Bergen, 1998.

[5] K. Hvistendahl Karlsen, K. Brusdal, H. K. Dahle, S. Evje, and K.-A. Lie. The corrected operator splitting approach applied to an advection-diffusion problem. *Comput. Methods Appl. Mech. Engrg.*, To appear.

[6] S. Evje, K. Hvistendahl Karlsen, K.-A. Lie, and N. H. Risebro. Front tracking and operator splitting for nonlinear degenerate convection-diffusion equations. Report No. 1, Institut Mittag-Leffler, Sweden., 1997/98.

[7] H. Holden, L. Holden, and R. Høegh-Krohn. A numerical method for first order nonlinear scalar conservation laws in one dimension. *Comp. Math. Appl.*, 15:595–602, 1988.

[8] N. H. Risebro and A. Tveito. A front tracking method for conservation laws in one dimension. *J. Comp. Phys.*, 101:130–139, 1992.

[9] F. Bratvedt, K. Bratvedt, C. F. Buchholz, T. Gimse, H. Holden, L. Holden, and N. H. Risebro. Frontline and frontsim: two full scale, two phase, black oil reservoir simulators based on front tracking. *Surv. Math. Ind.*, 3:185–215, 1993.

[10] T. Gimse. Front tracking for porous media flow. Dr. Scient. thesis, Dept. of Mathematics, Univ. of Oslo, 1992.

[11] T. Gimse. A triangular riemann solver. Cand. Scient. thesis, Dept. of Mathematics, Univ. of Oslo, 1988.

[12] J. A. Kok. Front tracking for three-phase flow in porous media. Final report of the postgraduate program Mathematics for industry. Eindhoven, Netherlands, 1994.

[13] K. Osnes. Den triangulære metoden med variasjoner. Cand. Scient. thesis, Dept. of Mathematics, Univ. of Oslo, 1997. In norwegian.

[14] K. Aziz and A. Settari. *Petroleum Reservoir Simulation.* Elsevier Applied Science Publishers, 1985.

[15] Ø. Pettersen. *Grunnkurs i reservoarmekanikk.* Matematisk institutt - UIB, 1990.

[16] J. B. Bell, J. A. Trangenstein, and G. R. Shubin. Conservation laws of mixed type describing three-phase flow in porous meida. *Siam appl. math.*, 46(6):1000–1017, 1986.

[17] K. Hvistendahl Karlsen. Numerical solution of nonlinear convection-diffusion equations: Operator splitting, front tracking and finite differences. Dr. Scient. thesis, Dept. of Mathematics, Univ. of Bergen, 1998.

[18] J. R. Natvig. Operatorspliting basert på frontfølging for polymersystemet. Cand. Techn. thesis, Inst. of Phys., Info. and Math., NTNU Trondheim, 1998.

[19] O. A. Oleinik. Discontinuous solutions of non-linear differential equations. *Amer. Math. Soc. Transl. Ser. 2*, 26:95–172, 1963.

[20] H. Holden and N. H. Risebro. Front tracking for conservation laws. Lecture notes, Dept. of Mathematics, Univ. of Oslo, 1997.

[21] L. Holden and R. Høegh-Krohn. A class of n nonlinear hyperbolic conservation laws. *Journal of Differential Equations*, 84:73–99, 1990.

[22] R. J. LeVeque. *Numerical Methods for Conservation Laws.* Birkhäuser Verlag, 1992.

[23] V. Alexiades, G. Amiez, and P. Gremaud. Super-time-stepping for explicit schemes. *Com. Num. Meth. Eng.*, 12:31–42, 1996.

[24] T. Nishida and J. Smoller. A class of convergent finite difference schemes for certain nonlinear parabolic systems. *Comm. Pure Appl. Math.*, 36:785–808, 1983.

[25] D. Hoff and J. Smoller. Error bounds for finite-difference approximations for a class of nonlinear parabolic systems. *Mathematics of Computation*, 45(171):35–49, 1985.